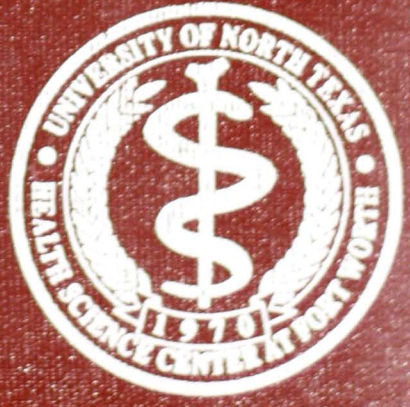
UNIVERSITY OF NORTH TEXAS
HEALTH SCIENCE CENTER AT FORT WORTH
1970

Shepard, Athena A., Anisotropy of Myosin and Actin in Contraction of Skeletal Muscle. Doctor of Philosophy (Molecular Biology and Immunology), December, 2004, 161 pp., 1 table, 42 illustrations, bibliography, 253 titles.

Muscle contraction results from the interaction of myosin and actin proteins contained in the muscle sarcomere. During actomyosin interactions, myosin consumes ATP and imparts an impulsive force to actin resulting in sliding of myosin and actin filaments to produce work. These proteins constitute the elementary motor responsible for cellular motility. The overall goal of this research project was to elucidate the mechanism of the actomyosin interaction on a molecular level. Novel time-resolved optical microscopic techniques followed myosin and actin orientation changes during skeletal muscle contraction.

Fluorescence anisotropy was used to study the real time orientation changes of myosin, actin, and nucleotide during a single cross bridge cycle beginning in a state of rigor. Rabbit psoas fibers were isolated on a microscopic slide and labeled with fluorescently labeled regulatory light chain to monitor orientation changes of the lever arm of myosin, with fluorescent phalloidin to monitor orientation changes of actin and/or with Alexa ADP to monitor ATP hydrolysis. Caged ATP was perfused into the fiber prior to analysis to allow a small population of cross-bridges to execute a single cross-bridge cycle. Flash photolysis with UV light during analysis converted caged ATP from an inactive from to an active from. Confocal and multi-photon imaging allowed illumination of a small population of fluorescently labeled cross-bridges to measure orientation changes over time.

The conclusions of this dissertation are: 1) The regulatory light chain rotates during skeletal muscle contraction and the lever arm model is supported, 2) Release of ADP from S1 corresponds to a single rotation of the lever arm, 3) Actin rotates during skeletal muscle contraction, 4) The rotation of actin is passive, i.e. it rotates as a consequence of dissociation of S1 from actin.

The results revealed orientation changes in key contractile proteins during muscle contraction in the non-disease state organism. By understanding the mechanism of muscle contraction in the healthy scenario, hopefully a better understanding of diseased states stemming from mutations in contractile proteins (Usher's Syndrome, Snell's Waltzer Disease, and certain familial hypertrophic cardiomyopathies) will be made available, leading to better preventative measures or treatments to treat such diseases in the future.

ANISOTROPY OF MYOSIN AND ACTIN

IN CONTRACTION

OF SKELETAL MUSCLE

Athena A. Shepard, B.S.

APPROVED:

T. Borejdo

Major Professor

Thomas P. Burghardt

Committee Member

Committee Member

Committee Member

University Member

Chair, Department of Molecular Biology and Immunology

Dean, Graduate School of Biomedical Sciences

ANISOTROPY OF MYOSIN AND ACTIN IN CONTRACTION OF SKELETAL MUSCLE

DISSERTATION

Presented to the Graduate Council of the

Graduate School of Biomedical Sciences

University of North Texas
Health Science Center at Fort Worth

in Partial Fulfillment of the Requirements

For the Degree of

DOCTOR OF PHILOSOPHY

By

Athena A. Shepard, B.S.

Fort Worth, Texas

December 2004

ACKNOWLEDGEMENTS

I am deeply grateful to Dr. Julian Borejdo, who motivated me to work hard and was a source of inspiration. I would also like to thank the members of my committee, Drs. Thomas Burghardt (Mayo Clinic, Rochester, MN), Ben Harris, Ming-Chi Wu, and my university member, Dr. Robert Mallet for their suggestions, comments and support. My lab research associate, Dr. Irina Akopova has provided excellent expertise, as have my fellow lab mates Disha Dumka, Mahalakshmi Ramini, and John Talent.

I am sincerely grateful to Dr. Alaknanada Basu, Dr. Jerry Simecka, Dr. Thomas Yorio, to the faculty, staff and students of the Department of Molecular Biology and Immunology, the Graduate School of Biomedical Sciences and the University of North Texas Health Science Center at Fort Worth for their constant encouragement and support.

Special thanks to the following sources of funding: National Institute of Health, Texas Higher Education Coordinating Board, and the National Science Foundation.

Most of all, I would like to thank my husband, Allan. For everything, I love you.

TABLE OF CONTENTS

LIST OF TABLES.....v

LIST OF ILLUSTRATIONS.....vi

Chapter

I. INTRODUCTION.....1

II. ANISOTROPY OF MYOSIN.....39

III. CORRELATION BETWEEN MECHANICAL AND ENZYMATIC EVENTS IN CONTRACTING SKELETAL MUSCLE FIBER.....81

IV. ANISOTROPY OF ACTIN.....111

V. CHANGES OF ACTIN ORIENTATION DURING MUSCLE CONTRACTION ARE PASSIVE.....136

VI. CONCLUSION.....160

List of Tables

Table I. The classes of myosin.....3

List of Illustrations

Chapter 1

Figure 1. Structure of skeletal muscle.....6

Figure 2. Schematic of sarcomere within striated muscle.....7

Figure 3. Schematic of cross-bridge formation.....7

Figure 4. Schematic of the myosin filament.....8

Figure 5. X-ray crystallographic structure of myosin II S1 from chicken skeletal muscle in the absence of ATP.....9

Figure 6. Schematic showing the weak to strong binding of actin to myosin.....13

Figure 7. Schematic of the cross-bridge cycle.....13

Figure 8. Electron microscope reconstruction of F-actin from X-ray crystal structure.....15

Figure 9. The lever arm hypothesis.....19

Figure 10. Representation of dipole of a fluorophore labeled on RLC (green chain).....21

Figure 11. The resolution of anisotropy over time varies with the number of cross-bridges observed over time.....22

Figure 12. Schematic of the illumination volume impinging on the muscle.....23

Figure 13. Comparison of the depth-of-focus of 1P and 2P illumination.....24

Figure 14. Simplified schematic of the experimental set-up for 1P LSM.....25

Figure 15. Experimental set-up for 2P imaging.....28

Chapter 2

Figure 1. Schematic representation of the expected time course of anisotropy over time of a single cross-bridge cycle.....44

Figure 2. RLC purification.....54

Figure 3. RLC exchange.....56

Figure 4. ELC exchange.....58

Figure 5. Unlabeled control fiber versus labeled fiber 62

Figure 6. 1P and 2P image of muscle fiber labeled with IATR-RLC.....67

Figure 7. The photobleaching effect.....65

Figure 8. Intensities and anisotropy of a muscle fiber containing IATR-RLC.....67

Figure 9. Anisotropy of 1P and 2P IATR-RLC and 2P IATR-ELC.....69

Figure 10. Anisotropy of 1P and 2P IATR-ELC.....71

Chapter 3

Figure 1. Excitation anisotropy of Alexa-ATP.....92

Figure 2. Myosin labeling with Alexa ATP and actin labeling with fluorescent phalloidin in the same fiber results in staining of the A- and I-bands.....94

Figure 3. Parallel anisotropy and parallel polarized intensity following ATP photogeneration in the fiber labeled with Alexa-ATP.....95

Figure 4. Excitation anisotropy of IATR-RLC.....96

Figure 5. Parallel anisotropy and parallel polarized intensity following ATP photogeneration in the fiber labeled with IATR-RLC.....97

Figure 6. Correspondence between anisotropy and intensity signals.....98

Figure 7. Images of a fiber labeled with IATR-RLC and viewed through an LP 590 (rhodamine) filter and Alexa-ATP viewed through an LP 647 (Cy5) filter....100

Figure 8. Correlation between rotations of the perpendicular polarized intensity of RLC and the parallel polarized intensity of Alexa-ATP.....101

Figure 9. Conventional scheme of cross bridge action and time course of anisotropy...102

Chapter 4

Figure 1. Labeling of thin filaments in a fiber with FITC-phalloidin.....119

Figure 2. Anisotropy of IATR-phalloidin bound to thin filaments of a muscle fiber....125

Chapter 5

Figure 1. Triple labeling of muscle.....146

Figure 2. Simultaneous measurement of polarized intensities of IATR-RLC, FITC-phalloidin, and Alexa-ADP.....148

Figure 3. Anisotropies of myosin, actin, and Alexa-ATP.....150

Figure 4. Excitation anisotropy spectra of free RLC labeled with rhodamine and IATR-RLC incorporated into myosin.....151

Figure 5. Excitation anisotropy spectra of FITC-phalloidin incorporated into F-actin...153

Figure 6. Excitation anisotropy spectra of Alexa-ATP incorporated into the active site of myosin.....154

CHAPTER 1

INTRODUCTION TO THE STUDY

Background to Myosin Superfamily

Cellular motility is a fundamental property of all living organisms. For example, within a cell, cargo may be transported via various myosin classes along actin filaments or kinesins and dyneins which travel along microtubules. Myosins are actin-based motors which function in cell motility, cytokinesis, phagocytosis, growth cone extension, contraction, and organelle/cargo trafficking (8, 9). Muscle myosins are called myosin II and are referred to as conventional myosins. Unconventional myosins refer to all other myosins, including non-muscle myosin. To date, 40 myosin genes in humans have been identified and categorized into fifteen classes (8). The bulk of myosin II genes have been found on chromosome 17, including 6 skeletal muscle myosin heavy chains (MHC), 2 cardiac muscle MHC, and 1 smooth muscle MHC, with the total number of myosin II genes numbering around 15. Recently, a human cDNA has been cloned (**Table 1**, Acc. # AB040945(8)) that is 70% identical to human skeletal myosin II, but its muscle and/or tissue expression distribution is unknown. Additionally, the gene maps to chromosome 20 and not to chromosome 17. Consequently, the identification and characterization of the myosin superfamily is an ongoing process.

Human

	Gene	Chr.	Acc. #	Comments
M1	*MYO1A*	12q	AF009961	Brush border myosin-I
	MYO1B	2q	X68199 (*Rn*)	*Rn* myr1, *Mm* M1α, *Hs* AK000160 (partial)
	MYO1C	17p	X98507	*Rn* myr2, *Mm* and *Hs* M1β
	MYO1D	17p	X71997 (*Rn*)	*Rn* myr4, *Mm* M1γ, *Hs* AK026920, KIAA0727
	MYO1E	15q	U14391	*Rn* myr3, *Hs* U14391 ("Myosin-IC")
	MYO1F	19q	X97650 (*Mm*)	*Hs* U57053 + X98411
	**MYO1G?*	7p	[AC004847]	Predicted; 50% identical to *Rn* myr4
	**MYO1H?*	12q	[NT_002188]	Predicted; 50% identical to *Rn* myr2
M2	*MYH1*	17p	AF111785	Myosin-IIx/d
	MYH2	17p	AF111784	Myosin-IIa
	MYH3	17p	X13988	Myosin-II embryonic
	MYH4	17p	AF111783	Myosin-IIb
	MYH5	(reserved)		
	MYH6	14q	P13533	Cardiac myosin II-alpha
	MYH7	14q	P12883	Cardiac myosin II-beta
	MYH8	17p	P13535	Myosin-II perinatal
	MYH9	22q	P35579	Non-muscle myosin-IIa
	MYH10	17p	P35580	Non-muscle myosin-IIb
	MYH11	16p	P35749	Smooth muscle myosin-II
	MYH12	(withdrawn)		
	MYH13	17p	AF111782	Myosin-II extraocular
	**MYH?*	20q	AB040945	KIAA1512 and predicted from AL132825
	**MYH?*	3	AB023217	KIAA1000 and predicted from AC069499
	**MYH?*	19q	[AC020906 +AC10515]	Predicted; similar to non-muscle myosins
M3	*MYO3A*	10p	AF229172	NinaC-like with N-terminal kinase
	**MYO3B?*	2q	[AC012594]	Predicted; similar to myosin-IIIa
M5	*MYO5A*	15q	U90942	Myosin-Va, Griscelli syndrome, "*dilute*"
	MYO5B	18	U60416 (*Rn*)	*Rn* myr6, *Hs* KIAA1119
	MYO5C	15q	AF272390	Myosin-Vc
M6	*MYO6*	6	U90236	Myosin-VI, reverse direction, "*Snell's waltzer*"
M7	*MYO7A*	11	U55208	Myosin-VIIa, Usher syndrome 1b, "*shaker-1*"
	MYO7B	2q	– pending –	Myosin-VIIb
M9	*MYO9A*	15q	AJ001714	*Hs* Myosin-IXa, *Rn* myr7, GAP for Rho
	MYO9B	19	U42391	*Hs* Myosin-IXb, *Rn* myr5, GAP for Rho
M10	*MYO10*	5p	AF247457	Myosin-X, PH domains, vertebrate specific
M15	*MYO15A*	17p	AF144094	Myosin-XV, DFNB3, "*shaker-2*"
	**MYO15B?*	17q	[AC019214]	Predicted novel class XV myosin
M16	*MYO16*	13	AF209114 (*Rn*)	*Hs* KIAA0865, *Rn* myr8
M18	*MYO18A?*	17	D88970	*Hs* KIAA0216, *Mm* MysPDZ
	**MYO18B?*	22q	[AL080245 +Z98949]	Predicted; similar to MysPDZ with coiled-coil tail
Orphan or not numbered				
	**MYO?*	17q	[AC023133]	Predicted; novel myosin with short tail

Drosophila

	Chr.	Acc. #	Comments
M1	31DF	S45573	Myosin-IA
	61F	U07596	Myosin-IB
M2	36A	P05661	MHC, alt. spliced
	60E	U35816	NMM-II "*zipper*"
M3	28A	J03131	"*ninaC*"
M5	43C	AF003826	"*didum*"
M6	95F	X67077	"*jaguar*"
M7	28B	AF233269	
	*35B	AAF44915	"*crinkled*"
M15	*10A	[AE003484]	CG2174
M18	*89B	[AE003711]	CG10218
Orphan or not numbered			
	*29CD	[AE003621]	CG10595
	*95E	[AE003746]	Novel, basic tail

Dictyostelium

	Name	Acc. #	Comments
M1	MyoA	P22467	
	MyoB	P34092	SH3
	MyoC	L35323	SH3
	MyoD	P34109	SH3
	MyoE	L06805	
	MyoK	AF090534	
M2	MhcA	P08799	
M7	MyoI	L35321	Phagocytosis
M11	MyoJ	U42409	
Orphan or not numbered			
	MyoM	AF090533	GEF for Rac1
	MyoF	L35319	~260bp partial
	MyoH	L35320	~299bp partial
	"MyoG"	No sequence	
	"MyoL"	No sequence	

C. Elegans

	Gene	Acc. #	Comments
M1	*hum-5*	X75564	
	hum-1	U52515	
M2	*mhc-A*	P12844	
	mhc-B	P02566	Unc-54
	mhc-C	P12845	
	mhc-D	P02567	
	**mhc-?*	[Z93382]	F45G2.2
	**mhc-?*	[U50309]	F58G4.1
	nmy-1	U41990	
	nmy-2	U49263	
	**nmy-?*	[AL032632]	Y11D7A.14
M5	*hum-2*	U52516	
M6	*hum-3*	U52517	
	**hum-8*	[AF125462]	Y66H1A.6
M7	**hum-6*	[U80848]	T10H10.1
M9	**hum-7*	[AF067217]	F58A6.2
M12	**hum-4*	[Z66563]	F46C3.3

Arabidopsis

	Gene	Acc. #	Comments
M8	ATM1	X69505	
	ATM2	Z34292	
	*F14I3.6	[AC007980]	
	*M4I22.180	[AL030978]	
M11	MYA1	Z28389	
	MYA2	Z34293	
	MYA3	Z34294	
	*F4I10.130	[AL035525]	
	*F11A3.16	[AC006569]	
	*F16A16.180	[AL035353]	
	*F20D22.7	[AC002411]	
	*F20M17.6	[AC006533]	PCR11 (S51821)
	*F22O13.20	[AC003981]	PCR43 (T00727)
	*F25I18.2	[AC002332]	
	*T1G11.15	[AC002376]	
	*T22H22.1	[AC005388]	PCR1 (S51820)
	*F7C8	[AF296833]	

S. Cerevesiae

	Gene	Acc. #	Comments
M1	*MYO3*	S76960	
	MYO5	Q04439	
M2	*MYO1*	[NP_011888]	
M5	*MYO2*	P19524	Vesicle transport
	MYO4	M90057	mRNA transport

S. Pombe

	Gene	Acc. #	Comments
M1	*myo1*	T39427	
M2	*myo2*	U75357	
	myp2	AF029788	*myo22, myo3*
M5	*"myo51"*	[AL035075]	*"myo5"*
	"myo52"	[AL031788]	*"myp5"*

Table 1. The classes of myosin. Taken virtually verbatim from (8): Classes are designated by the letter M (myosin) followed by the class number. Genes predicted in full or in part from genomic sequence are indicated by an asterisk. Accession numbers are for cDNA/protein sequences or genomic clones in square brackets. The numbering of the budding yeast myosins (MYO1–5) and the unconventional myosins from *C. elegans* (HUM1–8; *h*eavy chain of *u*nconventional *m*yosin) and rat (myr1–8; *m*yosin from *r*at) corresponds to the order of discovery in these organisms and not their phylogenetic class. *Drosophila* myosins have traditionally been referred to by their chromosomal locus. *Dictyostelium* myosins are lettered (MyoA-MyoM). *Arabidopsis* myosins ATM = class VIII and MYA = class XI. Chr = chromosome, *Rn* = *Rattus norvegicus*, *Mm* = *Mus musculus*, *Hs* = *Homo sapiens*.

Non-conventional Myosins

Typically, one thinks of myosin as present in the muscles; however, there is a plethora of (**Table I**) myosins that exist outside muscle and brief introduction of some, but not all of the classes, is provided here. A detailed introduction to conventional myosin or myosin II (myosin class II), including smooth, cardiac, and skeletal, the last one being the focus of this thesis, follows this. Myosin I, the first non-conventional myosin to be purified, has been implicated in cytoskeletal reorganization and organelle translocation (11). Various isoforms have been identified in the cytoplasm, plasma membranes, lamellipodia, regions of cell-cell contact within the cell, brush border of the intestinal microvillus, mitochondria of photoreceptor cells, auditory hair cells, microvilli of kidney cells, and membranes of neuronal cell bodies and dendrites (11). Mutated myosin IB heads with nucleotide analogues in the ATP and ADP state resulted in a reduction of *in vitro* actin motility and myosin ATPase activity (12). This was done by site-directed mutagenesis rendering only the IB isoform sensitive to binding the nucleotide, thus specifically studying the function of the 1B isoform. This exemplifies a common mutagenesis technique to study the function of myosin.

Myosin V is associated with transport of cargo along actin filaments and falls under the category of a processive motor, meaning that for each encounter with actin, myosin V goes through multiple ATPase cycles, travels long distances, and carries cargo before dissociating from actin (13). Myosin V is similar in job function to kinesin/dynein traveling along microtubules. However the kinetics between myosin and kinesin and dyneins differ, and myosin V movements take place by a long lever arm with

3 light chains connecting it to a coiled rod domain. Kinesin and dynein lack such a structure and possibly rely on some sort of diffusion for movement along microtubules (14). In yeast, myosin V has been shown to deliver vesicles, perhaps vacuoles, to the emerging bud tip, and to interact with members of the kinesin family to enhance docking of vesicles at the bud (15).

Myosin V transports cargo toward the barbed end; myosin VI transports cargo toward the pointed end of actin (16). Myosin VI may also serve as an intermediary motor, putatively transferring clathrin coated pits onto cytosolic actin filaments during endocytosis (17). Defects in myosin VI have been associated with Snell's Waltzer leading to deafness.

Myosin VIIb is normally expressed in the receptor cells of the inner ear and the pigment epithelium of the retina. A mutation in myosin VIIb has been associated with Usher syndrome (deafness and retinal degeneration) (18).

As a segue into the conventional myosin II genes within muscle, some myosins which are structurally most similar to myosin in muscle and hence fall into the myosin II category, exist actually in non-muscle cells. For example, non-muscle myosin II is essential for cytokinesis (19, 20). The *Drosophila* genome contains a single muscle myosin II gene and a single nonmuscle myosin II gene, using alternative splicing to generate specific isoforms (21). In *C. elegans* however, 9 of the 17 or so conventional myosin IIs are present. Hence, from an evolutionary standpoint, some organisms such as vertebrates and worms appear to have many single genes encoding for a single myosin

heavy chain isoform, while other organisms such as the fruit fly only carry a single muscle myosin gene which codes for many isoforms within that class.

Conventional Myosin, Myosin II

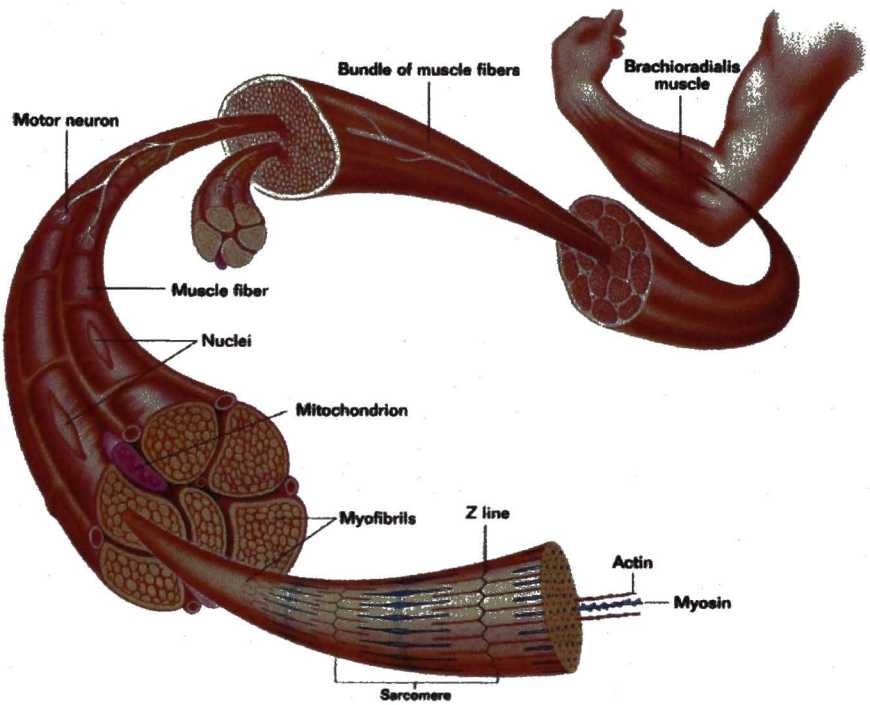

Figure 1: Structure of skeletal muscle from http://www.sirinet.net/~jgjohnso/amuscle.html.

Myosin movement coupled to actin and ATP hydrolysis is the mechanism of providing motion to muscles. As shown in **Figure 1**, skeletal muscle is made up of a bundle of fibers. Each fiber is comprised of a bundle of myofibrils. Each myofibril consists of repeating units called sarcomeres. Within one sarcomere, myosin and actin form filaments that are arranged in the highly organized structure of the sarcomere (22).

The Z lines flank the sarcomeric unit and anchor the actin thin filaments, which extend toward the M-line in the middle of the sarcomere (**Figure 2**). The area where myosin and actin overlap is designated the A-band between each side of the M-line. The H-zone is the region extending away from the M-line and ending where the actin and myosin filaments overlap. During contraction, the A-band stays constant, and the I-band and H-zone shorten (23). Other proteins which are part of the sarcomere, which appear to afford stability and support to the sarcomere are: titin (1,200 kDa (22)), located from the Z-line to the M-line, tropomodulin, which caps the end of the actin filament, and myosin binding protein-C (MyBp-C), which is interspersed every 14.3 nm along the A-band on myosin and titin (24, 25). The M-line appears to be associated with myosin and M-line protein (165 kDa), putatively adding support by binding myosin and titin. The Z-line is anchored by alpha-actinin, desmin, a cap Z protein (24, 25) and flanked by nebulin or nebulette (22). More such accessory/binding proteins are likely to exist.

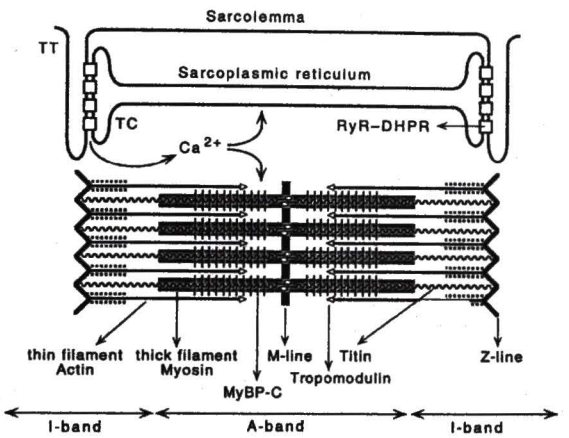

Figure 2. Schematic of sarcomere within striated muscle (4).

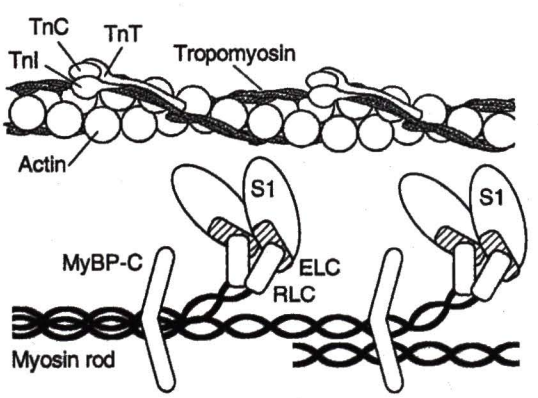

Figure 3. Schematic of cross-bridge formation between myosin and actin (4). The lever arm is represented by the rectangular capsules (ELC and RLC).

When an impulse down the α-motor neuron (**Figure 1**) approaches the motor nerve endplate located on the muscle sarcolemma, acetylcholine is released at the presynaptic cleft (26). The release of acetylcholine causes a depolarization down the t-tubules (TT) to the terminal cisternae (TC) (**Figure 2**). The depolarization is detected by the voltage sensor dihydropyridine receptor (DHPR) coupled to Ryanodine receptors (RyR) on the surface of the sarcoplasmic reticulum, eliciting calcium release from the sarcoplasmic reticulum. Free cytosolic calcium binds Troponin C (**Figure 3**). Troponin C is part of a trimeric complex where Troponin I transfers the signal to Troponin T to cause a conformational change in filamentous tropomyosin (66kDa monomer), located along the actin filament. The conformational change induced by tropomyosin causes exposure of the myosin binding site on actin, allowing the head to bind first 1 and then 2 actin monomers and initiate contraction (27). As contraction ceases, calcium is sequestered back into the sarcoplasmic reticulum via a Ca-ATPase. This provides the calcium gradient for the next contraction.

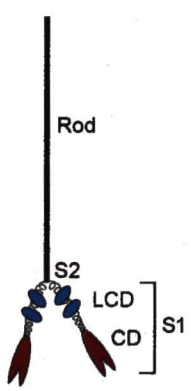

Figure 4. Schematic of the myosin filament (5).

Myosin head is the site for nucleotide and actin binding:

Myosin is a 500kDa molecular mass protein which can be cleaved by trypsin into light meromyosin (the tail coiled-coil filaments or Rod) and heavy meromyosin (S1 + S2) (**Figure 4**) (28). Heavy meromyosin is further digested with papain *in* vitro into subfragment-2 (S2) and subfragment-1 (S1). S1 is comprised of the "head" or catalytic domain (CD) which contains the actin and nucleotide binding sites, as well as the

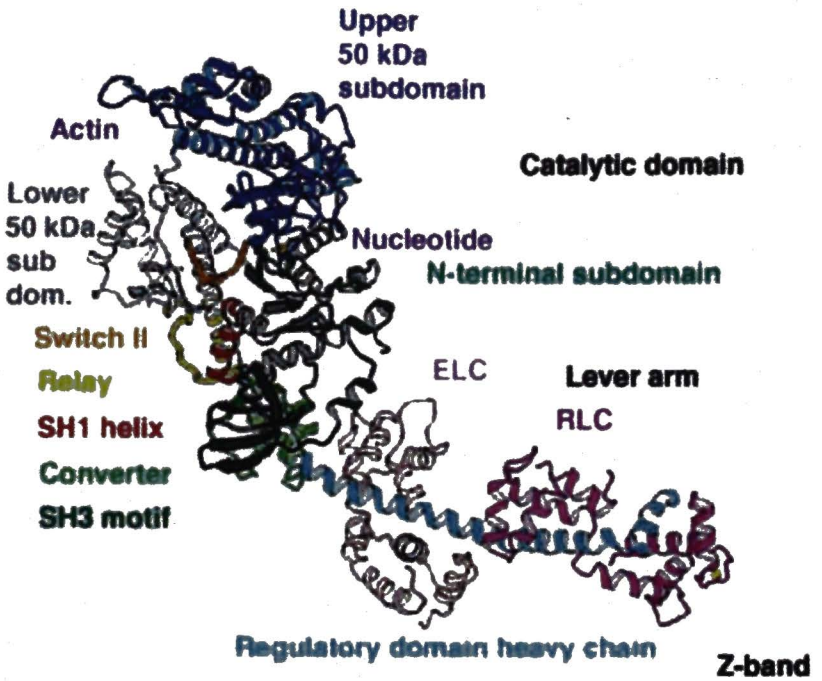

Figure 5. X-ray crystallographic structure of myosin II S1 from (7). Picture taken from (5).

light chain domain (LCD) which contains two light chains, the essential light chain (ELC) and the regulatory light chain (RLC). Further digestion of S1 with trypsin cleaves S1 into three heavy chain fragments, the N-terminal 25kDa fragment (green), 50kDa fragment (upper in periwinkle, lower in gray), and C-terminal 20kDa (light blue) fragment (29) in **Figure 5** which is collectively called S1 (subfragment 1). The myosin head (S1) is an actin-activated adenosine triphosphatase (ATPase) which has been resolved from chicken skeletal S1 at 2.8Å resolution (30). The switch II region (orange), relay region (yellow) and SH1 helix (red) change conformation in response to the nucleotide status. This status is relayed to the converter domain (light green) which transduces into movement of the lever arm containing ELC (faint white-pink) and RLC (magenta-pink). The interface between the 25kDa fragment and the upper 50 kDa domain contains the nucleotide binding site cleft. Specifically the gamma phosphate interacts with the lysine residue in the highly conserved sequence of sites that are ATPases. The site, called a P-loop is 15 amino

acids N terminal to Loop 1, which separates the 25kDa and 50kDa fragment and consists of GESGAGKT (22). The interface between the upper and lower 50kDa domain comprises the actin binding domain. The ATP binding site is about 4.0 nm (40Å) from the actin binding site (29). The converter domain functions as a socket to allow regulatory domain rotation (31). The C-terminal tail with ELC and RLC are called the "regulatory domain" or "neck" and the 25kDa and 50kDa fragments are called the motor domain. A given myosin class will differ functionally from other myosin classes within the loop domain sequence (32). Two loop domains exist between the 25kDa and 50kDa fragments (Loop 1) and the 50kDa and 20kDa fragments (Loop 2). Analysis of these fragments shows that myosins with similar kinetic properties (activation of myosin ATPase and ADP release) have similar loop sequences. These regions may be essential in conferring myosin function specificity.

The two light chains, the essential (ELC) and regulatory (RLC) light chains bind the heavy chain of myosin at an IQ-motif consisting of Ile-Gln-x-x-x-Arg-Gly-x-x-x-Arg (33). C-terminal to this, the myosin tails form an alpha-helical coiled-coil which assembles into the myosin filaments. RLC is 171 amino acids (approximately 18kDa) (34) and is non-covalently bound to the heavy chain at the lever arm or hinge region of the myosin head within the skeletal, cardiac and smooth muscle. ELC exists in two isoforms, alternatively spliced from one gene: ELC-1 (20,700Da) and ELC-3 (16,500 Da) (35). ELC is also termed in the literature as alkali light chain. Mutations in ELC alter shortening velocity and filament velocity (35, 36). ELC and RLC belong to a family of EF hand calcium-binding proteins and display the characteristic folding of other EF hand

proteins, which include calmodulin, troponin C and parvalbumin (37-40). These proteins are composed of four EF hands (helix-loop-helix), each consisting of an alpha-helix (called E), a divalent cation binding site (loop), and an alpha-helix (called F) (41, 42). RLC binds calcium and magnesium (preferentially to calcium) to regulate the interaction of myosin and actin (43-45). **Although the exact functions of RLC and ELC still remain obscure, good evidence suggests they serve as a lever arm to amplify force-generating movements.** Verifying whether this is true is the underlying thesis of this dissertation.

Uyeda and others showed that sliding velocity of filaments was proportional to the number of light chains on S1 (46). In smooth muscle, the phosphorylation of RLC by calcium-calmodulin-myosin light chain kinase has been well documented (26). The specifics regarding the significance and function of RLC phosphorylation in skeletal muscle are more controversial (47-50). It appears that RLC may be phosphorylated in skeletal muscle, however there seems to be no downstream effect resulting from the phosphorylation. Indeed, whether there is a modulatory effect is debatable and what that "modulatory effect" actually means remains obscure (47, 51).

In general, the N terminal motor domain is more conserved among the myosin classes compared to the C terminus neck and tail domain, which is diverse both in size and sequence (52). Some myosins do not contain tails at all (myosin I) and some myosins contain six light chains per head (myosin V, XI) (19). To this, the head domain of myosins interact in a similar manner with actin, utilizing energy from ATP hydrolysis to fuel movement along actin, as in the case of myosin V (13).

Historical Overview--the cross-bridge cycle: The discovery of myosin dates back to 1859 (53). It was originally thought that actin and myosin were one molecule and existed as a copolymer (23). In the late 1950s, Huxley discovered that actin and myosin exist as separate filaments that cross-link in the absence of ATP and described contraction in terms of actin and myosin filaments sliding against one another (54, 55). In the 1970s, Lymn & Taylor described energy released from ATP hydrolysis coupled to force production as a mechanism for the contractile cycle, later coined the cross-bridge cycle (56).

In 1974, Bagshaw and Trentham developed a model which showed that intrinsic protein fluorescence of S1 changed with conformational states of S1 dependent on ATP hydrolysis, as shown below (57).

$$M + T \leftrightarrow M.T \leftrightarrow M^{*}T \leftrightarrow M^{**}D.P_i \leftrightarrow M^{*}D.P_i \leftrightarrow M^{*}D \leftrightarrow M.D \leftrightarrow M + D \quad \textbf{(Eqn. 1)}$$

M is myosin or S1, T is ATP, D is ADP, P_i is phosphate (**Eqn. 1**). One asterisk indicates tryptophan fluorescence (58). Two asterisks indicates greater fluorescence in this state. This model indicates that S1 conformation changes are dependent on ATP hydrolysis.

In the 1980s, an attempt to correlate ATP binding and hydrolysis was developed by Geeves and Holmes and termed a two-state model of actomyosin association (**Figure 6**) (3, 59). In this model the **A** state (for **A**ttached) denoted that actin was weakly attached to myosin but the nucleotide was tightly attached to myosin. A conformational

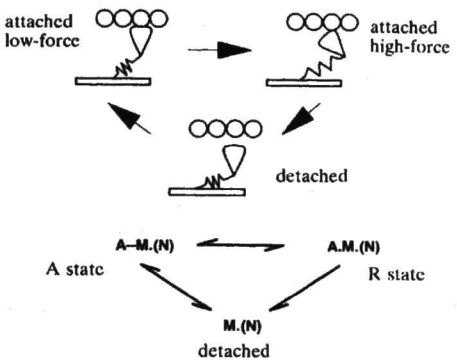

Figure 6. Schematic showing the weak binding to strong binding of actin to myosin (3).

change occurred to the **R** (for **R**igor) state in which the opposite occurred; actin was strongly attached to myosin and the nucleotide was weakly attached to myosin. The switch from the **A** to **R** state would then provide the powerstroke. They later expanded upon this model based on studies explaining how the tropomyosin only allowed S1 to partially bind actin and that a conformational change in S1 (or other molecule) moved tropomyosin away further, allowing a tighter binding of S1 to actin in the R state (60).

While the sliding filament theory is universally accepted, the detailed mechanism of transduction of chemical energy from ATP hydrolysis into mechanical work in terms of force production remains under intense research (13). The generally accepted model of the cross-bridge cycle is as follows **(Figure 7)**: The cross-bridge refers to the interface of the myosin head and the actin filament. Within the sarcomere (one structural unit of a

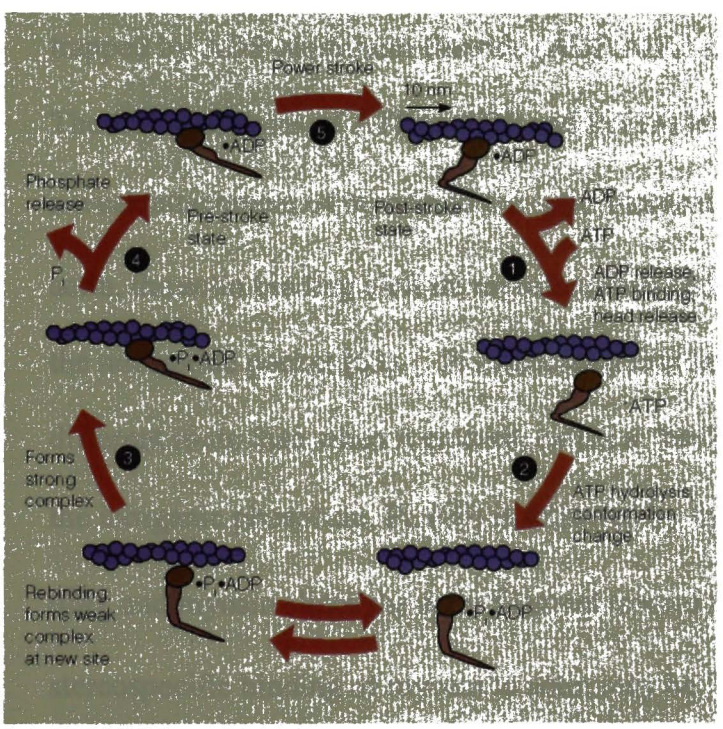

Figure 7. Schematic of the cross-bridge cycle from (1).

muscle cell), the rigor state describes the state in which the myosin head is bound to the actin filament. Cytosolic ATP (①), binds to and causes a conformational change in the S1 (myosin head) (see also text body from Figure 6). The nucleotide cleft which is termed "OPEN" in the biophysical muscle field at this stage appears to be due to the conformational change elicited when ATP binds myosin (29). Binding of the nucleotide causes the affinity of S1 for actin to decrease and S1 dissociates from actin. Such conformational stages have been determined by nucleotide analogues which trap the nucleotide in one state. For example, the state before number ① corresponds to just prior to ATP binding when ATP is just bound to myosin. This was isolated with the analogue ADP-beryllium fluoride (ADP.BeFx) (61). The state after number ② represents the transition state in hydrolysis of ATP to ADP and Pi. This state was trapped by ADP-aluminum fluoride ($ADP.AlF_4$) and ADP-vanadate ($ADP\text{-}VO_4$) (62). The fast hydrolysis of ATP to ADP and Pi (13) leads to transient relaxation, followed by a weak attachment of myosin to the actin filament (just prior to ③). When S1 binds actin, the actin binding cleft on myosin closes and is believed to be coupled to opening of the nucleotide pocket (63). Pi dissociates first but exits the nucleotide cleft by a different route than when it entered, called a "back-door" enzyme (61). The release of the inorganic phosphate, Pi, (④) is followed by the power stroke, where ADP is released (⑤), and myosin slides the actin filament toward the center of the sarcomere. The stereospecific binding of myosin to actin may be "stiffened" and solidified at the end of the powerstroke, shown by Electron Paramagnetic Resonance (EPR) spin-labeled studies

(64). On the other hand, good evidence also suggests that the power stroke is concident with phosphate release (52, 65). Which state the power stroke corresponds to is still under debate.

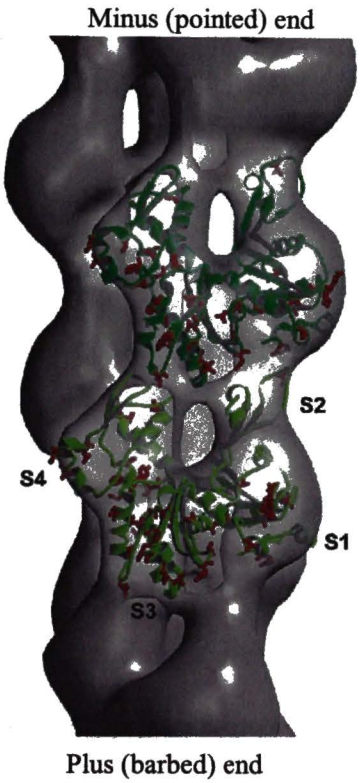

Figure 8. Electron microscopic reconstruction of F-actin from X-ray crystal structures from (2). Subdomains 1-4 are shown. Top= minus pointed end, bottom, plus barbed end, so filament extends downwards.

Actin:

Actin is an abundant and highly conserved protein, functioning in cell motility, cytokinesis, and cargo transport (66). G-Actin (**Figure 8,** two monomers highlighted, yellow and green) is a 42 kDa monomer with four subdomains (S1-S4) and polymerizes into F-actin (**Figure 8,** entire molecule) by hydrolysis of ATP to ADP (66). It is not certain how depolymerization occurs; however, one report states that F-actin is actually in the ADP + Pi state and that release of Pi promotes depolymerization (67). Actin exists in up to 6 isoforms in mammals, but the amino acid sequences are highly conserved (2, 66). As illustrated in **Figure 8,** atomic models predict that when two X-ray crystallographic monomers of bovine β cytoplasmic G-actin are fit into electron microscopic resconstructions of yeast F-actin, only 39 (red) residues out of 375 (green) total residues are different (2). Actin filaments are thinner and more flexible than microtubules and have a slow-growing/inert minus end (pointed end) and fast-growing plus end (barbed end, due to the arrow like appearance). The actin filament in

skeletal muscle is stabilized at the Z-disk (one sarcomeric unit) via the actin-binding protein Filamin C (68). Crosslinking studies (Cys10 to Ala19) have shown that subdomain 1 interacts with the acting-binding site on myosin S1 (69). G-actin can be polymerized into F-actin by addition of S1 to actin monomers and studies show that the DNase I binding loop (residues 38-52) on subdomain 2 of actin does not interact with S1 (70). During the cross-bridge cycle, a single myosin head binds the N-terminus of two adjacent actin monomers (71). *In vitro* motility assays show that the sliding velocity of actin varies with the type of myosin, whether the myosin be fast skeletal from rabbit, turkey gizzard, or bovine cardiac myosin, when the actin type is held constant (72).

Present biophysical approaches aim to understand how myosin interacts with actin and nucleotide hydrolysis during the cross bridge cycle. One such approach involves cross-linking studies, to determine which amino acids of proteins interact, in this case, S1 and actin, within the actomyosin complex. Nucleotide-induced intramolecular movements have been found to be confined to the 50kDa/20kDa and 20kDa/ELC interface (73). The acto-S1 interface has been cross-linked during rigor and complexed to nucleotides or nucleotide analogs (74). These studies revealed that apolar amino acids 48-113 on the subdomain 1 of actin interact with apolar amino acids 506-561 of the S1 actin binding site located on the lower 50kDa subdomain. Studies of this nature illustrate the specific influence of the gamma-phosphate, the release of which is purported in force generation. Site-directed mutagenesis has been used to probe the structure-function relationship in actin and myosin. Movement of myosin at Trp510 whose fluorescence is sensitive to

the open-close transition of the active site on binding of nucleotide has been quantified with respect to different state of the cross bridge cycle. ATP and ADP have been labeled with extrinsic fluorophores (75) to study ATPase movement during different stages of the cross bridge cycle and with respect to actin movement. For instance, Cy3-ADP has shown to display an exchange rate constant of 3.2 sec^{-1} concerning myofibrils of rabbit slow skeletal muscle (soleus) (76). These approaches are designed to probe the mechanism of actin/myosin/nucleotide interaction at the single molecule level. In the present studies, the rotation of the S1 regulatory domain and actin will be measured using anisotropy of fluorescence emitted by probes attached to specific amino acid residues on the protein. Cross-linkers serve as a means to determine which inter-monomer motions within F-actin are necessary for actin sliding filament velocity and *in vitro* motility (77, 78).

In vitro studies of the movement of the lever arm during contraction have been verified by X-ray crystallographic studies in which ATP and ADP analogues are trapped in the active site of S1 (7). This is useful for dissecting the contractile cycle of myosin because one kinetic state is isolated and how nucleotides bind the myosin head may be determined (79, 80). The X-ray structure of the motor domain of *Dictyostelium discoideum* complexed with MgADP-BeF_x and MgADP-Vanadate (62) (both are nucleotide analogues mimicking the ATP bound state) and MgADP-$AlF4^-$ (a nucleotide mimicking the hydrolysis transition state) at 2.0Å and 2.6Å resolution have been isolated and are consistent with chicken S1 X-ray crystallographic structures (81), even though both light chains are missing. In this particular study, conformational changes at the

narrow cleft in the lower 50kDa segment of the heavy chain and are propagated into signals toward the NH_2-terminal of ELC leading to movement of the lever arm. The "hinge" region represents the interface between the 50kDa lower domain and the amino terminal of ELC (82). *D. discoideum* was used because an expression system for chicken skeletal muscle myosin was not available and *D. discoideum* is somewhat homologous to skeletal muscle myosin. Previously, only NMR could provide such 2-2.5Å resolution of proteins in their "natural state", which was only precise enough for proteins over 100 amino acids and often offered only in the backbone conformation, due to the complex spectra from side-chain definitions (83). More recently, 6 non-nucleotide analogues have been crystallized to *D. discoideum* which appear to coincide well with the MgADP-BeF_x state (79). Our understanding of the states of the contractile cycle continues to increase and become clearer with time.

The lever arm hypothesis: Initial reports postulated that the 50kDa myosin S1 subdomain would be responsible for force generation (10, 84). Subsequent studies, in which fluorescent probes were attached to key amino acid residues, showed little rotation during the contractile cycle. Furthermore, when fluorescent probes were attached to more distal portions of the myosin head, specifically at the regulatory domain, much larger rotations were seen, up to 30 degrees. The current opinion seems to hold that the bulk of the head might not rotate after all; rather, actin binding and ATP hydrolysis tranduces into a lever arm movement of the regulatory domain (**Figure 9**) (84).

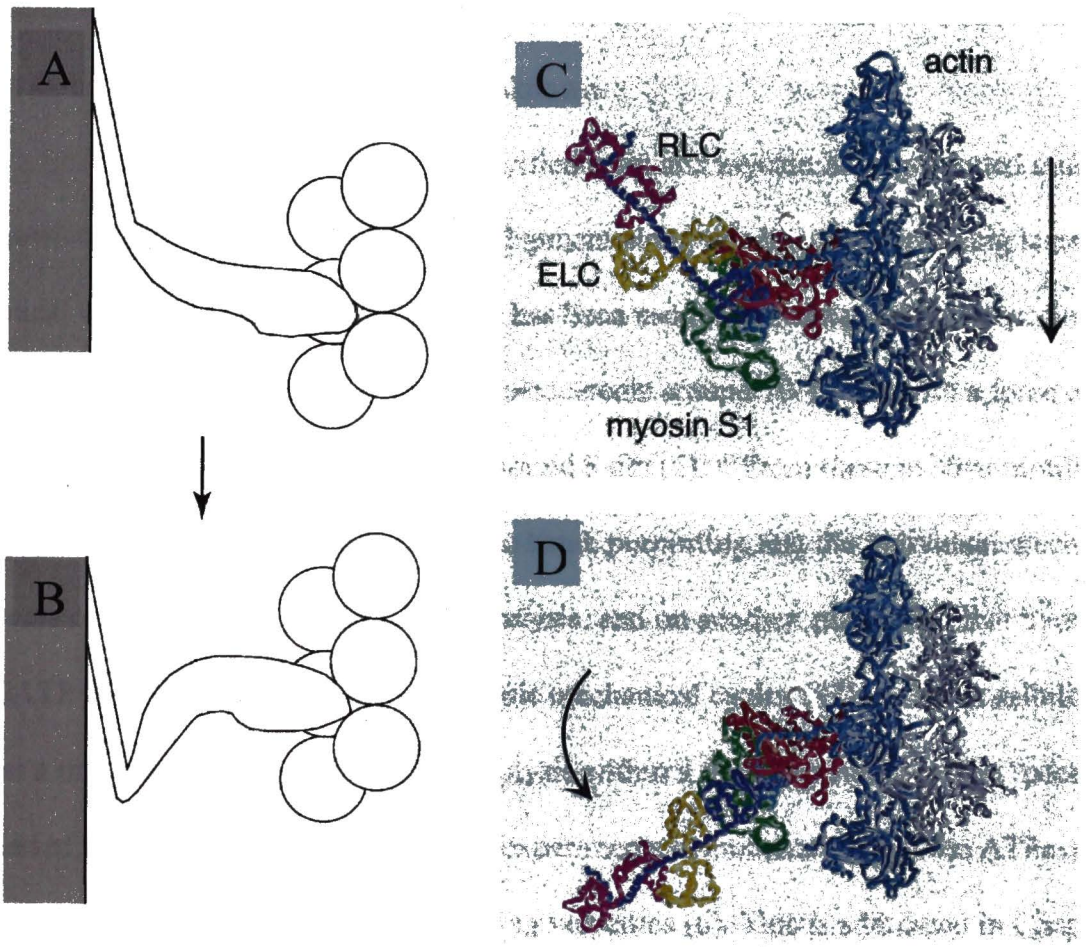

Figure 9. The lever arm hypothesis: the lever arm rotates during power-stroke of contraction. **A)** Pre-power stroke state, the schematic shows myosin catalytic domain displaying less rotation and the regulatory domain rotating more (6). **B)** post-power stroke. **C)** Pre-power stroke computer modeling of x-ray crystallography of 5 monomers of actin: 3 light blue, 2 gray and decorated with myosin S1: 25kDa fragment (green), 50 kDa fragment (red), 20kDa fragment (dark blue), ELC (yellow), RLC (magenta) (10). **D)** Post-power stroke.

This regulatory domain is 8nm long and the myosin heavy chain (20kDa fragment) is composed of a long uninterrupted alpha helix, which may offer rigidity to prevent the purported lever arm from collapse or offer support to the light chains surrounding it (10). Further reports show there are light chain domain rotations relative to the actin-binding and catalytic domain of S1, and that the latter domains do not rotate during contraction

(85). This hypothesis is tested *ex vivo* in Chapter 2. If this is the case, how binding of nucleotide and actin at the N-terminal portion of S1 translates to lever arm movement at the distal regulatory domain remains unknown.

In vitro motility assays using purified actin and myosin have generated much knowledge in the field. A recent development along this line involves using laser-based optical traps or optical tweezers. This has been used to understand single myosin interactions and elucidate myosin II displacements around 10-12 nm with a force of 3-5 pN (86) and myosin V displacements around 8 nm (6). From these *in vitro* motility assays, controversy has emerged, on one hand, purporting that the individual mechanical events correspond to a single ATP hydrolysis, and on another, purporting that hydrolysis of ATP allows myosin to execute multiple mechanical cycles (87). One possibility is that a muscle fiber may vary ATP hydrolysis within a fiber depending on the "pace" or need of the fiber; this was purported in experiments demonstrating that the ATPase hydrolysis rate was low at high shortening velocities (6). This is addressed in Chapter 3.

The fundamental question of how hydrolysis of how ATP is coupled to motion has been difficult to answer because the cross bridge cycle occurs quickly and it has not been possible to isolate each state in its native environment. There is controversy whether force generation is powered by changes primarily in the myosin head or by conformational changes in the actin filament itself (88). This is addressed in Chapter 4.

Chemical modifications to S1 through site-directed mutagenesis, crosslinking, proteolysis or other modifications have revealed areas of S1 important for ATPase activity, force production, and motility (89).

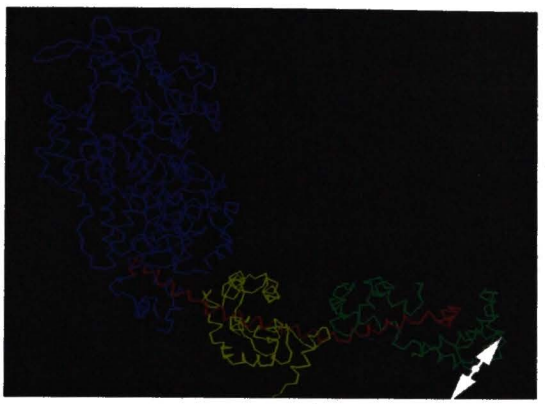

Figure 10. Representation of dipole of a fluorophore labeled on RLC (green chain). X-ray structure from (7).

Therefore, this research project has two parts: Chapters 2 and 3 focuses on the rotation of myosin, the second part on the rotation of actin. The first part focuses on the rotation of RLC within S1. Fluorescence anisotropy from a probe attached to RLC will be measured during one cross bridge cycle in an isolated muscle fiber using confocal microscopy. Release of ATP from a caged precursor will be used to synchronize myosin rotation. **Figure 10** shows a representation of myosin RLC labeled with a fluorescent probe, with an arrow representing the dipole moment of the probe. Chapters 4 and 5 focus on the rotation of actin during the cross bridge cycle. The conventional theory of muscle contraction stipulates that actin is a passive structure, i.e., it does not by itself split ATP, and that the change in its orientation is due to interactions with myosin. This hypothesis will be tested using a small number of actin filaments in contracting muscle fiber. Fluorescence anisotropy of a probe attached to actin will be measured in an isolated mounted muscle fiber using confocal microscopy. Release of ATP from a caged precursor will be used to synchronize actin rotation. The present goal is to investigate the kinetics of a small number of myosin molecules in contracting muscle fiber.

Rationale:

Anisotropy is a technique used in biophysics which allows the observation of orientation of a fluorescently labeled molecule over time, e.g., during one cross-bridge cycle. A fluorescent dye is attached to a specific molecule such as RLC, and anisotropy follows, by virtue of the dye, the movement of RLC. By nature, fluorescent dyes exhibit a dipole moment or direction. It is this direction or orientation (using the formula for anisotropy) of the dye on the RLC that is measured. Information regarding rotation during skeletal muscle contraction from a small number of molecules will be obtained. My studies will test these ideas in a number of molecules of myosin in live fibers.

Figure 11A shows how the orientation of one cross-bridge can be monitored. A value of 1 here means the orientation of a molecule is very ordered and has a distinct orientation or direction. A value of zero means the molecule is tumbling in all directions and has a random orientation. The stage at time zero represents the orientation of the myosin head when it is in a state of rigor. Myosin is attached to actin, so the myosin head has a distinct orientation and value. The state at around

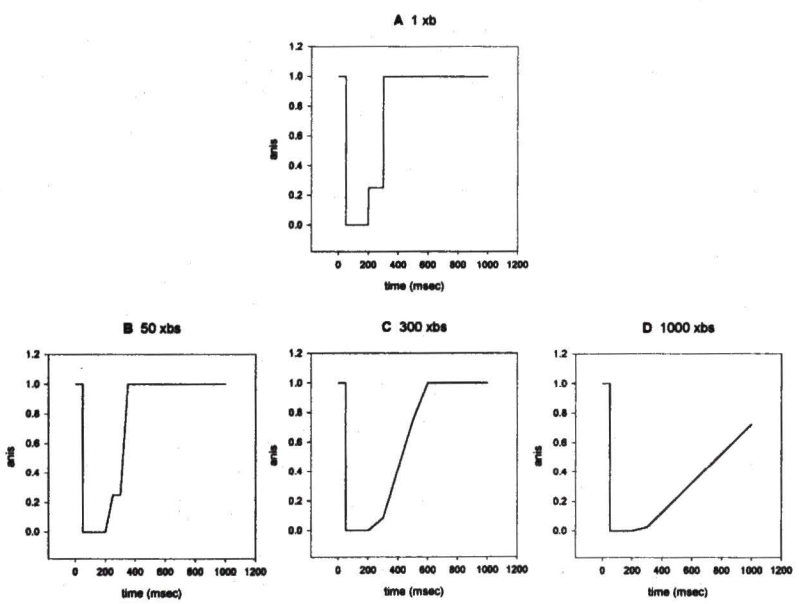

Figure 11. The resolution of anisotropy (anis) over time varies with the number of cross-bridges (xbs) observed over time.
A) 1 cross-bridge. **B)** 50 cross-bridges. **C)** 300 cross-bridges.
D) 1000 cross-bridges.

time equals 50 milliseconds represents the orientation of S1 as it dissociates from actin and it has a low value because the head is freer to rotate as it is not attached to something. The state at around 220 milliseconds represents the orientation of myosin as it is weakly bound to actin. The state at 300 milliseconds represents the powerstroke where the myosin head is pulling actin towards itself. By 600 milliseconds the state is back to the original state of rigor.

It is important to investigate as few molecules as possible because each molecule behaves differently and a large population provides only gross information about a whole muscle, not individual molecules. Each individual myosin head has its own rate of transient relaxation, weak attachment, and strong attachment to actin. Hence, the kinetics of orientation can be lost when the signal is coming from too many cross-bridges. With 1 cross bridge (**Figure 11A**), each intermediate orientation is clearly differentiated, with 50 cross-bridges (**Figure 11B**) one can see some intermediate states, with 300 cross-bridges (**Figure 11C**) a little more information is lost, and with 1000 cross-bridges (**Figure 11D**) even more information is lost.

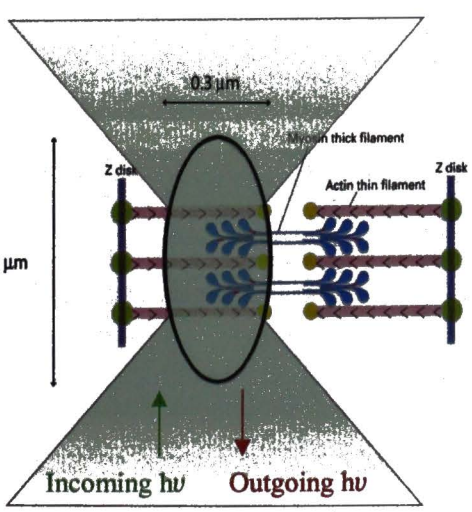

Figure 12: Schematic of the illumination volume impinging on the muscle (adapted, courtesy of J. Borejdo).

The introduction of an extremely small observational volume of 0.3 microns^3 defined by diffraction-limited laser beams and confocal detection (**Figure 12**), has made it possible to limit the number of cross-bridges contributing to signal to around 500 for 1P microscopy and half that for 2P microscopy. To determine

the size of the illumination volume, the formula for the volume of a cylinder was used. This is because the actual illumination volume is Gaussian, however the calculations to determine this volume would be complex and only an estimate is required. The diameter of the cylinder top was equal to the diffraction limit (wavelength of excitation light/numerical aperture) or 568μm/1.2. The length of the cylinder was determined by measuring the depth-of-focus of 1mm fluorescent microspheres (Molecular Probes Orange FluorSpheres) (**Figure 13A**). This value was determined to be approximately 3μm. Two-photon imaging offers an advantage over confocal imaging (1P imaging) because the illumination volume is decreased to about half that (**Figure 13B**) so the number of cross-bridges observed is lower.

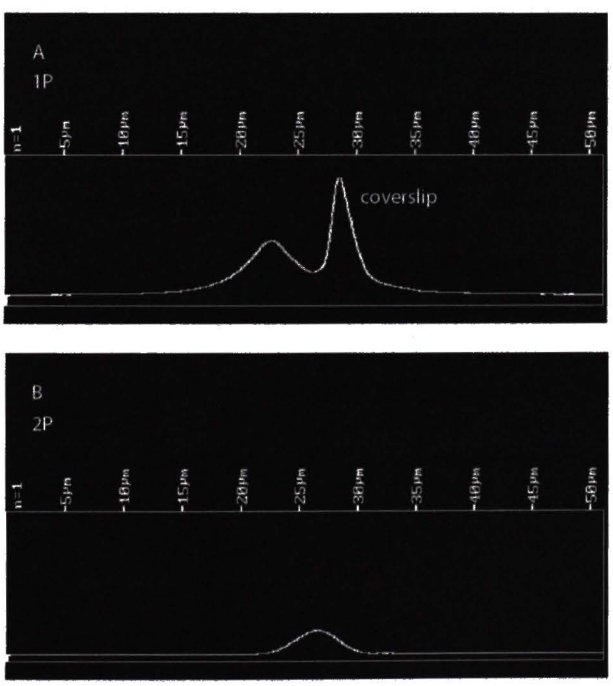

Figure 13: Comparison of the depth-of-focus of 1P and 2P illumination. 1 μm fluorescent microspheres were dried on a coverslip and immobilized in a mounting medium provided with MP PS-Speck Microscope Point Source Kit. A center of a microsphere was scanned in the Z direction in 0.1 μm steps. A – 1P scan. Pinhole diameter 35 μm, excitation wavelength=568 nm, LP 590 nm emission filter. The bright peak at right is the light reflected by a coverslip. Microsphere profile is at left. Half-Width-at-Full-Height (HWFH) of the profile=2.2 μm. B – 2P scan. No pinhole. Excitation wavelength=820 nm, no emission filters, HWFH=1.2 μm.

1P Laser Scanning Microscopy

In one-photon (confocal) microscopy, a pinhole is placed at the focal point of the image, which focuses the rays to high resolution and eliminates out of focus rays. A diffraction limited laser beam is used here, which limits the area to a small volume where the converging focal point rays are in focus. The Zeiss 410 confocal microscope has been modified to measure anisotropy (**Figure 14**). Polarized light from the Ar/Kr Laser (top light blue) is linearly selected by the filter (LSF) and passed to the half-wave plate ($\lambda/2$), which selects the direction of excitation. The UV beam (dark blue dashed line) photolyzes caged ATP. Dichroic combiners 1 & 2 (DC1,2) merge visible and UV beams. Dichroic mirror 1 (DM1) directs the beam onto the beam scan system (BSS), producing a scanned laser. A mirror (MR1) directs the beam through the objective (OBJ) and onto a muscle fiber (MUS), mounted on the stage. The emitted light (green line) is projected on a confocal pinhole plate (not shown). Photodetectors record intensities of perpendicular ($I_\perp$) and parallel ($I_\parallel$) components of polarized

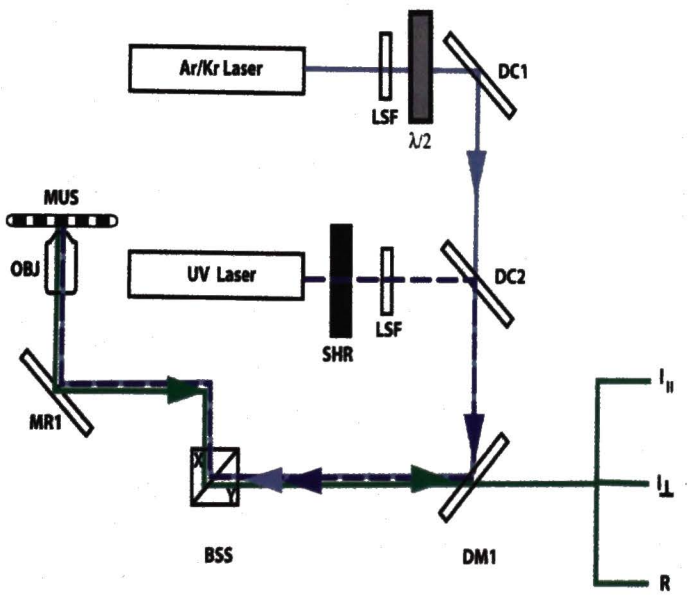

Figure 14. Simplified schematic of the experimental set-up for 1 Photon (1P) Laser Scanning Microscopy (LSM), adapted from the Zeiss 410 confocal LSM user manual.

fluorescence in separate channels. Anisotropy (r) is a ratio of the horizontal ($I_{\parallel}$) and vertical ($I_{\perp}$) emission intensities of the dye, where $r = (I_{\parallel} - I_{\perp}) / (I_{\parallel} + 2I_{\perp})$ (90). Anisotropy is plotted as graph of anisotropy in arbitrary units (a.u.) over time. In the proposed experiments, the emitted light intensity in the horizontal direction will be measured in one photomultiplier channel to obtain $I_{\parallel}$. At the same time, emitted light is passed through a polarizer in the vertical direction and will be measured in a second photomultiplier channel to obtain $I_{\perp}$. These two values will be fit into the formula (anisotropy)*256+128 (Zeiss confocal software allows for these variables to be input into the equation recording real-time anisotropy). The additional functions, *256+128, were required to allow the viewer to observe all three channels within one screen. By multiplying the pixel size (512x512), this translates to 262,144 intensity values being collected every 25 microseconds for seven seconds. The confocal screen displays these data points every 14.3 milliseconds. Therefore, perpendicular anisotropy $R_{\perp}(t)=[({}_{\perp}I_{\perp}(t) - {}_{\perp}I_{\parallel}(t))/({}_{\perp}I_{\perp}(t) + 2{}_{\perp}I_{\parallel}(t))]*256+128$. Parallel anisotropy $R_{\parallel}(t)=[({}_{\parallel}I_{\parallel} (t) - {}_{\parallel}I_{\perp} (t))/({}_{\parallel}I_{\parallel} (t) + 2{}_{\parallel}I_{\perp} (t))]*256+128$. Unless otherwise specified, no half-wave plate was used and parallel anisotropy was measured.

2P Laser Scanning Microscopy

In this technique, two photons at twice the excitation wavelength raise an electron to an elevated state. Imaging occurs at the focal point where the photon density is sufficiently high for two photons to be absorbed simultaneously by the fluorophore essentially. To achieve such a high concentration of photons, high energy light (laser)

delivers bursts of 100 femtosecond pulses with a repetition rate of around 80-100 MHz and an average laser power around 700mW with an incident laser power of 10-50mW within wavelength ranges of 700-900nm (91). A high peak-power, pulsed laser is moderated so that the sample power does not damage the specimen.

The high density necessary for two-photon excitation is achieved only at the focal point of the lens, where the requirement for probability of 2P excitation (proportional to the square of the photon density) is met, so no pinhole is necessary as in 1P microscopy (92). With imaging, the signal-to-noise ratio decreases the deeper an image is obtained from the sample, but with 2P imaging, this ratio decreases less because the wavelength used in 2P is longer. In 2P, the fluorescence will occur only at the focal point where the photon density is highest.

Photobleaching of scattered light above and below the focal point is reduced more so than in 1P because the illumination volume is smaller. Unlike in 1P, photobleaching of the fluorophore in focal planes above and below the illumination volume are eliminated because of the requirement for high photon density required for excitation to the excited state (92). Photobleaching is restricted to the plane of focus (91).

The reduced effects of light scattering in 2P are achieved because longer red and near-IR wavelengths are used for 2P, so the longer wavelengths penetrate deeper into the muscle with less absorption and scattering along the way there or back. Because only two coincident photons excite a fluorophore, scattered light does not excite the fluorophore. In sum, 2P is advantageous over 1P microscopy because 1) no pinhole is necessary, 2) there is greater penetration depth due to longer wavelengths,

3) photobleaching is reduced because the excitation volume is smaller, and 4) in our instrument, the illuminated volume is smaller (**Figure 13B**).

In 1P aborption, this is called linear absorption because the absorption of light is proportional to the intensity of the excitation light. In other words, fluorescence yield is proportional to pump intensity. 2P absorption is referred to as nonlinear because absorption of the two photons depends on the square of the light intensity. Therefore, fluorescence yield is proportional to the square of the pump intensity. Hence, while high peak power is required for 2P absorption, this also results in localized excitation only within the focal point of the laser beam. In order to maintain such a high average power (around 1 Watt) and produce 700-900nm wavelengths, Ti:sapphire lasers, commonly used for two-photon microscopy was used in the present experiments. The power that reaches the sample is less than 10mW, thus avoiding damage to the sample or reducing the lifetime of the fluorophore.

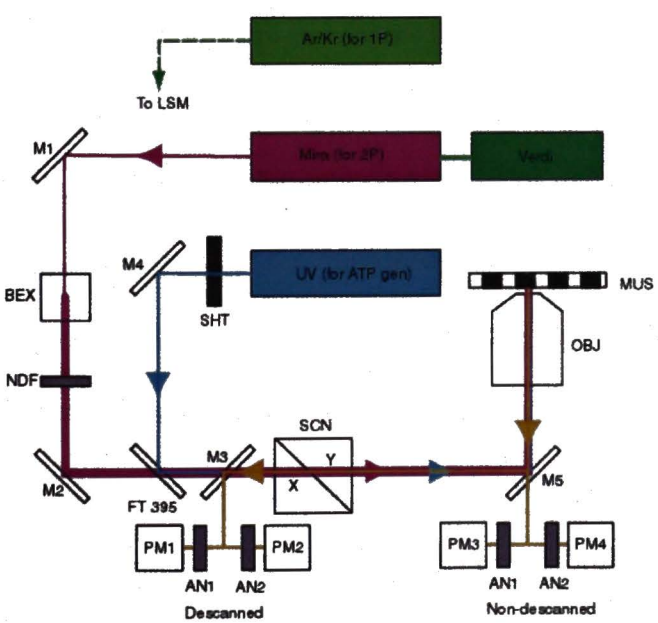

Figure 15. Experimental set up for 2 photon (2P) imaging, adapted from Coherent, Inc., Santa Clara, CA.

Figure 15 shows a schematic diagram of the 2P set up. A 2P laser (Mira, Coherent Inc., Santa Clara, CA) is pumped by 6.5 W of 532 nm light (green) from a Verdi Solid State laser (Coherent, Santa Clara, CA), generating a femtosecond 820 nm pulses at 80 MHz (magenta), directly coupled to the microscope (Zeiss

Axiovert 135). IR light (magenta) is focused by the objective on a muscle fiber mounted on a stage of a microscope. The fluorescent light (yellow) is measured by cooled photomultipliers (Hamamatsu 6060-02). The UV light (blue) is used to generate ATP from a caged precursor. The 1P data is obtained using Ar/Kr laser (green). IR laser beam is expanded by the beam expander (BEX), attenuated by the Neutral Density filters and passed to the X-Y scanner, which projects the scanned beam onto the objective (OBJ) (Zeiss Apo C 40x, NA=1.2 water immersion) and muscle fiber (MUS). The IR power impinging on muscle is ~65 mW. Fluorescent light (yellow) is collected by the objective, passed by the same scanner and reflected by the dichroic mirror M3 into photomultipliers 1 & 2, which detect orthogonally polarized light passed by crossed analyzers (AN1 and AN2). Since the fluorescent light is scanned again on the way to the detectors, it is termed descanned detection. Alternatively, mirror M5 can be substituted by a dichroic filter to pass the fluorescent light to another set of photomultipliers 3 & 4. Since the fluorescent light does not pass through the scanner, it is termed non-descanned detection. The significant advantage of this mode of detection is that the distance between the detectors and the sample is shortened, and the fluorescent light does not enter the microscope at all. It does not pass through the scanner or is not otherwise attenuated by the internal optics. Unless otherwise stated, all the experiments described in this thesis were done in non-descanned mode. The 351+ 364 nm light from the UV laser (blue) (Enterprise, Coherent) is made collinear with the IR beam by the dichroic filter FT395. A fast shutter SHT (Vincent Associates, Model T132) is opened

for 10 msec to admit UV light to a muscle fiber. The UV power impinging on muscle is 700 μW, giving a power flux of 9×10^{-4} mJ/μm^2.

The limitations of 2P are (which do not apply in my case): 1) it works only with fluorescence imaging 2) thermal damage and interference can occur if molecules are present which absorb at the same excitation wavelength (such as pigments, *e.g.* melanin) (92).

Problem/Hypothesis:

The long term objective is to understand how muscle contraction works. A consensus opinion holds that muscle contraction involves splitting of ATP and subsequent rotation of the myosin molecule at the regulatory domain. The goal here is to determine the rotational aspects of myosin and actin contributing to the mechanism of muscle contraction.

The specific hypotheses to be tested are as follows:

1) To determine whether RLC rotates during contraction, thereby contributing to the body of evidence that force production results largely from rotation of the lever arm. This hypothesis is addressed in Chapter 2.

2) To test whether the splitting of one molecule of ATP corresponds to a single rotation of the regulatory domain in a small population of crossbridges in contracting muscle. This hypothesis is addressed in Chapter 3.

3) To test in a small population of molecules in contracting muscle, whether actin rotates during contraction. This hypothesis is addressed in Chapter 4.

4) To test in a small population of muscles in contracting muscle, whether actin rotation plays an active or passive role during the cross bridge cycle. This hypothesis is addressed in Chapter 5.

Significance:

The present experiments will be performed *ex vivo*, in contracting muscle fibers, within a small illumination volume of $0.3\mu m^3$, the equivalent of observing around 400 fluorescently labeled myosin molecules. Also, defects in myosins have been shown to underlie blindness, deafness, and in particular for myosin II, cardiomyopathies. For example, mutations in or (more often) in combination with certain other sarcomeric proteins are associated with a group of familial hypertrophic cardiomyopathies (FHC) (93). Based on analysis of tissue from persons with this disease, so far, researchers have pinpointed this disease to 5 mutations in cardiac RLC (12q23-12q24.3), 15 mutations in troponin T (1q32), 8 mutations in troponin I (19q13.4), 76 mutations in the beta-cardiac heavy chain of myosin (14q12) (94), 8 mutations in essential light chain (3p21.2-3p21.3), 33 mutations in myosin-binding protein C (11p11.2) and 1 mutation in titin (2q24.3), and 1 mutation in troponin C (93, 95, 96). An up-to-date database compiling mutations in various genes known to cause FHC can be found at: http://www.angis.org.au/Databases/Heart/heartbreak.html. More likely exist. FHC are characterized by abnormal electrocardiograms, myofibrillar disarray and result from benign effects, to severe heart failure, to sudden cardiac death. Of the different subsets of FHC, mid-left ventricular obstruction has been associated specifically with three

mutations in cardiac RLC. Two additional RLC mutations at different sites have been identified with hypertrophic cardiomyopathies, involving increased ventricular wall thickness and abnormal electrocardiography (97). One application of this study is the greater understanding of the role of RLC with respect to familial hypertrophic cardiomyopathies (FHC). Perhaps rotation in RLC-associated FHC is altered; but the research here will not provide answers to these questions. The work here will however provide insight into the fundamental mechanism of muscle contraction. Diseases stemming from myosin related defects are difficult to explain unless the healthy scenario is elucidated first.

REFERENCES

1. Spudich, J. A., How molecular motors work, *Nature, 372*, 515 (1994).
2. Egelman, E. H., Actin allostery again?, *Nat Struct Biol, 8*, 735 (2001).
3. Geeves, M. A., The actomyosin ATPase: a two-state system, *Philos Trans R Soc Lond B Biol Sci, 336*, 63 (1992).
4. Schaub, M. C., Hefti, M. A., Zuellig, R. A., and Morano, I., Modulation of contractility in human cardiac hypertrophy by myosin essential light chain isoforms, *Cardiovasc Res, 37*, 381 (1998).
5. Reedy, M. C., Visualizing myosin's power stroke in muscle contraction, *J Cell Sci, 113 (Pt 20)*, 3551 (2000).
6. Cooke, R., White, H., and Pate, E., A model of the release of myosin heads from actin in rapidly contracting muscle fibers, *Biophys J, 66*, 778 (1994).
7. Rayment, I., Rypniewski, W. R., Schmidt-Base, K., Smith, R., Tomchick, D. R., Benning, M. M., Winkelmann, D. A., Wesenberg, G., and Holden, H. M., Three-dimensional structure of myosin subfragment-1: a molecular motor, *Science, 261*, 50 (1993).
8. Berg, J. S., Powell, B. C., and Cheney, R. E., A millennial myosin census, *Mol Biol Cell, 12*, 780 (2001).
9. Dickinson, M. H., Farley, C. T., Full, R. J., Koehl, M. A., Kram, R., and Lehman, S., How animals move: an integrative view, *Science, 288*, 100 (2000).
10. Block, S. M., Fifty ways to love your lever: myosin motors, *Cell, 87*, 151 (1996).
11. Barylko, B., Binns, D. D., and Albanesi, J. P., Regulation of the enzymatic and motor activities of myosin I, *Biochim Biophys Acta, 1496*, 23 (2000).
12. Gillespie, P. G., Gillespie, S. K., Mercer, J. A., Shah, K., and Shokat, K. M., Engineering of the myosin-ibeta nucleotide-binding pocket to create selective sensitivity to N(6)-modified ADP analogs, *J Biol Chem, 274*, 31373 (1999).
13. Duke, T. A., Molecular model of muscle contraction, *Proc Natl Acad Sci U S A, 96*, 2770 (1999).
14. Hirose, K., and Amos, L. A., Three-dimensional structure of motor molecules, *Cell Mol Life Sci, 56*, 184 (1999).
15. Beningo, K. A., Lillie, S. H., and Brown, S. S., The yeast kinesin-related protein Smy1p exerts its effects on the class V myosin Myo2p via a physical interaction, *Mol Biol Cell, 11*, 691 (2000).
16. Spudich, J. A., and Rock, R. S., A crossbridge too far, *Nat Cell Biol, 4*, E8 (2002).
17. Frank, D. J., Noguchi, T., and Miller, K. G., Myosin VI: a structural role in actin organization important for protein and organelle localization and trafficking, *Curr Opin Cell Biol, 16*, 189 (2004).
18. Chen, Z. Y., Hasson, T., Kelley, P. M., Schwender, B. J., Schwartz, M. F., Ramakrishnan, M., Kimberling, W. J., Mooseker, M. S., and Corey, D. P., Molecular cloning and domain structure of human myosin-VIIa, the gene product defective in Usher syndrome 1B, *Genomics, 36*, 440 (1996).

19. Cope, M. J., Whisstock, J., Rayment, I., and Kendrick-Jones, J., Conservation within the myosin motor domain: implications for structure and function, *Structure, 4*, 969 (1996).
20. Feierbach, B., and Chang, F., Cytokinesis and the contractile ring in fission yeast, *Curr Opin Microbiol, 4*, 713 (2001).
21. Morgan, N. S., The myosin superfamily in Drosophila melanogaster, *J Exp Zool, 273*, 104 (1995).
22. Stryer, L., *Biochemistry*, W. H. Freeman and company, New York (1988).
23. Huxley, H. E., Getting to grips with contraction: the interplay of structure and biochemistry, *Trends Biochem Sci, 23*, 84 (1998).
24. Schaub, M. C., Hefti, M. A., Harder, B. A., and Eppenberger, H. M., Various hypertrophic stimuli induce distinct phenotypes in cardiomyocytes, *J Mol Med, 75*, 901 (1997).
25. Schiaffino, S., and Reggiani, C., Molecular diversity of myofibrillar proteins: gene regulation and functional significance, *Physiol Rev, 76*, 371 (1996).
26. Rhoades RA, T. G., *Medical Physiology*, Lippincott Williams and Wilkins, Baltimore (2003).
27. Holmes, K. C., The actomyosin interaction and its control by tropomyosin, *Biophys J, 68*, 2S (1995).
28. Szent-Gyorgyi, A. G., Meromyosins, the subunits of myosin, *Arch Biochem Biophys, 42*, 305 (1953).
29. Geeves, M. A., and Holmes, K. C., Structural mechanism of muscle contraction, *Annu Rev Biochem, 68*, 687 (1999).
30. Rayment, I., Holden, H. M., Whittaker, M., Yohn, C. B., Lorenz, M., Holmes, K. C., and Milligan, R. A., Structure of the actin-myosin complex and its implications for muscle contraction, *Science, 261*, 58 (1993).
31. Houdusse, A., and Cohen, C., Structure of the regulatory domain of scallop myosin at 2 A resolution: implications for regulation, *Structure, 4*, 21 (1996).
32. Goodson, H. V., Warrick, H. M., and Spudich, J. A., Specialized conservation of surface loops of myosin: evidence that loops are involved in determining functional characteristics, *J Mol Biol, 287*, 173 (1999).
33. Cheney, R. E., and Mooseker, M. S., Unconventional myosins, *Curr Opin Cell Biol, 4*, 27 (1992).
34. Zavodny, P. J., Petro, M. E., Kumar, C. C., Dailey, S. H., Lonial, H. K., Narula, S. K., and Leibowitz, P. J., The nucleotide sequence of chicken smooth muscle myosin light chain two, *Nucleic Acids Res, 16*, 1214 (1988).
35. Sweeney, H. L., Function of the N terminus of the myosin essential light chain of vertebrate striated muscle, *Biophys J, 68*, 112S (1995).
36. Sweeney, H. L., Kushmerick, M. J., Mabuchi, K., Sreter, F. A., and Gergely, J., Myosin alkali light chain and heavy chain variations correlate with altered shortening velocity of isolated skeletal muscle fibers, *J Biol Chem, 263*, 9034 (1988).
37. Baba, M. L., Goodman, M., Berger-Cohn, J., Demaille, J. G., and Matsuda, G., The early adaptive evolution of calmodulin, *Mol Biol Evol, 1*, 442 (1984).

38. Dong, W. J., Xing, J., Villain, M., Hellinger, M., Robinson, J. M., Chandra, M., Solaro, R. J., Umeda, P. K., and Cheung, H. C., Conformation of the regulatory domain of cardiac muscle troponin C in its complex with cardiac troponin I, *J Biol Chem, 274*, 31382 (1999).
39. Nakayama, S., Moncrief, N. D., and Kretsinger, R. H., Evolution of EF-hand calcium-modulated proteins. II. Domains of several subfamilies have diverse evolutionary histories, *J Mol Evol, 34*, 416 (1992).
40. Ikura, M., Clore, G. M., Gronenborn, A. M., Zhu, G., Klee, C. B., and Bax, A., Solution structure of a calmodulin-target peptide complex by multidimensional NMR, *Science, 256*, 632 (1992).
41. Herzberg, O., and James, M. N., Structure of the calcium regulatory muscle protein troponin-C at 2.8 A resolution, *Nature, 313*, 653 (1985).
42. Strynadka, N. C., and James, M. N., Crystal structures of the helix-loop-helix calcium-binding proteins, *Annu Rev Biochem, 58*, 951 (1989).
43. Reinach, F. C., Nagai, K., and Kendrick-Jones, J., Site-directed mutagenesis of the regulatory light-chain Ca2+/Mg2+ binding site and its role in hybrid myosins, *Nature, 322*, 80 (1986).
44. Malnasi-Csizmadia, A., Hegyi, G., Tolgyesi, F., Szent-Gyorgyi, A. G., and Nyitray, L., Fluorescence measurements detect changes in scallop myosin regulatory domain, *Eur J Biochem, 261*, 452 (1999).
45. Szczesna, D., Regulatory light chains of striated muscle myosin. Structure, function and malfunction, *Curr Drug Targets Cardiovasc Haematol Disord, 3*, 187 (2003).
46. Uyeda, T. Q., Abramson, P. D., and Spudich, J. A., The neck region of the myosin motor domain acts as a lever arm to generate movement, *Proc Natl Acad Sci U S A, 93*, 4459 (1996).
47. Butler, T. M., Siegman, M. J., Mooers, S. U., and Barsotti, R. J., Myosin light chain phosphorylation does not modulate cross-bridge cycling rate in mouse skeletal muscle, *Science, 220*, 1167 (1983).
48. Butler, T. M., and Siegman, M. J., Chemical energy usage and myosin light chain phosphorylation in mammalian smooth muscle, *Fed Proc, 42*, 57 (1983).
49. Swynghedauw, B., Developmental and functional adaptation of contractile proteins in cardiac and skeletal muscles, *Physiol Rev, 66*, 710 (1986).
50. Davis, J. S., Satorius, C. L., and Epstein, N. D., Kinetic effects of myosin regulatory light chain phosphorylation on skeletal muscle contraction, *Biophys J, 83*, 359 (2002).
51. Sweeney, H. L., Bowman, B. F., and Stull, J. T., Myosin light chain phosphorylation in vertebrate striated muscle: regulation and function, *Am J Physiol, 264*, C1085 (1993).
52. Goldman, Y. E., Wag the tail: structural dynamics of actomyosin, *Cell, 93*, 1 (1998).
53. Stull, J. T., Myosin minireview series, *J Biol Chem, 271*, 15849 (1996).
54. Huxley, A. F., Muscle structure and theories of contraction, *Prog Biophys Biophys Chem, 7*, 255 (1957).

55. Huxley, H. E., Structural difference between resting and rigor muscle; evidence from intensity changes in the lowangle equatorial x-ray diagram, *J Mol Biol, 37*, 507 (1968).
56. Lymn, R. W., and Taylor, E. W., Mechanism of adenosine triphosphate hydrolysis by actomyosin, *Biochemistry, 10*, 4617 (1971).
57. Bagshaw, C. R., and Trentham, D. R., The characterization of myosin-product complexes and of product-release steps during the magnesium ion-dependent adenosine triphosphatase reaction, *Biochem J, 141*, 331 (1974).
58. Werber, M. M., Szent-Gyorgyi, A. G., and Fasman, G. D., Fluorescence studies on the interaction between heavy meromyosin and magnesium ions. Effect of EDTA, *J Mechanochem Cell Motil, 2*, 35 (1973).
59. Geeves, M. A., Goody, R. S., and Gutfreund, H., Kinetics of acto-S1 interaction as a guide to a model for the crossbridge cycle, *J Muscle Res Cell Motil, 5*, 351 (1984).
60. Geeves, M. A., and Conibear, P. B., The role of three-state docking of myosin S1 with actin in force generation, *Biophys J, 68*, 194S (1995).
61. Rayment, I., Smith, C., and Yount, R. G., The active site of myosin, *Annu Rev Physiol, 58*, 671 (1996).
62. Smith, C. A., and Rayment, I., X-ray structure of the magnesium(II).ADP.vanadate complex of the Dictyostelium discoideum myosin motor domain to 1.9 A resolution, *Biochemistry, 35*, 5404 (1996).
63. Holmes, K. C., Angert, I., Kull, F. J., Jahn, W., and Schroder, R. R., Electron cryo-microscopy shows how strong binding of myosin to actin releases nucleotide, *Nature, 425*, 423 (2003).
64. Raucher, D., Fajer, E. A., Sar, C., Hideg, K., Zhao, Y., Kawai, M., and Fajer, P. G., A novel electron paramagnetic resonance spin label and its application to study the cross-bridge cycle, *Biophys J, 68*, 128S (1995).
65. Goldman, Y. E., Hibberd, M. G., and Trentham, D. R., Initiation of active contraction by photogeneration of adenosine-5'-triphosphate in rabbit psoas muscle fibres, *J Physiol, 269*, 55 (1984).
66. Alberts, B., Bray, D., Lewis, J., Raff, M., Roberts, K., and Watson, J. D., *Molecular Biology of The Cell*, Garland Publishing, New York (1994).
67. Belmont, L. D., Orlova, A., Drubin, D. G., and Egelman, E. H., A change in actin conformation associated with filament instability after Pi release, *Proc Natl Acad Sci U S A, 96*, 29 (1999).
68. Bonnemann, C. G., Thompson, T. G., van der Ven, P. F., Goebel, H. H., Warlo, I., Vollmers, B., Reimann, J., Herms, J., Gautel, M., Takada, F., Beggs, A. H., Furst, D. O., Kunkel, L. M., Hanefeld, F., and Schroder, R., Filamin C accumulation is a strong but nonspecific immunohistochemical marker of core formation in muscle, *J Neurol Sci, 206*, 71 (2003).
69. Eli-Berchoer, L., Reisler, E., and Muhlrad, A., Structural implications of the chemical modification of Cys(10) on actin, *Biophys J, 78*, 1482 (2000).

70. Eligula, L., Chuang, L., Phillips, M. L., Motoki, M., Seguro, K., and Muhlrad, A., Transglutaminase-induced cross-linking between subdomain 2 of G-actin and the 636-642 lysine-rich loop of myosin subfragment 1, *Biophys J, 74*, 953 (1998).
71. Bonafe, N., and Chaussepied, P., A single myosin head can be cross-linked to the N termini of two adjacent actin monomers, *Biophys J, 68*, 35S (1995).
72. Cuda, G., Pate, E., Cooke, R., and Sellers, J. R., In vitro actin filament sliding velocities produced by mixtures of different types of myosin, *Biophys J, 72*, 1767 (1997).
73. Blotnick, E., and Muhlrad, A., Effect of nucleotides and actin on the intramolecular cross-linking of myosin subfragment-1, *Biochemistry, 33*, 6867 (1994).
74. Bertrand, R., Derancourt, J., and Kassab, R., Probing the hydrophobic interactions in the skeletal actomyosin subfragment 1 and its nucleotide complexes by zero-length cross-linking with a nickel-peptide chelate, *Biochemistry, 36*, 9703 (1997).
75. Bagshaw, C., ATP analogues at a glance, *J Cell Sci, 114*, 459 (2001).
76. Shirakawa, I., Chaen, S., Bagshaw, C. R., and Sugi, H., Measurement of nucleotide exchange rate constants in single rabbit soleus myofibrils during shortening and lengthening using a fluorescent ATP analog, *Biophys J, 78*, 918 (2000).
77. Prochniewicz-Nakayama, E., Yanagida, T., and Oosawa, F., Studies on conformation of F-actin in muscle fibers in the relaxed state, rigor, and during contraction using fluorescent phalloidin, *J Cell Biol, 97*, 1663 (1983).
78. Hegyi, G., Mak, M., Kim, E., Elzinga, M., Muhlrad, A., and Reisler, E., Intrastrand cross-linked actin between Gln-41 and Cys-374. I. Mapping of sites cross-linked in F-actin by N-(4-azido-2-nitrophenyl) putrescine, *Biochemistry, 37*, 17784 (1998).
79. Gulick, A. M., Bauer, C. B., Thoden, J. B., Pate, E., Yount, R. G., and Rayment, I., X-ray structures of the Dictyostelium discoideum myosin motor domain with six non-nucleotide analogs, *J Biol Chem, 275*, 398 (2000).
80. Smith, C. A., and Rayment, I., X-ray structure of the magnesium(II)-pyrophosphate complex of the truncated head of Dictyostelium discoideum myosin to 2.7 A resolution, *Biochemistry, 34*, 8973 (1995).
81. Fisher, A. J., Smith, C. A., Thoden, J. B., Smith, R., Sutoh, K., Holden, H. M., and Rayment, I., X-ray structures of the myosin motor domain of Dictyostelium discoideum complexed with MgADP.BeFx and MgADP.AlF4, *Biochemistry, 34*, 8960 (1995).
82. Fisher, A. J., Smith, C. A., Thoden, J., Smith, R., Sutoh, K., Holden, H. M., and Rayment, I., Structural studies of myosin:nucleotide complexes: a revised model for the molecular basis of muscle contraction, *Biophys J, 68*, 19S (1995).
83. Bax, A., Two-dimensional NMR and protein structure, *Annu Rev Biochem, 58*, 223 (1989).
84. Cooke, R., The mechanism of muscle contraction, *CRC Crit Rev Biochem, 21*, 53 (1986).

85. Dos Remedios, C. G., Millikan, R. G., and Morales, M. F., Polarization of tryptophan fluorescence from single striated muscle fibers. A molecular probe of contractile state, *J Gen Physiol, 59*, 103 (1972).
86. Finer, J. T., Mehta, A. D., and Spudich, J. A., Characterization of single actin-myosin interactions, *Biophys J, 68*, 291S (1995).
87. Yanagida, T., Loose coupling between chemical and mechanical reactions in actomyosin energy transduction, *Adv Biophys, 26*, 75 (1990).
88. Schutt, C., and Lindberg, U., Actin as the generator of tension during muscle contraction, *Proc Natl Acad Sci U S A, 89*, 319 (1992).
89. Root, D. D., The dance of actin and myosin: a structural and spectroscopic perspective, *Cell Biochem Biophys, 37*, 111 (2002).
90. Lackowicz, J., *Principles of Fluorescence Spectroscopy*, Kluwer Academic/Plenum Publishers, New York, NY (1999).
91. Denk, W., Strickler, J. H., and Webb, W. W., Two-photon laser scanning fluorescence microscopy, *Science, 248*, 73 (1990).
92. Centonze, V. E., and White, J. G., Multiphoton excitation provides optical sections from deeper within scattering specimens than confocal imaging, *Biophys J, 75*, 2015 (1998).
93. Szczesna, D., Ghosh, D., Li, Q., Gomes, A. V., Guzman, G., Arana, C., Zhi, G., Stull, J. T., and Potter, J. D., Familial hypertrophic cardiomyopathy mutations in the regulatory light chains of myosin affect their structure, Ca2+ binding, and phosphorylation, *J Biol Chem, 276*, 7086 (2001).
94. Roopnarine, O., and Leinwand, L. A., Functional analysis of myosin mutations that cause familial hypertrophic cardiomyopathy, *Biophys J, 75*, 3023 (1998).
95. Bashyam, M. D., Savithri, G. R., Kumar, M. S., Narasimhan, C., and Nallari, P., Molecular genetics of familial hypertrophic cardiomyopathy (FHC), *J Hum Genet, 48*, 55 (2003).
96. Hoffmann, B., Schmidt-Traub, H., Perrot, A., Osterziel, K. J., and Gessner, R., First mutation in cardiac troponin C, L29Q, in a patient with hypertrophic cardiomyopathy, *Hum Mutat, 17*, 524 (2001).
97. Flavigny, J., Richard, P., Isnard, R., Carrier, L., Charron, P., Bonne, G., Forissier, J. F., Desnos, M., Dubourg, O., Komajda, M., Schwartz, K., and Hainque, B., Identification of two novel mutations in the ventricular regulatory myosin light chain gene (MYL2) associated with familial and classical forms of hypertrophic cardiomyopathy, *J Mol Med, 76*, 208 (1998).

CHAPTER 2

ROTATION OF THE LEVER-ARM OF MYOSIN IN CONTRACTING SKELETAL MUSCLE FIBERS MEASURED BY ONE-PHOTON AND TWO-PHOTON ANISOTROPY

Rationale:

While the sliding filament theory is universally accepted, the detailed mechanism of transduction of chemical energy from ATP hydrolysis into mechanical work in terms of force production remains under research. For example, prior research pointed to the whole head, including the catalytic domain moving together as shown on the left. More recent reports have suggested that the catalytic domain in fact show little movement and that hydrolysis of ATP is coupled to a large movement in the regulatory domain.

In this chapter, the rotation of myosin via anisotropy of the regulatory light chain (RLC) and the essential light chain (ELC) using 1 photon and 2 photon microscopy was measured. In order to measure movement of the regulatory domain, *in vitro* purified and fluorescently tagged RLC was exchanged with endogenous RLC in 1-5 isolated fibers depleted of endogenous ATP. The fiber was perfused with caged ATP which converted the inactive form of ATP into an active form via a pulse of UV light, synchronizing the muscle to execute one cross-bridge cycle.

This was established before correlating the mechanical rotation (RLC) to the enzymatic event (release of nucleotide) as discussed in Chapter 3. Using 2P microscopy, we determined that the power stroke occured approximately 200 milliseconds following flash photolysis of caged ATP from a fiber in a state of rigor.

ABBREVIATIONS

S1: myosin subfragment-1

1P: one-photon excitation

2P: two-photon excitation

IR: infrared light

S/N: Signal-to-Noise ratio

SD: Standard Deviation

5'-IATR: 5'-iodoacetamido-tetramethyl-rhodamine

IATR-RLC or IATR-RLC: RLC labeled with 5'-iodoacetamido-tetramethyl-rhodamine

IATR-ELC or IATR-ELC: ELC labeled with 5'-iodoacetamido-tetramethyl-rhodamine

TRITC-Ph: tetramethylrhodamine-5-isothiocyanate (TRITC) phalloidin

DMNPE-caged ATP: 5-dimethyoxy-2-nitrobenzyl-caged ATP

RLC: regulatory light chain

ELC: essential light chain-1

msec: milliseconds

nsec: nanoseconds

ABSTRACT. The rotation of the lever-arm of myosin cross-bridges causes muscle to contract. To resolve details of this rotation, it is necessary to observe either a single, or small population, of cross-bridges. In muscle fibers, it is still impossible to resolve a single cross-bridge, but it is possible to investigate a small population by simultaneously activating cross-bridges in a femtoliter volume by rapid release of caged ATP. One-photon (1P) microscopy was used, in which the number of observed cross-bridges is limited to ~600, to measure the rates of cross-bridge detachment and re-binding to thin filaments. In this case, the power-stroke was not resolved, perhaps because the number of observed cross-bridges was too large. In an attempt to decrease this number, data was also obtained using two-photon (2P) microscopy which permitted observation of approximately half as many cross-bridges as before. With the 2P excitation, the number of cross-bridges was small enough to resolve the beginning of the power stroke. My results indicate that the power stroke begins ~200 msec after the rigor cross-bridge first binds ATP.

INTRODUCTION

The hypothesis tested in this chapter supports the model that rotational motion of the light chain domain occurs during the cross-bridge cycle (*1*). The rotation of myosin cross-bridges in muscle is the mechanical event responsible for muscle contraction. Resolving distinct myosin structural states in muscle has been difficult, because each myosin head has its individual state of cycling and each cycle has different structural states. When a small enough population of cross-bridges is activated by rapid release of caged ATP, they move in synchrony and their behavior is expected to be equivalent to that of a single cross-bridge (*2*). Using electron paramagnetic resonance (EPR), two distinct orientations of a spin labeled attached to cys108 of chicken gizzard RLC exchanged into scallop muscle have been observed during contraction (*3*). However, disorder is present due to the nature in which the bundles are perfused and the probe is detected, besides using smooth muscle exchanged into a skeletal muscle of a eukaryotic lower organism. Some Fluorescence Resonance Energy Transfer (FRET) reports do not show a difference in the distance between Cys177 on ELC and Lys553 on the catalytic domain of S1 upon addition of various nucleotide analogues or addition of actin (*4*). The introduction of extremely small observational volumes defined by diffraction-limited laser beams and confocal detection (*5*) has made it possible to observe exceedingly small populations of cross-bridges in vivo. Isolated S1 labeled with probes on ELC and RLC with and without actin showed greater phosphorescence anisotropy than probes at the catalytic domain, supporting the idea of the so-called "swinging lever arm", "wobble in a cone", and "Brownian ratchet" models of force generation (*6*). In the present

experiments, the orientation change of ~600 fluorescently labeled myosin cross-bridges during single turnover of ATP in skeletal muscle fibers was measured.

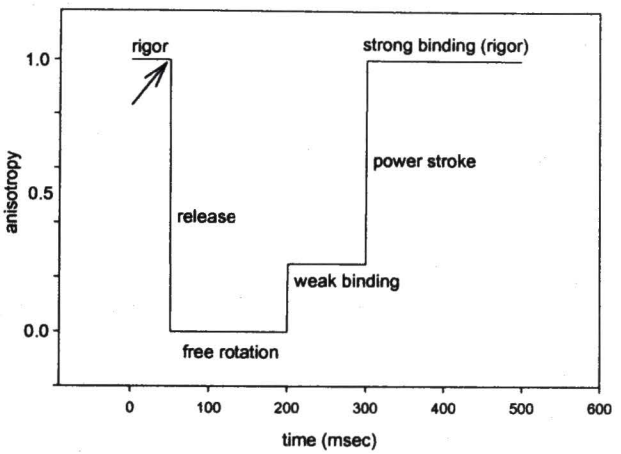

Figure 1. Schematic representation of the expected time course of anisotropy over time of a single cross-bridge cycle.

Figure 1 shows a schematic representation of the expected time course of anisotropy change of a single cross-bridge. Creation of ATP (arrow) is followed by a release of a cross-bridge from thin filaments. For 150 msec, the cross-bridge is rotating freely in solution (anisotropy=0), and eventually binds to actin in a short-lived or partially disordered pre-powerstroke (labeled "weak" in the field) conformation. It remains weakly bound until Pi/ADP dissociates (100 msec in this case) when it produces power stroke and returns to the original, strongly bound configuration. If a small population of cross-bridges were acting in perfect synchrony, the anisotropy of the lever-arm would be expected to change in three phases. Beginning with the heads in rigor, when they are immobilized by actin, the first phase after creation of ATP (arrow) is an increase in rotational mobility, reflecting dissociation of heads from thin filaments. At the end of this process, myosin heads rotate freely. The second phase is a partial immobilization, reflecting binding of the heads to thin filament in a short-lived or partially disordered pre-powerstroke state (*7*). The final phase is the power stroke -- transition of the weakly bound, partially

immobilized heads to strongly bound, completely immobilized state triggered by product release. Following synchronous activation, the cross-bridges started to rotate rapidly (indicating dissociation from actin) after which they were slowly immobilized (indicating binding to actin) (*2, 8*). However, in the experiments using one-photon (1P) excitation in a confocal microscope, the power stroke was conspicuously absent. It is possible that the reason for the absence of clearly defined power stroke was that the observed population of cross-bridges (~600) was still too large. In an attempt to decrease this number, two-photon (2P) microscopy was also used. In a conventional (1P) confocal microscopy, the thickness of the observational volume is defined by the diameter of the confocal aperture. In the present experiments, the aperture was 35 μm (2.37 Airy units)[1]. This made the depth-of-focus equal to 3 μm, the volume equal to 0.3 μm^3 and the number of observed cross-bridges ~600. In 2P microscopy on the other hand, which is now possible because of the wide availability of ultra-short pulsed near-infrared lasers, the signal originates only from the focal plane where the laser power density is high enough to produce 2P absorption (*9*). In my experiments, the plane was ~1.4 μm thick, allowing less than ~270 cross-bridges to be observed.

In spite of the fact that number of observed cross-bridges was less than half, the S/N ratio was unchanged. This was due to the fact that 2P photobleaching was reduced and that absolute values of 2P anisotropy were larger. It is well known that out-of-focus photobleaching is reduced in 2P because out-of-focus planes are illuminated by less

---

[1] It could not be further decreased, because closing it decreased the Signal-to-Noise ratio (S/N) to the extent that measurements became impossible.

damaging IR light. Surprisingly, in the case of muscle exchanged with myosin regulatory light chain labeled with rhodamine, photobleaching in the plane of focus was also reduced. The anisotropy was larger because absorption/emission of two photons depends on the fourth power, not the second power (like 1P absorption) of the cosine of the angle between the dye dipole and the direction of polarization of exciting light.

The time-courses of anisotropy using 2P excitation during muscle contraction were sufficiently different to allow determination of the onset of the power stroke. With the 2P excitation, the power stroke began on the average ~200 msec after a cross-bridge first binds ATP.

MATERIALS AND METHODS

Psoas muscle isolation from rabbit: The psoas muscle was isolated from isoflurane-anesthetized young adult New Zealand White rabbits and stored in glycerinating solution at -20°C for no more than 3-5 months. The glycerinating solution was comprised of 0.15M KCl, 6mM $MgCl_2$, 5mM EGTA, 5mM ATP, 10mM Tris-HCl (pH 7.5), 1mM DTT in 50% glycerol.

Expression of RLC: RLC cDNA cloned into pT7-7 from chicken skeletal muscle was generously provided by Dr. S. Lowey (University of Vermont). RLC containing a single cysteine at position 73 was prepared by expression of RLC in a pT7-7 plasmid in

BL21(DE3) cells. The construct contains the following mutations: S73C, C126A, C155A, thus ensuring only one binding site for the thiol-specific fluorescent dye.

RLC purification: The purification was performed following transformation and expression from BL21(DE3) cells as previously described (*10*). The concentration of leupeptin in the lysis buffer was added at 1ug/mL. Once purified, the RLC was detected in the eluent fractions by Western blot analysis using an anti-RLC antibody. A 12% denaturing SDS-PAGE gel was used to separate the protein fractions by size followed by Western Bloting (*11*). The molecular weight used were ColorBurst Markers (Sigma, Saint Louis, MO). The anti-RLC antibody was generously provided by Dr. Danuta Szczesna, University of Miami School of Medicine, Miami, FL.

RLC stability: RLC was eluted according to the protocol for RLC purification supplied by Lowey using increasing salt concentrations or ion exchange chromatography (*12*). RLC was purified under denaturing conditions, because it has a tendency to form inclusion bodies and Guanidine HCl was used to break up inclusion bodies. Once the correct fraction was identified, 5mM sodium azide was added as an antibacteriostatic and 2 mM DTT was added to keep the protein reduced and prevent it from aggregating.

RLC labeling: The RLC-containing fraction was dialyzed overnight in 1 Liter of 50mM KCl, 10mM Tris-Cl pH 7.5. This removed DTT, which interferes with labeling. A 10-fold molar excess 5'-IATR (Molecular Probes, Eugene OR) was added. The 5'-

IATR was dissolved from powder in methanol just before labeling, per suggestions from the supplier for optimum labeling. The sample was covered in aluminum foil to protect the fluorophore from light and incubated on ice for 7 hours. Unlabeled dye was dialyzed out overnight at 4 degrees Celsius protected from light in 50mM KCL, 10mM Tris-Cl pH 7.5 and 2mM DTT. The concentration of labeled protein was calculated where the molar coefficient of extinction for RLC at 280nm was 220,000 and dye at 555nm was 87,000. The concentration of protein in mg/mL = (A280-A555/3)/0.22 and that value is divided by 0.02 (molecular weight of RLC is approximately 20,000) to yield the μM concentration of protein. The concentration of dye in μM = A555/0.87. The degree of labeling is determined by dividing the μM concentration of dye by the μM concentration of protein multiplied by 100%. The IATR-RLC adduct contained 14% rhodamine.

ELC expression, purification and labeling: ELC was prepared as described (*13*). Briefly, human fast skeletal muscle ELC (gift from Dr. S. Lowey, University of Vermont) was subcloned into the pQE60 vector (Qiagen, Valencia, CA) using DNA polymerase chain reaction with the 3'- end containing a tag of 6 histidines. The presence of the his-tag at the N-terminus of ELC was confirmed by DNA sequencing and then expressed and purified from *E. coli* M15[pREP4] cells (QIAGEN, Valencia, CA). The expressed recombinant proteins were purified on the Ni-NTA-agarose columns (QIAGEN, Valencia, CA). Labeling was done as described earlier (*2*), except that stock IATR was dissolved in methanol just before the experiment.

Myofibril Exchange: As a control to show that the protein is tagged and is exchanged into the fiber (Figure 3 and Figure 4), the exchange procedure described below was performed the same, but using a solution of myofibrils. This is because it is easier to load myofibrils on a gel than homogenize a fiber and load it on a gel. Myofibrils may be directly loaded on a 12% denaturing SDS-PAGE gel. The anti-RLC (Figure 3) and anti-ELC antibodies were generously provided by D. Sczcesna, University of Florida.

Muscle fiber preparation: Labeled RLC was exchanged into fibers as described earlier (*14*). Briefly, single fibers were dissected from glycerinated rabbit psoas muscle bundles in glycerinating solution. Opened bottles containing glycerinated bundles were discarded after a week. Fibers were mounted on a microscope slide containing aluminum clips glued ~5 mm apart. Tautly stretched fibers were attached to the clips. Mounted fibers were thoroughly washed with 200μL rigor solution (50mM KCl, 2mM $MgCl_2$, 10mM Tris-Cl pH 7.5). The fiber was incubated for 3-5 minutes in 100uL RLC exchange solution (50mM KCl, 20mM EDTA, 10mM potassium monophosphate buffer pH 7.0, 0.5 mM DTT). The fiber was incubated in100μL of 0.5mg/mL RLC in extracting solution at 30°C for 30 minutes. The fiber was rinsed with 300μL Calcium-rigor solution (50mM KCl, 2mM $MgCl_2$, 10mM Tris-Cl pH 7.5, 0.1 mM $CaCl_2$). 50μL 2mM caged ATP + 10mM glutathione was added to the fiber. A glass cover slip was placed over the fiber and rested on ~2 mm layer of Vaseline lined along the edge of the microscopic slide to prevent evaporation and drying out of the fiber.

Force tension measurements: This was performed to ensure that the fibers were viable and that the transgenic fibers developed the same force as a normal rabbit fiber. A MKB force transducer (Scientific Instruments, Heidelberg, Germany) was coupled to an analogue counter (Model 6024E, National Instruments, Austin, TX). As described in (*15*), isometric contraction was recorded in fiber strips stretched to about 1.2 times slack length after mounting between a fixed arm and a force transducer.

Statistical analysis of anisotropy graphs: Anisotropy of myosin and actin after release of ATP from the cage was recorded. Anisotropy change was divided into two phases. The half-times of the first phase, indicating cross-bridge dissociation, and that of the second phase, corresponding to a slow relaxation back to a rigor, were measured in milliseconds using SigmaPlot 7.101. The point at which pulse was administered (denoted by a deflection in polarized emission intensities or anisotropy) until the inflection stopped denoted the first phase. The point at which the inflection returned toward the original value until approximately 3-4 seconds later denoted the second phase. Anisotropy was detrended to account for photobleaching effects and also examined on an expanded scale (1 second versus 7 second time scale) to inspect the trend more closely.

One-way Analysis of Variance (ANOVA) was performed to show that the half times in the fast phase were not statistically different between muscle samples on different days and within different illumination volumes of the muscle fiber. For each fiber, 5-10 anisotropy responses were recorded. The average half-times of 5-10 samples were recorded with a standard deviation. N-1 degrees of freedom were allowed for the

denominator in determining the standard deviation. The confidence interval was 0.05 (95% confidence).

Confocal Analysis: Using a Zeiss 410 confocal microscope (Thornwood, NY), a muscle fiber was placed horizontally on a stage of a confocal microscope and observed through rhodamine filters. The objective (Zeiss C-Apo, 40x, numerical aperture (NA) = 1.2, water immersion) focused visible laser light onto the A-band. The width and depth of the illumination volume were approximately equal to the diffraction limit of ~0.3 μm^3. Around 500 fluorescent crossbridges were isolated within that illumination volume, depending on the degree of labeling for that batch of labeled protein. The excitation wavelength was 568nm. When taking an anisotropy data point, the laser scanned the muscle fiber at the illumination volume every 25 μseconds for seven seconds.

Photogeneration of ATP: ATP was photogenerated from a caged precursor by perfusing fibers with 2 mM caged ATP (Molecular Probes, Eugene, OR) in rigor solution. The UV beam was focused by the objective to a Gaussian spot with width, length and depth of ~0.2x0.2x3 μm. Approximately 3 seconds after beginning the scan, a shutter admitting the UV light was opened for exactly 10 milliseconds. The UV beam at a wavelength of 384nm photolyzed caged ATP. The energy flux through the illuminated area during the time ATP stayed in the experimental volume (~300 μsec) was 9×10^{-4} $mJ/\mu m^2$. The amount of released ATP is enough for a single turnover of ATP (*16, 17*).

Fluorescence anisotropy of fibers. Fluorescence was measured with a high aperture lens (C-Apo, 40x, numerical aperture=1.2). Calculations showed that high numerical aperture of the objective causes minimal distortion to the polarized intensities (*18*). The subscripts after the intensity indicate the direction of polarization of emitted light relative to the axis of the muscle fiber. The excitation light was always parallel to the axis of fiber. The muscle axis was oriented horizontally on a stage of a microscope. Photomultipliers 1 & 2 in descanned mode, and photomultipliers 2 & 3 in non-descanned mode recorded $I_{\perp}$ & $I_{\parallel}$, respectively.

RESULTS

RLC purification: **Figure 2** top right is Western Blot showing the noninduced (lane 1) and induced (lane 2) cell lysate, indicating RLC was being expressed by the bacterial system and identified by the antibody. **Figure 2** at the top left and bottom left show purification of RLC. Lane 3 shows that the non-purified cell extract is not heavily marked in the Sypro-stain but it is heavily marked by the antibody shown in the western blot. This shows that the antibody is specific for RLC. The purification is also quite clean (lane 5 and 6) after column chromatography, compared to just before loading the expressed sample onto the column (*i.e.* lane 2). It is noted that no protease inhibitors were added, because the protocol for purification of RLC was followed from a paper (*12*) and the paper did not specify to use protease inhibitors. RLC before purification was around 18 kDa (i.e. lane 3) and around 12 kDa after purification or truncated by 30% (lane 5 and 6). After this was recognized, communication was made with Dr. Lowey's

lab and an updated protocol was obtained, which specified use of protease inhibitors. I looked into sequencing the protein to determine the actual sequence; however, for Edman degradation (cheapest and easiest to contract out), the N-terminus of a protein is not allowed to be blocked. In the case of RLC, it was, shown by an internet search at www.pubmed.gov. Another alternative was to use mass spectroscopy; however, that was beyond our lab's budget. A second batch of RLC was purified again (**Figure 3, lane 3)** and this time the protein was full-length. Both proteins appeared to be functional, shown by fluorescent striated patterns and anisotropy results. The results from anisotropy were identical to the batch of RLC purified without protease inhibitors added. I speculated that the part of this batch of RLC that was missing must not have been the part containing rhodamine (cys 73). In the published papers (Chapter 3 and 5), some figures contain data obtained from the truncated RLC and some figures contain data from full length RLC. The results between the two RLCs were comparable to one another.

Dr. Lowey, who provided the RLC clone and purification protocols stated that RLC will be cleaved at the N-terminal amino acid sequence near the phosphorylation site (Ser 19) (personal communication). This omitting of protease inhibitors would not affect labeling or binding to the myosin heavy chain. In the past, her lab has seldom used protease inhibitors, but if problems arise, the protease inhibitors will be added.

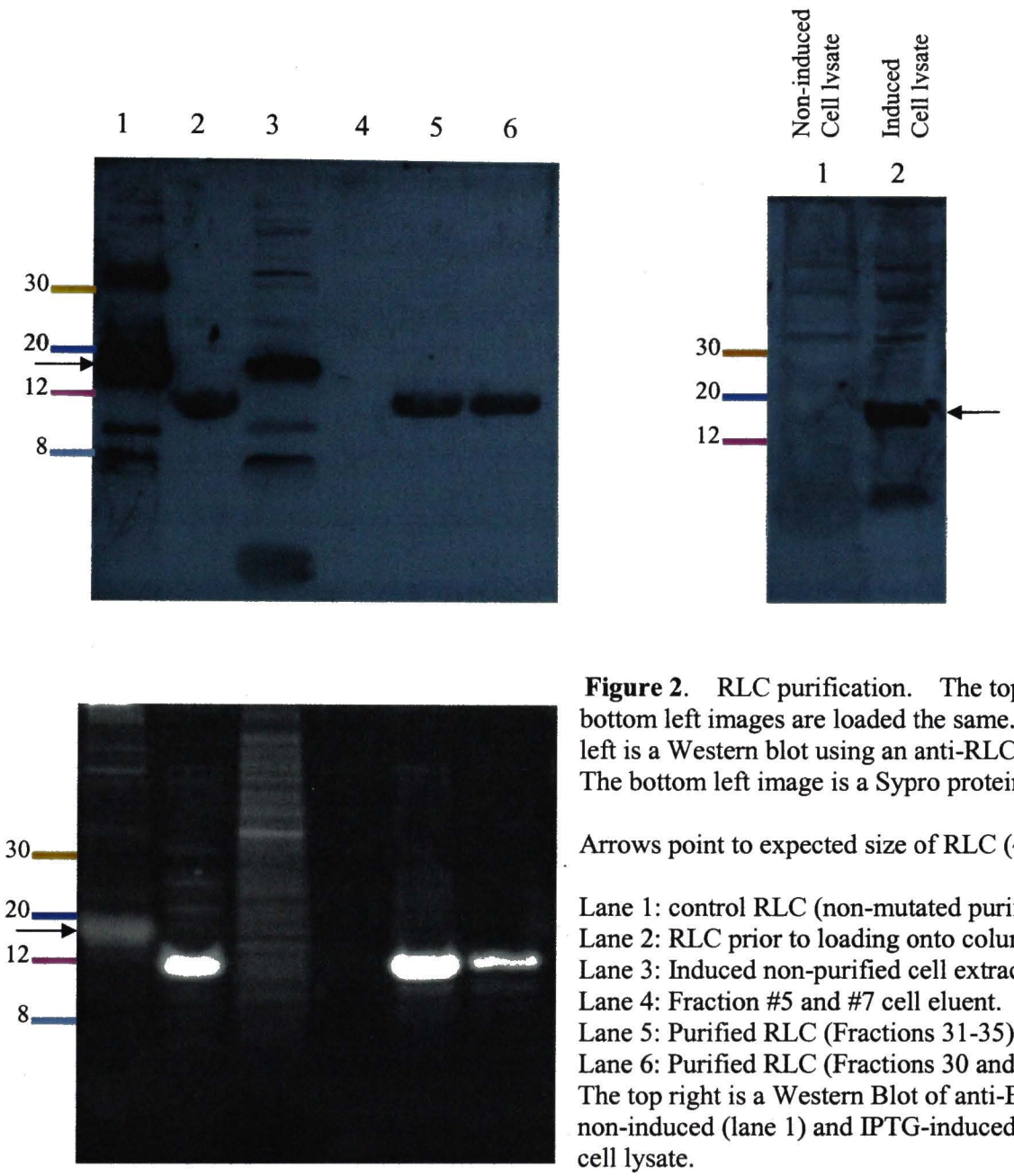

Figure 2. RLC purification. The top left and bottom left images are loaded the same. The top left is a Western blot using an anti-RLC antibody. The bottom left image is a Sypro protein stain.

Arrows point to expected size of RLC (~18kDa).

Lane 1: control RLC (non-mutated purified RLC).
Lane 2: RLC prior to loading onto column.
Lane 3: Induced non-purified cell extract.
Lane 4: Fraction #5 and #7 cell eluent.
Lane 5: Purified RLC (Fractions 31-35).
Lane 6: Purified RLC (Fractions 30 and 36).
The top right is a Western Blot of anti-ELC in non-induced (lane 1) and IPTG-induced (Lane 2) cell lysate.

Labeling myosin in muscle with IATR-RLC and IATR-ELC. Labeled RLC was exchanged into fibers as described earlier (*14*). Labeled ELC was exchanged with endogenous light chains of myosin in muscle fibers at 30°C using the exchange solution as described before (*19, 20*). The degree of labeling was ~3% for 5'-iodoacetamido-

tetramethyl-rhodamine (IATR)-RLC and ~1%-2% for IATR-ELC. The microscope had no trouble detecting such lightly labeled fibers.

Additionally, experiments were performed to verify that labeled light chains were actually exchanged into the fibers while the endogenous protein was exchange/extracted out (**Figure 3** for RLC and **Figure 4** for ELC). This procedure is consistent with other methods of exchange, such as exchanging native troponin I in single rabbit psoas muscle fibers for externally fluorescently labeled troponin I at Cys 133 (*21*). The procedure is based on molecules that can reversibly dissociate from their binding sites that can be replaced by externally applied proteins competing for the free binding sites. Furthermore, the labeled exogenous protein specifically folds into the site due to its conformational affinity for the binding site.

The procedure of removing RLC from permeabilized muscle fibers is not new (*22*). Other laboratories have used this procedure in order to replace native RLC with RLC that has been fluorescently labeled at either endogenous or engineered cysteine amino acid sites (*23, 24*). I did not perform experiments to examine the structural effect of the light chain removal and recombinant exchange into myosin beyond force tension experiments, myofibril exchange, and visual striation patterns using confocal microscopy. Others have however, (*25-27*) and report that normal function was regained upon RLC removal and addition of either native or recombinant RLC. The effect of RLC exchange on the X-ray pattern from contracting fibers is unknown.

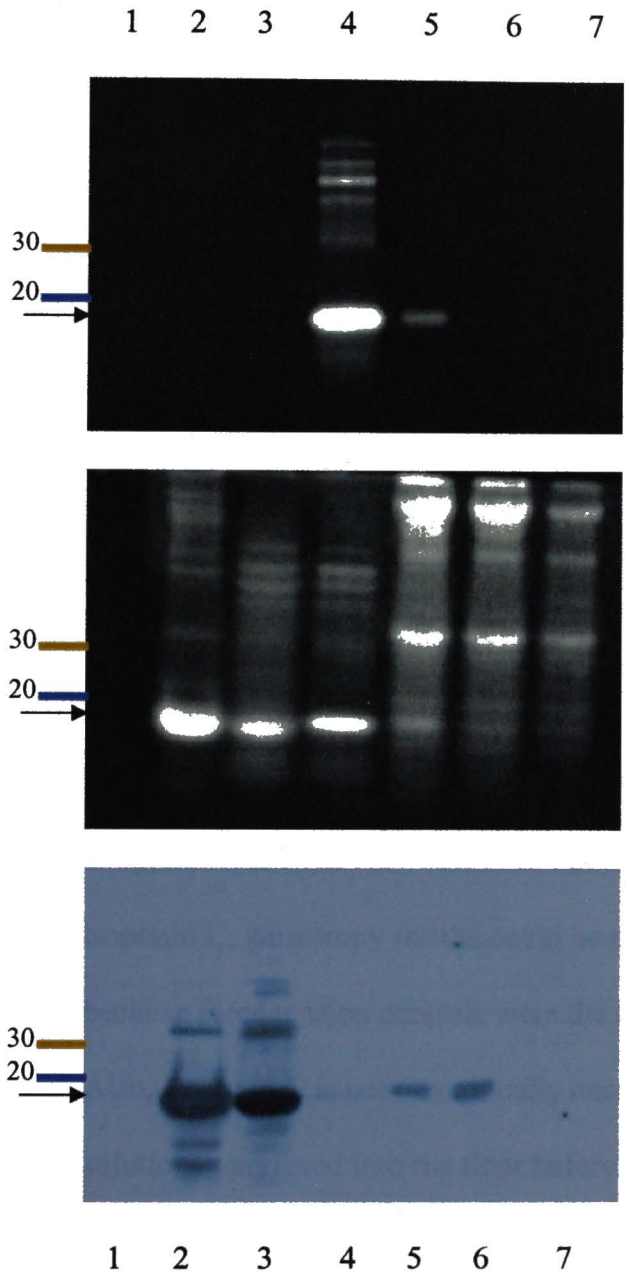

Figure 3. RLC Exchange
Top: UV transluminator (350nm)
Middle: Sypro Protein Stain
Bottom: Western Analysis

Arrows point to the expected size of RLC (~18 kDa)

Lane 1: MW
Lane 2: Control RLC
Lane 3: Unlabeled purified RLC
Lane 4: IATR-RLC
Lane 5: Exchanged RLC
Lane 6: Extracted RLC
Lane 7: Plain skeletal myofibrils

As shown in **Figure 3**, control RLC in lane 2 (non-mutated human fast skeletal muscle RLC, D. Sczcesna, University of Florida) shows the expected size of RLC. Lane 3 shows another control of the expected size of purified RLC, purified from our lab. Lane

4 shows that RLC is fluorescently labeled and the fluorescent tag does not affect the size mobility of RLC. An RLC band is present in the original autoradiogram, but it is faint in the reproduced image in Figure 3, because the amount loaded was not well detected by the antibody. Lane 5 shows that RLC is exchanged into the myofibrils because RLC is picked up by the antibody (Western blot) and shows up under UV light at the correct size. Lane 6 shows that endogenous RLC indeed is extracted out into the supernatant (this was the step prior to addition of recombinant labeled RLC). Lane 7 shows the protein extract of plain rabbit skeletal myofibrils. Endogenous RLC is not picked up by the antibody in lane 7 of the Western blot as no sample was loaded in the well of this gel. The top and middle images are from the same gel, a second gel was used for the Western blot. Otherwise, both gels were loaded the same.

One deviation from the protocol for RLC exchange (*25*) was not adding troponin C. Troponin C is apparently removed during RLC exchange step and because I did not add troponin C, anisotropy results could be affected. This is probably not a major concern, because force tension controls were the same as force tension of RLC-exchanged fibers. Also, troponin C is not theoretically necessary in this set-up, because calcium-rigor solution is perfused into the fiber before exchange. The solution allows tropomyosin to roll over when troponin C is present and expose the myosin heads so that the cross-bridges would attach. Without ATP, the fiber becomes fixed in the rigor state. This would prepare the muscle for contraction as soon as caged ATP is activated and hold myosin stiff as recombinant RLC is exchanged for native endogenous RLC.

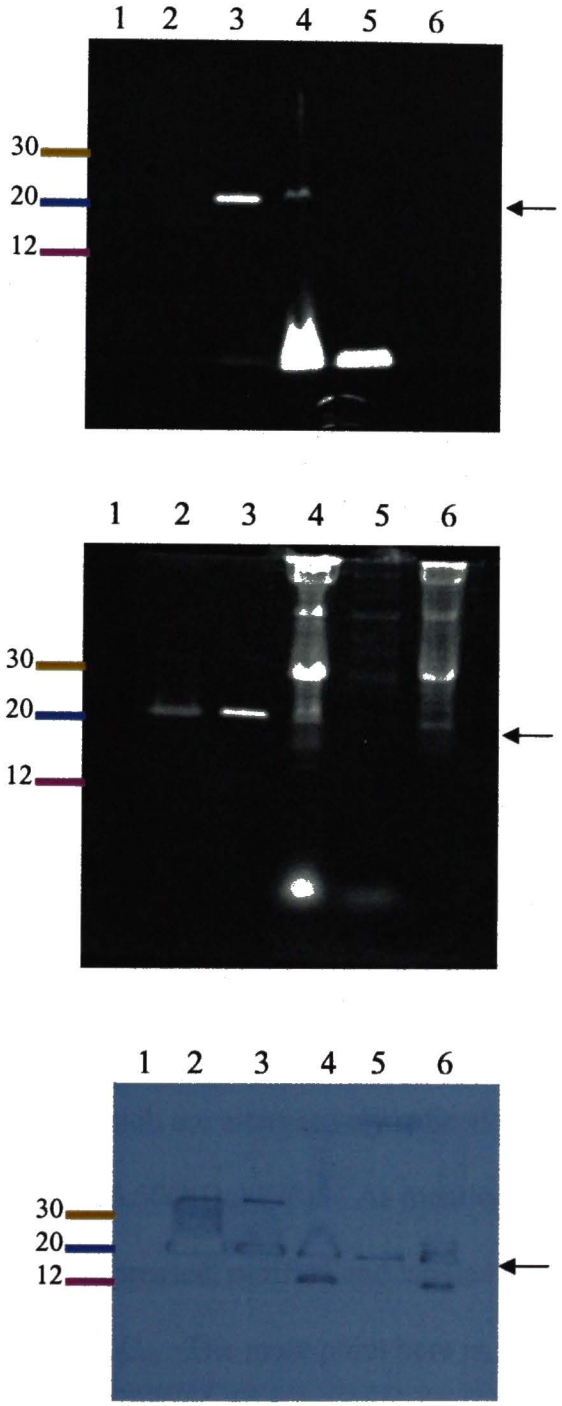

Figure 4. ELC Exchange
Top: UV transluminator
Middle: Sypro Protein Stain
Bottom: Western Analysis

Arrows point to the size expected for ELC (~21 kDa)

Lane 1: MW
Lane 2: Purified ELC
Lane 3: IATR-ELC
Lane 4: Myofibrils exchanged with ELC
Lane 5: Extracted ELC
Lane 6: Plain skeletal myofibrils

As shown in **Figure 4,** control experiments were performed to ensure that ELC was properly purified (Lane 2), fluorescently labeled (Lane 3), and exchanged into the myofibril (Lane 4). All gels were loaded the same. Lane 1 shows the molecular weight lane. No bands appear because these proteins are not fluorescent and can be visualized using Sypro Staining only under longer exposure times. Lane 2 shows the ELC purification is clean (middle) and identifiable by anti-ELC antibody (bottom). Lane 3 (top) shows that ELC is labeled and able to be visualized under ordinary UV fluorescence, the protein is clean during purification and that the antibody recognizes ELC (bottom). Lane 4 shows that the fluorescently-tagged ELC is exchanged into the myofibrils (top). Lane 5 shows that the exchange solution does remove native ELC (the main ingredient in the protocol is trifluorperizine (TFP) used to chemically remove ELC) and the antibody detection verifies this (bottom). Lane 6 shows plain skeletal myofibrils, which shows that the antibody picks up ELC. In Lanes 4 and 6 of the Western blot (bottom), a second band is seen below ELC. This is ELC-3 (approximately 16 kDa). There are two isoforms of ELC that exist in skeletal muscle, which are alternatively spliced from one gene: ELC-1 (20,700 kDa) and ELC-3 (16,500kDa) (*20*). As mentioned in the abbreviations, the ELC which has been expressed, purified and labeled here is ELC-1. In this thesis, ELC-1 is referred to as ELC. The main point here is, although both isoforms are expressed in psoas muscle, mainly the endogenous ELC-1 was extracted through this TFP-based procedure, (lane 5, antibody does not detect ELC-3) leaving ELC-3 presumably intact. The ELC-3 band does not appear in Lane 2 or 3 because this represents purified ELC, which was

expressed from bacteria and bacteria do not contain ELC-3. In lanes 2 and 3, a small portion of the ELC, which does not become fluorescently labeled, can be seen as dimers, shown by the antibody. At the bottom in Lanes 3, 4, and 5, it is possible to see either UV fluorescence or protein staining. This is due to unbound free fluorophores (Lane 4), the dye front, or small proteins being detectable. In conclusion, ELC is labeled and does exchange into myofibrils. This was extrapolated to be the case in fibers.

The procedure for ELC exchange in permeabilized rabbit muscle fibers was used from Sweeny's lab and their lab performed functional studies showing normal function of fibers upon endogenous ELC removal and re-addition of recombinant ELC (*20, 28*). I did not perform experiments to examine the structural effect of the light chain removal and recombinant exchange into myosin beyond force tension experiments, myofibril exchange, and visual striation patterns using confocal microscopy. No troponin C was added, but based on the aforementioned controls, the fiber contractility appeared viable. The effect of ELC exchange on the X-ray pattern from contracting fibers is unknown.

Functionality of exchanged fibers. Tension development was studied by a MKB force transducer (Scientific Instruments, Heidelberg, Germany) coupled to an analog counter (Model 6024E, National Instruments, Austin, TX). Control (unlabeled) fibers developed normal 0.94±0.05 mN/fiber (mean±SEM, n=32) maximum isometric tension. Fibers exchanged with fluorescently labeled RLC developed 0.96±0.03 mN/fiber tension. This is in agreement with others researching orientation changes of RLC who have determined that tension using photolysis of caged ATP in a rigor fiber were insensitive to

RLC exchange (*29*). Studies where half of the endogenous RLC were exchanged with rhodamine-labeled chicken gizzard RLC had little effect on isometric tension (*25*) or tension transients after rapid length steps (*30*). Fibers exchanged with fluorescently labeled LC1 also developed normal tension. Fibers labeled with 0.3 μM TRITC-Phalloidin developed tension within 10% of control fibers.

Other Controls. The following control experiments were performed in addition to the above exchange experiments:

To control for the response that the anisotropic response is due to a contraction, not an artifact such as the mechanical response to flicking the button for the UV pulse, a separate experiment with no caged ATP added was performed. With no ATP present, no rotation occurred and no change in anisotropy was observed (data not shown).

To control for the polarization of the free dye as not being what was measured in the fiber, free rhodamine dye (not conjugated to protein) was added in the same molar concentration using the same exchange procedure in a separate experiment one. If rhodamine was free to bind anywhere within sarcomere, it should bind cysteine residues present on RLC, ELC and any other molecule containing cysteine, cause a net dipole in all directions, cancel each other out, and display no anisotropy. This is what was seen; no ansisotropy. In these controls, 1) the photobleaching spot was not as big probably due to excessive light scattering; 2) More detailed striations were seen. This indicates that cysteines are preferentially displayed in proteins that form the A and I bands, M-line and Z-line; 3) The fiber appeared pinker than IATR-RLC labeled fibers. This is likely

because excess IATR-RLC that does not integrate into the position of the endogenous RLC is rinsed away through the calcium-rigor solution. In the case of the rhodamine dye, the larger protein it is conjugated to is absent, so therefore it would make sense that the free rhodamine would randomly bind to any and all proteins containing cysteine, and therefore less rinsed away, leaving the fiber pinker in appearance. The fact that the photobleaching spot was less intense, striations were seen, and the fiber was pink whereas in 9 spots no significant anisotropy change was detected, is indicative that: 1) all Rh conjugated to RLC bind in the same direction, 2) IATR-RLC integrates into the native spot with Rh in the same direction and 3) each individual rotation of Rh is distinct enough but synchronized enough to see a change in anisotropy upon stimulation of one cross bridge cycle.

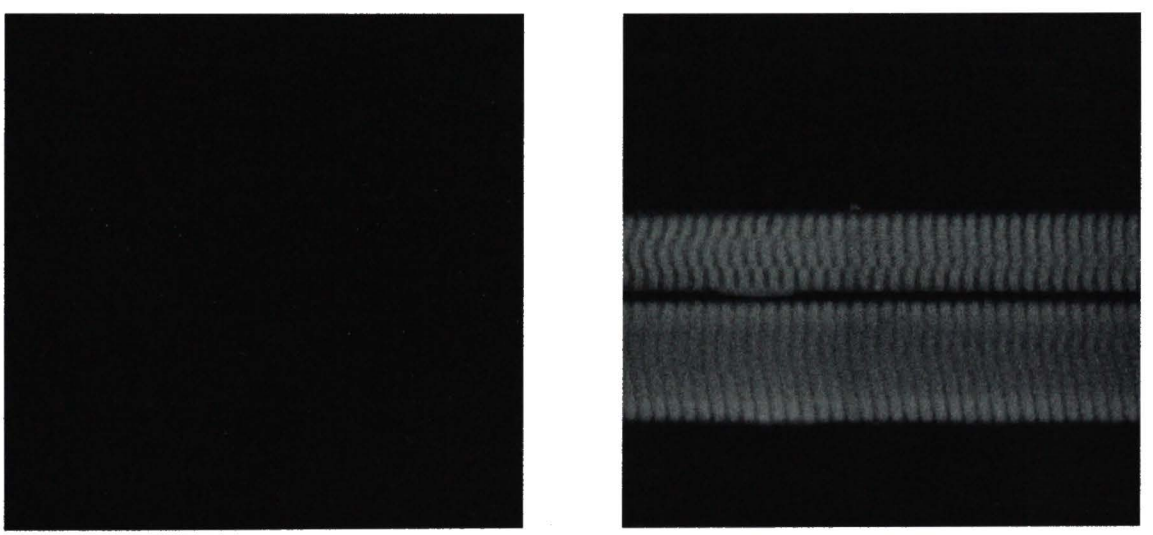

Figure 5. Unlabeled control fiber versus labeled fiber. Left: unlabeled fiber viewed with: 30x attenuation, 488nm and 364nm excitation. Right: 1-photon labeled with 42uM IATR-ELC under same viewing conditions.

Unlabeled vs. labeled fiber. To control for the fact that autofluorescence was not a factor, the experiment was be performed at 568 and 488 nm using a fiber that is not fluorescently tagged (**Figure 5**). A negligible amount of autofluorescence was detected. No response with measurement of anisotropy during flash photolysis was detected. Also, striations should not be visible using this wavelength. When a fiber was unlabeled and viewed under 568nm or 488nm excitation wavelength, no striations were present. This verifies that dyes conjugated to myosin specifically labeled myosin and that the labeled myosin conforms to the endogenous myosin's place in the A-band. The fact that no striations were seen and the screen was black indicated that the level of background autofluorescence was negligible. The control was performed after a fiber was triple-labeled with fluorescent rhodamine, actin, and ATP and measurements recording intensity of fluorescence taken. This ensured the instrumental setup was working to eliminate the possibility that no fiber was seen due to set-up error. This type of control was repeated on separate days using a different bundle of fibers and on 5 separate spots per isolated, mounted fiber.

The major controls for functionality of labeled RLC were: 1) Anti-RLC antibodies from Western blotting analysis recognized the protein sequence; 2) A striated pattern was visualized by confocal microscopy; 3) Force tension experiments of the RLC exchanged fiber showed the muscle contracts. These are reasonable conclusions that the protein is functional. The striated pattern visualized using confocal microscopy is supportive evidence that RLC selectively incorporates into the myosin thick filaments (the A-band) and not non-specific sites in the fiber.

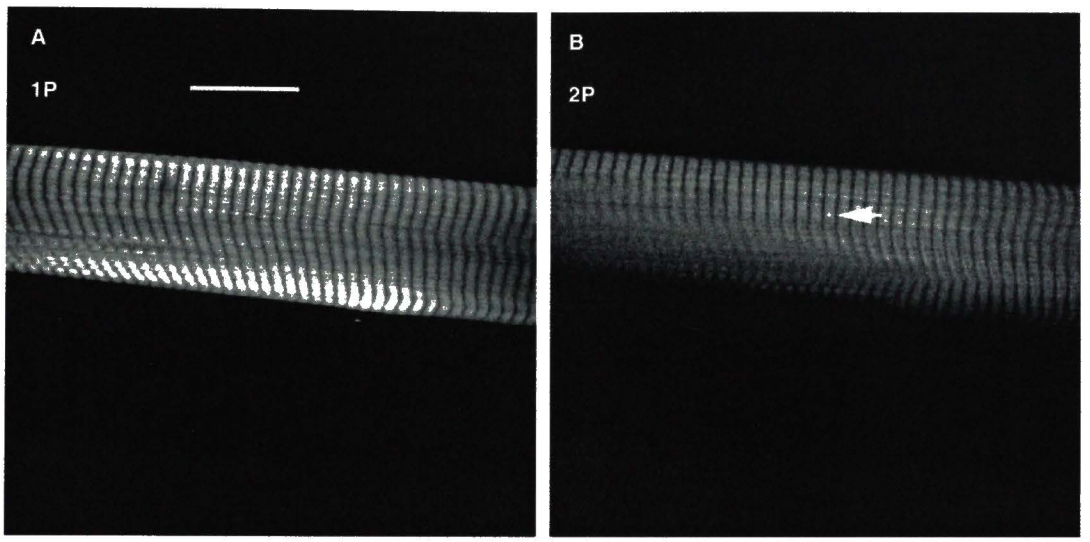

Figure 6. **A)** Confocal (1P) and **B)** 2P image of the same area of a muscle fiber labeled with IATR-RLC. To obtain a confocal image, the muscle was illuminated with 568 nm light and viewed through a 35 μm pinhole and LP 590 nm filter. To obtain a 2P image, the muscle was illuminated with 820 nm light and viewed without a pinhole. A 700 nm short-wavelength pass filter was used to block the intra-microscope reflections of the excitation beam. The two images represent slices through muscle ~2 μm apart, because the two images are not exactly parfocal. The bar=20 μm. The sarcomere length=2.62 μm. The round spot in B (pointed to by the arrow) shows the relative size of the illuminated spot.

1P and 2P spectra of IATR-RLC incorporated into myosin. The observational volume (and therefore number of observed cross-bridges) is smaller in 2P than in 1P experiment. 2P image has shallower depth of focus. **Figure 6** compares 1P and 2P images of muscle fiber. The entire fiber section (97 x 24 μm) was in focus using conventional 1P imaging (**Figure 6A**), but only the top portion was in focus using 2P imaging (**Figure 6B**).

Observed number of cross-bridges. The concentration of labeled cross-bridges was measured by comparing the fluorescence intensity of labeled fibers with the intensity of a capillary containing a known concentration of dye. In eight experiments using 1P excitation, fibers exchanged with 1.1 mg/mL ELC were 4.1 ± 1.4 (mean SE) dimmer than

a 10 μM solution of IATR rigor buffer. In eight experiments using 2P excitation, fibers were 5.9 ± 0.8 dimmer than dye alone. On average, fibers were 5.0 ± 0.8 dimmer than the known concentration of dye, i.e. the concentration of the dye in the fiber was 2 uM.

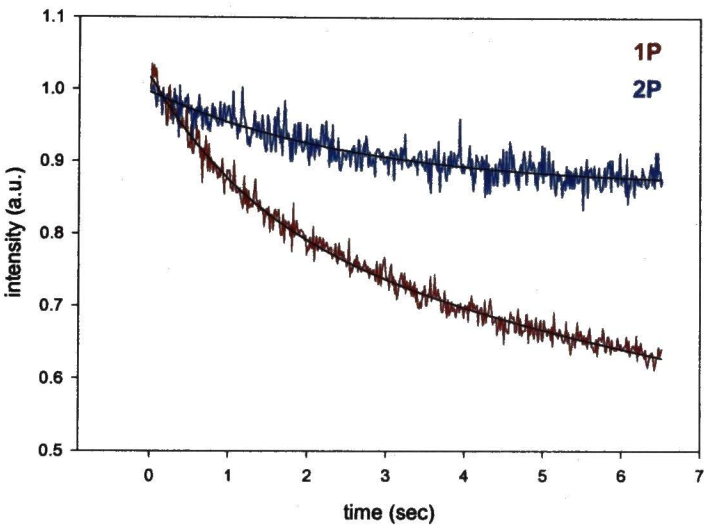

Figure 7. The photobleaching effect of muscle illuminated with visible (568 nm, red) versus IR (820 nm, blue) laser beams. The lasers had the same intensity as used in the experiments.

2P photobleaching. The rate of 2P photobleaching is lower in comparison with the rate of 1P photobleaching. **Figure 7** compares the rate of bleaching of a fiber illuminated with 568 nm (red line) and 820 nm (blue line) light. 1P intensities bleach faster than 2P intensities. The out-of-focus areas of a sample are known to bleach slowly (*9*) and although the intensities shown in the figure originate from the focal plane, 1P light scattering. Photobleaching of scattered light above and below the focal point is reduced more so than in 1P because the illumination volume is smaller. Unlike in 1P, photobleaching of the fluorophore in focal planes above and bellow the illumination

volume are eliminated because of the requirement for high photon density required for excitation to the excited state (*31, 32*).

Anisotropy of RLC: Muscle contraction was synchronized by depleting ATP from the isolated mounted fiber and adding just enough ATP in an in active form, such that when a short pulse of UV light illuminated a small spot on the fiber, the inactive form was converted into an active form of ATP. Enough ATP was released for one cross bridge cycle. The 2mM ATP used was in agreement with other similar studies (*33*) and the intracellular physiological ATP concentration (around 3-5mM). Upon ATP binding, hydrolysis and release of ADP, the ADP diffuses away and is not regenerated. This is in agreement with other reports where rhodamine probes bound to chicken gizzard RLC at the single cysteine 108 within muscle fibers changed their orientation promptly when ATP was released from caged ATP (*29*). **Figure 8** shows a representative graph of recombinant RLC labeled with 5-iodoacetamidofluorescein (Molecular Probes, Eugene, OR). The blue line represents anisotropy, or the ratio of the emission intensities measured via polarizers in the horizontal and vertical position. The graph began at the left where anisotropy is at a certain value because the fiber is in rigor (3 to just prior to 3.4 seconds). At around 3.4 seconds, the line dipped down, signifying the pulse of UV light (red arrow) which was administered for 10 milliseconds, releasing ATP from its caged precursor. This synchronized and initiated a cross bridge cycle that resulted in the RLC on myosin detaching from actin. The most likely reason for the decrease is dissociation of S1 from actin (*16, 29*). The slow creep upward is the re-association of cross bridges to rigor again as ATP is hydrolyzed and diffuses away. The fast phase

was the spike downwards and corresponded to the rate of dissociation of the myosin from actin. The slow phase was the curve after this that returned back to original anisotropy. This corresponded to the rate of re-association of the cross-bridges of myosin heads to actin. It is called slow and fast phase because the dissociation is fast, compared to the rate of re-association which is slower (*16, 34*). Horiuti (*35*) also observed slow changes in the intensity of X-ray reflections following single turnover of ATP. A cross-bridge that finished a turnover cycle may act as a load for cross-bridges that still did not complete the cycle.

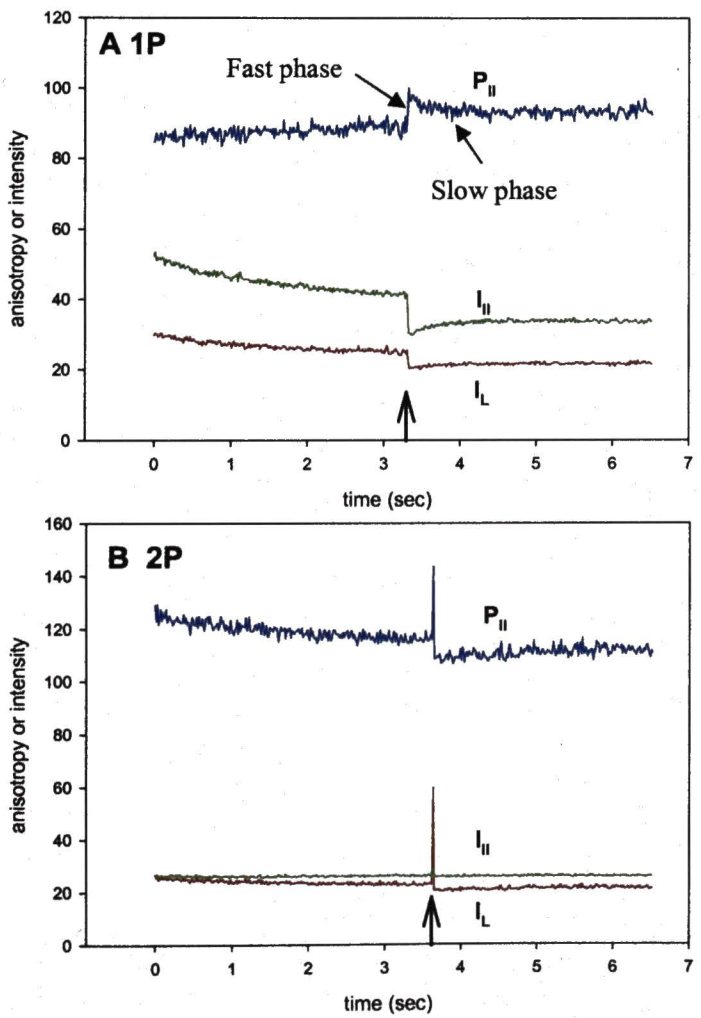

Figure 8. Orthogonal intensities ($I_\perp$ red; $I_\parallel$ green) and parallel anisotropy (blue) of a muscle fiber containing IATR-RLC. To adjust anisotropy values to the same scale as polarized intensities, it is plotted as $R_\parallel(t)=[(\parallel I_\perp(t)-\parallel I_\parallel(t))/(\parallel I_\perp(t)+2\parallel I_\parallel(t))]*256+128$, where $\parallel I_\perp(t)$, and $\parallel I_\parallel(t))$ are the instantaneous fluorescence intensities at time t. **A)** 1P signal, **B)** 2P signal.

Figure 8A is consistent with earlier results (*2*) for 1P analysis where anisotropy (blue) changed rapidly and later recovered slowly to the original level[2]. **Figure 8B** shows the time course of anisotropy change of 2P signal from the adjacent area of the same muscle fiber. The polarization of the IR laser illuminating the muscle was parallel to the fiber axis. The UV pulse is much more prominent in the 2P than in 1P experiment because no confocal aperture or emission filters were used. The anisotropy changed rapidly and recovered slowly to the original level. The rate of rapid change was too fast to measure.

Although photobleaching in 2P experiments is slower than in 1P experiments, it is not altogether absent. To correct for photobleaching, the data was fit to a single 3 parameter exponential and the fit subtracted from the raw data. The same was done for 1P anisotropy, allowing direct comparison between the two. The result is shown in **Figure 9A.** The S/N ratio, defined as a ratio of anisotropy change to the SD of the signal before the flash, was 4.3 and 5.1 for 2P and 1P experiments, respectively. In this, and 5 other experiments the difference in S/N was not statistically significant.

---

[2] $I_{\perp}$ and $I_{\parallel}$ change in the same direction. Whether they change in the same or opposite direction depends on the cross-bridge angle (29). Orthogonal anisotropies, not intensities, must change in opposite directions.

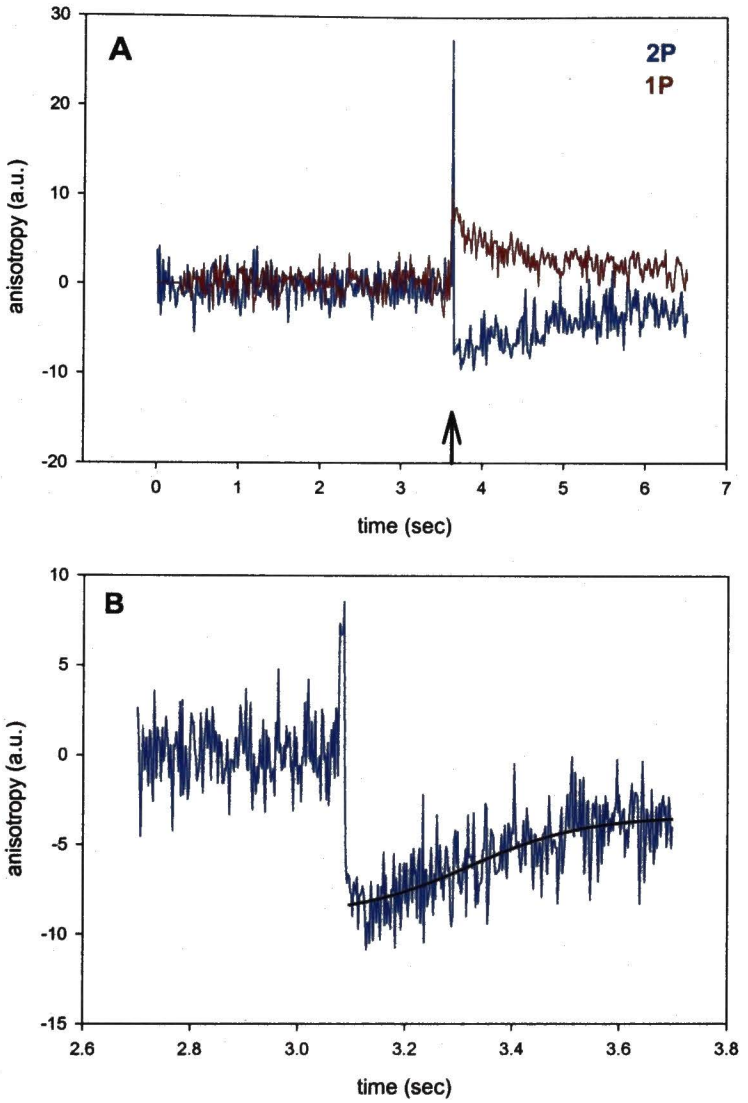

Figure 9. Anisotropy of 1P and 2P IATR-RLC and 2P IATR-ELC. **A)** Comparison of 1P (red) and 2P (blue) parallel anisotropy of muscle myosin labeled with IATR-RLC. To correct for photobleaching, the anisotropy data were fitted by a single 3 parameter exponential functions ($114.0+11.3e^{-0.450t}$ and $85.9+16.6(1-e^{-0.007t}$ for 2P and 1P, respectively). The fitted data was subtracted from the original data, so the curves normalized to 0.

B) 2P parallel anisotropy of muscle exchanged with IATR-ELC (blue). The rising phase of the signal was fitted to a three parameter sigmoidal (black) $r_1 = -8.97+5.58/(1+\exp-((x-3.32)/0.11))$.

The sigmoidal recovery of 2P signal (**Figure 9**): The anisotropy recovery curve is a superposition of step-like individual responses such as shown in Figure 1 and it should therefore reflect a power stroke. While the overall time courses of 1 & 2P anisotropy signals are similar (**Figure 9A**), the anisotropy during the 1P mode always rises after the UV pulse and then decays exponentially to the origin. In the 2P mode, anisotropy changes rapidly and then remains approximately constant for a few hundred milliseconds

before relaxing back to the origin. This is a sigmoidal character of the recovery and was present both in ELC and RLC labeled fibers. A typical record is shown in **Figure 9B**. The data has been detrended and fitted to a three-parameter sigmoidal. The average ± SE of the time that the inflection occurred after the creation of ATP for ELC was 165 ± 31 msec (n=10). The sigmoidal inflection in the fibers exchanged with Rh-RLC occurred approximately 245 ± 45 msec (n=10) after the creation of ATP. The sigmoidal shape was slightly more noticeable with fluorescent ELC experiments, as the number of observed cross-bridges labeled with ELC was less because the degree of labeling of the fiber was smaller. It makes sense that the inflection for ELC could occur sooner than for RLC, because RLC has further to swing since it is located more distal on the lever arm.

Anisotropy of ELC: Anisotropy transient is observed after application of 10 msec UV-light pulse to produce ATP (**Figure 10**). Just enough caged ATP is added to bind to myosin and calculations and experiments performed by my lab indicate virtually all caged ATP is converted to ADP via the myosin ATPase (*16*). Thus, soon after application of a pulse there is practically no free ATP in the experimental volume because it has been hydrolyzed to ADP. The sole nucleotide remaining in the volume is the one bound to the cross-bridges. The anisotropy change following the pulse reflects the rotation induced by a turnover of a single molecule of ATP. In a typical experiment (see also Chapter 1 methods), Ca^{2+}-rigor solution containing 2 mM caged ATP is added to the fiber. A 10 msec pulse of UV light is applied 2-4 sec after the beginning of the

experiment. The laser beam is focused on a selected spot within the muscle fiber for 6.55 sec. This can cause considerable photobleaching with 1 photon excitation. The problem is aggravated by the fact that the same fluorophores remain in the beam throughout the entire time, i.e. they do not get replenished through free diffusion. The photobleaching is the reason why in some of the graphs, the anisotropy curve displayed an upward trend prior to flash photolysis. Anisotropy changes consist of a fast decrease followed by a slow increase. The fast drop of anisotropy was also contributable to the fraction of heads undergoing dissociation from the actin filament. This is because all the cross-bridges are originally attached and therefore detach at the same/similar time. There comes a time, however, when the fraction undergoing dissociation during each time increment decreases sharply because a significant number of heads are already dissociated. This is followed by the slow recovery of the dipole to its original orientation.

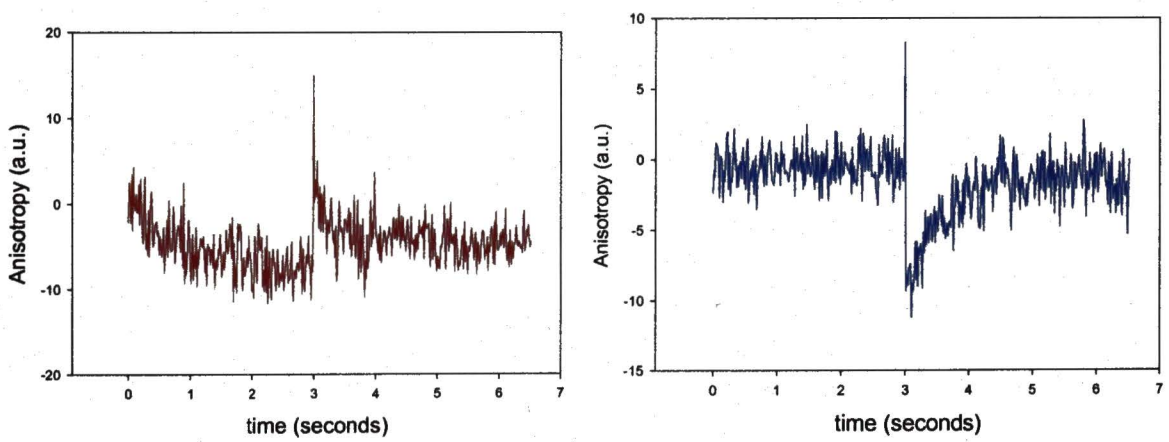

Figure 10. Anisotropy of 1P and 2P IATR-ELC. Left (red): 1P anisotropy of Rhodamine-labeled ELC. Right (blue): 2P anisotropy of Rhodamine-labeled ELC. Although both have been detrended to account for photobleaching, the 1P trace shows more photobleaching. Anisotropy measured in arbitrary units (a.u.).

Anisotropy is not within the limit for fluorophores of -0.4 to 0.4 for 1P and -0.57 to 0.57 for 2P (values from (*36*)) on the y-axis because the actual value for anisotropy was anisotropy*256+128 in order to fit all three lines onto one screen. If the additional functions were not added, then the anisotropy would fall within these limits. The traces were set to zero to account for photobleaching in the same manner as described for RLC in Figure 9. In 10 experiments using ELC, the average half times of re-association were 125±20 msec. In similar experiments, tension decreased from the rigor for approximately 20 msec, suggesting detachment of the cross-bridges, and then increased over the next 100-200 msec as cross-bridges reattached and generated force (*37, 38*).

DISCUSSION

The anisotropic response of fluorescently labeled RLC and ELC using 1P and 2P laser scanning microscopy was measured. The change in anisotropy of the regulatory domain is in agreement with the current model of lever arm movement as a force transducer (*39*). Mutations in RLC reduce step size of myosin against actin filaments (*40*). The rotational motion of RLC is different from the catalytic domain as shown by time-resolved phosphorescence anisotropy (*41*). Changes in rotation of RLC were also detected using chicken gizzard exchanged into rabbit psoas muscle using bifunctional rhodamine as a cross-linker (*42*). The advantage in this experiment was that bifunctional rhodamine allowed more rotational angles to be measured. However, static measurements could only be derived because the muscle was not activated to execute any cross-bridge cycles. The lever arm hypothesis is also supported by this data, as both

ELC and RLC showed anisotropy. The rotation of ELC and RLC in vivo supports the movement of the regulatory domain as present and necessary, and correlates well with *in vitro* data in which mutations in ELC reduce both sliding filament velocity (the velocity at myosin translocates actin filaments ATPase activity) (*43*) and data where removal of one or both light chains caused reduction in sliding filament velocity without altering the ATPase activity (*27*). The present results also correlate with studies in which chicken gizzard RLC (containing only one cysteine) labeled at Cys 108 was exchanged into a single skinned rabbit psoas fiber and fluorescence polarization transients measured, which revealed rotation of the lever arm at this site (*44*). A criticism of this work is that using a sequence whose amino acid sequence has point mutations is altering the protein itself. However, other reports using this clone shows the ATPase activity (*12*) is maintained. Also, chicken pectoralis skeletal RLC is expressed in rabbit psoas skeletal muscle. However, the sequences are 90% identical by doing a BLAST search on Pubmed.

ATP displacement from S1 in myofibrils has a rate constant of 0.3 s^{-1} to 0.7 s^{-1} (*45*). The range indicates that nucleotide displacement depends on shortening velocity. The rate can be estimated from displacement of fluorescent nucleotides bound to cross-bridges by flash photolysis of caged ATP (*46*). The ATP photolyzed in our experiments occurs quickly enough to observe the effects of synchronizing a single cross-bridge cycle.

The energy flux of UV light (0.0167 mJ/ μm^2) is not damaging to the muscle. The power of the UV light used to photolyse ATP impinging on the muscle was

measured with a power meter and was approximately 100-200 μW. This was the same for 1P and 2P. The energy flux was calculated as follows:

-- 0.1mW = 0.1mJ/sec (power = work/time)
-- UV shutter duration time = 10msec
-- Energy of UV light is 0.1mJ/sec x 0.01sec = 0.001mJ
-- Area of UV beam impinging on the muscle = 0.2μm x 0.3 μm or 0.06μm^2
-- Energy flux impinging on the muscle = 0.001mJ/0.06μm^2 or 0.0167mJ/μm^2

Therefore, this flux is not significant enough to endanger the muscle by virtue of using UV light.

Around 500 fluorescently labeled RLC molecules can be visualized using 1P, calculated as follows:

-- Concentration of myosin in frog satorius skeletal = 120uM (*47*).
-- 1M (molar) = 6.022 x 10^{23} molecules/liter
-- 120uM = 7.2x10^{9} myosin molecules/liter
-- Number of myosin molecules in the illuminated volume of a fiber:
7.2x10^{9} myosin molecules/liter x 0.310^{-15} liters = 21600
-- RLC = 12% labeled as IATR-RLC
-- Theoretical # of fluorescently labeled myosin molecules 0.012 x 21600 = 2592
-- Assume 20% efficiency of exchange, based on exchange experiments
-- Actual # fluorescently labeled myosin molecules = 0.2 x 2592 = 500

Around half as many fluorescently labeled molecules are visualized using 2P, because the photon density decreases the illumination volume to about half (based on fluorescent microspheres experiment in Chapter 1, Figure 13).

In the present experiments, anisotropy did not return to the original position as would be expected to complete a cross-bridge cycle. In a similar experiment where polarization transients were measured from a probe on RLC and made to undergo cross bridge cycling via application of rapid length steps, the transients also did not return to the original position, though no direct explanation was offered (*48*). One possibility might be that because contraction is initiated at one time, one cross-bridge that has completed its cycle does not have any more ATP to undergo a second cross bridge cycle and therefore will stay attach to the actin monomer, thereby presenting a load to the next cross-bridge, which slows its rate of return.

No clear powerstroke was observed with 1P analysis. One reason for this was that the population of observed cross-bridges was still too large. If a small enough population of cross-bridges were perfectly synchronized, the anisotropy of lever-arm would be expected to change in three steps as illustrated in Figure 1. In a normal contracting muscle, each cross-bridge has its only rate of cross bridge dissociation, weak attachment and strong attachment to actin. Therefore, the muscles may not be completely synchronized, within the illumination volume observed here, and anisotropy may result from averaging of signals. Researchers of similar experiments admit that interpretation of data during an active isometric contraction also requires consideration of a population of heads as being in different mechanical states (*48*). Also, the cDNA for RLC contained an inadvertent mutation F103L (40) and a recent paper showed that this reduced the step-size (power-stroke) during *in vitro* motility studies0, although the myosin ATPase was not affected. Hence the powerstroke in our experiments may be

smaller and therefore not as detectable for such a movement that ordinarily one would expect more from. The resolution of each step in cross-bridge cycle *in vivo* will be possible when a single cross-bridge within contracting muscle fiber can be followed.

Reports indicate that the change in angle of the lever arm is 3-5° (*30, 44, 48, 49*), while others detect an angle of 30° (*30*). No measurement of angle was made in this experiment and it would be interesting to be able to make such a calculation.

This experimental set-up cannot measure rotations in the azimuthal plane. However, it is unlikely that the rotational motion of the lever-arm occurs exclusively in the azimuthal plane.

In summary, the present experiments show that rotation of fluorescently labeled ELC and RLC were detected by 1P and 2P analysis of anisotropy. 2P microscopy provided a means to better resolve the power stroke of a cross-bridge in contracting muscle. The power stroke demonstrated itself as a sigmoidal change of anisotropy. On the average, the power stroke occured ~200 msec after the binding of ATP to fibers in the rigor state.

ACKNOWLEDGMENTS

Supported by NIH R21CA9732 and RO1AR048622 and by the grant 000130-0008-2001 from Texas Higher Education Coordinating Board and NCRR (RR-08119). Dr. Irina Akopova, Ph.D. and Ms. Disha Dumka provided expert technical assistance in determination of fiber viability in the force-tension experiments.

REFERENCES

1. Roopnarine, O., Szent-Gyorgyi, A. G., and Thomas, D. D., Microsecond rotational dynamics of spin-labeled myosin regulatory light chain induced by relaxation and contraction of scallop muscle, *Biochemistry, 37*, 14428 (1998).
2. Borejdo, J., and Akopova, I., Orientational Changes of Cross-Bridges During Single Turnover of ATP, *Biophys. J., 84*, 2450 (2003).
3. Baker, J. E., Brust-Mascher, I., Ramachandran, S., LaConte, L. E., and Thomas, D. D., A large and distinct rotation of the myosin light chain domain occurs upon muscle contraction, *Proc Natl Acad Sci U S A, 95*, 2944 (1998).
4. Smyczynski, C., and Kasprzak, A. A., Effect of nucleotides and actin on the orientation of the light chain-binding domain in myosin subfragment 1, *Biochemistry, 36*, 13201 (1997).
5. Eigen, M., and Rigler, R., Sorting single molecules: application to diagnostics and evolutionary biotechnology, *Proc Natl Acad Sci U S A, 91*, 5740 (1994).
6. Brown, L. J., Klonis, N., Sawyer, W. H., Fajer, P. G., and Hambly, B. D., Independent movement of the regulatory and catalytic domains of myosin heads revealed by phosphorescence anisotropy, *Biochemistry, 40*, 8283 (2001).
7. Warshaw, D. M., Hayes, E., Gaffney, D., Lauzon, A. M., Wu, J., Kennedy, G., Trybus, K., Lowey, S., and Berger, C., Myosin conformational states determined by single fluorophore polarization, *Proc Natl Acad Sci U S A, 95*, 8034 (1998).
8. Shepard, A., and Borejdo, J., Correlation between mechanical and enzymatic events in contracting skeletal muscle fiber, *Biochemistry, 43*, 2804 (2004).
9. Pawley, J. B. e., "Handbook of Biological Confocal Microscopy". *Plenum Press, , NY & London*, Second Edition. (1995).
10. Wolff-Long, V. L., Saraswat, L. D., and Lowey, S., Cysteine mutants of light chain-2 form disulfide bonds in skeletal muscle myosin, *J Biol Chem, 268*, 23162 (1993).
11. Laemmli, U. K., Cleavage of structural proteins during the assembly of the head of bacteriophage T4, *Nature, 227*, 680 (1970).
12. Wolff-Long, V. L., Saraswat, L. D., and Lowey, S., Cysteine mutants of light chain-2 form disulfide bonds in skeletal muscle myosin, *J Biol Chem, 268*, 23162 (1993).
13. Ushakov, D. S., Conformational transitions in myosin subfragment-1, in *Biochemistry*, Universitiy of North Texas Health Science Center, Fort Worth, pp. 72 (2000).
14. Ling, N., Shrimpton, C., Sleep, J., Kendrick-Jones, J. & Irving, M., Fluorescent probes of the orientation of myosin regulatory light chains in relaxed, rigor, and contracting muscle., *Biophys. J., 70* 1836 (1996).
15. Tang, D. C., Stull, J. T., Kubota, Y., and Kamm, K. E., Regulation of the Ca2+ dependence of smooth muscle contraction, *J Biol Chem, 267*, 11839 (1992).
16. Borejdo, J., Ushakov, D. S., and Akopova, I., Regulatory and essential light

CHAPTER 3

CORRELATION BETWEEN MECHANICAL AND ENZYMATIC EVENTS IN CONTRACTING SKELETAL MUSCLE FIBER

A. Shepard & J. Borejdo

Dept of Molecular Biology and Immunology

University of North Texas

3500 Camp Bowie Blvd, Fort Worth, TX 76107

Biochemistry. 2004 Mar 16;43(10):2804-11

Rationale:

The previous chapter contained information showing anisotropy of myosin ELC and RLC. In my next question, whether there was a correlation between dissociation of ATP and mechanical rotation of S1 during the cross bridge cycle was investigated. The existing conventional view pioneered by Huxley in 1968 and Lymn and Taylor in 1971 showed that ATP hydrolysis corresponded with one cross bridge cycle, and therefore the myosin head detached and reattached to actin only once per cycle. However in the 1990s, other researchers such as Yanagida's lab, showed that splitting of one ATP was enough energy for one myosin head to execute multiple cross bridge cycles. Therefore, a working hypothesis to test whether splitting of one molecule of ATP corresponds to a single rotation of the lever arm.

A fiber in rigor was co-labeled with fluorescent RLC and enough fluorescent nucleotide for a single turnover of ATP, then monitoring over time how many rotations of the lever arm occurred per that one nucleotide released. The same protocol to exchange in rhodamine labeled RLC was used as described in Chapter 1; this is the mechanical signal. When fluorescent Alexa ATP is perfused into the fiber, it attaches to the myosin and hydrolyzes to ADP. A brief pulse of non-fluorescent caged ATP is released from its precursor and which displaces the fluorescent ADP and synchronizes one cross-bridge cycle. The anisotropy of this fluorescent ADP as it comes off the myosin head is the enzymatic signal. In the following text, "tightly coupled" means that one dissociation of ATP is required for one myosin head to produce force. "Weakly coupled" denotes that not every cross-bridge that attaches to actin requires an ATP in order to detach.

ABBREVIATIONS

Caged-ATP: 5-dimethyoxy-2-nitrobenzyl-caged ATP

Alexa-ATP: adenosine 5'-triphosphate, Alexa Fluor® 647 2'-(or-3')-O-(N-(2-aminoethyl)urethane), hexa(triethylammonium) salt

RD: the regulatory domain of myosin

CD: the catalytic domain of myosin

S1: myosin subfragment-1

RLC: regulatory light chain

Rh or IATR: 5'-iodoacetamido-tetramethyl-rhodamine

Rh-RLC or IATR-RLC: RLC labeled with 5'-iodoacetamido-tetramethyl-rhodamine

Alexa-myosin: myosin containing Alexa-ADP at the active site

ABSTRACT. The conventional hypothesis of muscle contraction postulates that the interaction between actin and myosin involves tight coupling between the power stroke and hydrolysis of ATP. However, some *in vitro* experiments suggested that hydrolysis of a single molecule of ATP caused multiple mechanical cycles. To test whether the tight coupling is present in contracting muscle, we simultaneously followed mechanical and enzymatic events in a small population of cross-bridges of glycerinated rabbit psoas fibers. Such a small population behaves as a single cross-bridge when muscle contraction is initiated by a sudden release of caged ATP. Mechanical events were measured by changes of orientation of probes bound to the regulatory domain of myosin. Enzymatic events were simultaneously measured from the same cross-bridge population by the release of fluorescent ADP from the active site. If the conventional view were true, ADP desorption would occur simultaneously with dissociation of cross-bridges from thin filaments, and would be followed by cross-bridge rebinding to thin filaments. Such a sequence of events was indeed observed in contracting muscle fibers, suggesting that mechanical and enzymatic events are tightly coupled *in vivo*.

According to the conventional hypothesis of muscle contraction, the enzymatic chemistry and mechanics of myosin cross-bridges are tightly coupled, because hydrolysis of one molecule of ATP causes one swing of the regulatory domain (RD, also referred to as lever arm) of myosin subfragment-1. This view has been challenged by some *in vitro* experiments that suggested that hydrolysis of one ATP molecule is responsible for multiple mechanical cycles, resulting in myosin step size being many times larger than the dimension of a cross-bridge (*1, 2*). The absence of tight coupling between enzymatic and mechanical events was directly demonstrated by measuring both events simultaneously in a single myosin molecule *in vitro* (*3*).

While much information regarding the mechanism of the cross-bridge cycle has been made possible through *in vitro* studies (*3-5*), it is not certain that cross-bridges in functioning muscle behave like purified proteins in solution. The mechanism that may be responsible for different properties of myosins in solution versus muscle fibers is molecular crowding. Crowding influences protein solubility and conformation in solution (*6, 7*). Molecular crowding provides a rationale for the two distinct myosin cross-bridge orientations in rigor, which were observed to form at different degrees of saturation of actin filaments with myosin subfragment-1 (*8, 9*).

In the present work we asked whether the tight coupling exists in cross-bridges of contracting muscle fiber. Under ideal circumstances such experiments should be done on a single cross-bridge, to avoid averaging of asynchronous signals from large population of molecules. This

can be done *in vitro* by diluting solution of myosin, but in muscle this condition can only be approximated by collecting data from a small number (200-600) of cross-bridges, a circumstance that assures synchrony for at least 100 msec after sudden release of ATP from a cage (*10*). In this work, we measured simultaneously mechanical and enzymatic events in the same small population of cross-bridges that were synchronized by a sudden release of caged ATP.

The mechanical events were followed by measuring orientation changes of the regulatory domain (RD) of myosin subfragment-1 (S1). S1 consists of the N-terminal, globular catalytic domain and the C-terminal, α-helical regulatory domain. Recent evidence has confirmed earlier suggestions (*11, 12*) that the catalytic domain does not rotate during contraction, and thus a consensus has emerged that rotation of the regulatory domain around a pivot at Gly 699 (*13*) is responsible for cross-bridge cycle (*14-20*). The present experimental design is based on the fact that polarization of fluorescence (or anisotropy) of fluorescent probes bound to the regulatory domain of myosin reflect rotations of the RD (*10, 21, 22*).

Enzymatic events were followed by measuring the rate of dissociation from cross-bridges of Alexa-ADP, a fluorescent analog of ADP. Fluorescent ADP is displaced from the active site of myosin by excess of non-fluorescent ATP produced from caged precursor by a brief UV pulse. The rate of this release is measured by the rate of increase of rotational mobility of Alexa-ADP. The rotational mobility of a small ligand increases when it is released from a

large protein (*23, 24*). The rate of release of ADP reflects the rate of shortening of muscle (*25*). The displacement technique was first used by Bagshaw and collaborators (*26, 27*) who used changes of intensity of fluorescence of Cy3-EDA-ATP as a measure of ATPase of myofibrillar myosin.

The present results revealed that *in vivo* mechanical and enzymatic events occurred simultaneously, and that the lever arm rotated once for every molecule of ATP split. This suggests that rotations of cross-bridges are tightly coupled to the chemical events at the active site.

MATERIALS AND METHODS

Chemicals and solutions. Standard chemicals and nucleotides were from Sigma (St. Louis, MO). 5-dimethyoxy-2-nitrobenzyl-caged ATP (DMNPE-caged ATP), adenosine 5'-triphosphate, Alexa Fluor® 647 2'-(or-3')-O-(N-(2-aminoethyl)urethane) (Alexa-ATP) and 1-(4,5-dimethoxy-2-nitrophenyl)-1,2-diaminoethane-N,N, N',N'-tetraacetic acid (DMNP-EDTA) and 5'-iodoacetamido-tetramethyl-rhodamine (IATR) were from Molecular Probes (Eugene, OR). Ca-rigor solution contained 50 mM KCl, 4 mM $MgCl_2$, 0.1 mM $CaCl_2$, 1 mM DTT, 10 mM TRIS buffer pH 7.5. All solutions used in the photolysis experiments contained 10 mM reduced glutathione. The glycerinating solution contained 80 mM K-Acetate, 0.2 mg/mL PMSF, 2 mM mercaptoethanol and 50% glycerol.

Preparation and mounting of muscle fibers. Isolated muscle fibers were prepared from glycerinated rabbit psoas muscle bundles by dissecting single fibers in glycerinating solution and attaching the ends of the tautly stretched fiber to aluminum clips glued to the microscope cover-slip. The cover-slip fit into a 22mm x 22mm x 0.2mm home-made perfusion temperature controlled chamber (volume =100 μL). Mounted fibers were thoroughly washed with Ca-rigor solution and covered with a cover slip.

Preparation of the regulatory light chain. Rabbit myosin was prepared from back and leg muscles by the method of Tonomura et al. (*28*). RLC containing a single cysteine at position 73 (*29*) was prepared by expression of RLC in a pT7-7 plasmid in BL21(DE3) cells. The construct was a gift from Dr S. Lowey (University of Vermont). A one liter culture was prepared and RLC isolated as described (*30*).

Labeling of RLC. Newly purified RLC in 10 mM KP_i buffer pH 7.5 & 2 mM DTT was dialyzed overnight at 4°C against 50 mM KCL, 10 mM TRIS-Cl pH 7.5. RLC was incubated with a 10 fold excess of 5'-IATR for 7 hrs on ice in the dark. Excess IATR was removed by overnight dialysis at 4°C against 50 mM KCl, 20 mM EDTA, 0.01 M KP_i buffer pH 7.0 and 0.5 mM DTT. The degree of labeling was 14%.

Labeling myosin with IATR-RLC. Labeled RLC was exchanged into fibers as described earlier (*31*). Briefly, a fiber was mounted on the coverslip, thoroughly washed with Ca-rigor solution and incubated with 100 μL 35 μM RLC in 50 mM KCL, 20 mM EDTA, 0.5 mM

DTT, 10 mM KP_i pH 7.0 for 30 min in the dark at 0°C. The fiber was rinsed 3 times with 100 μL Ca-rigor. Then, 50 μL of 2 mM caged ATP in Ca-rigor plus 10 mM glutathione was added and the muscle was covered with a coverslip. The concentration of fluorophore incorporated into muscle was estimated by comparing fluorescent intensity of fiber with the intensity of known concentration of free IATR-RLC. Fluorescence of the fiber viewed with a wide-field microscope using a 10x (NA=0.22) objective was equal to fluorescent intensity given by ~ 2 μM of free IATR-RLC. The number of myosin molecules observed by the confocal microscope is equal to this concentration multiplied by the experimental volume. The width and depth of the observational (confocal) volume are approximately equal to the diffraction limit (~0.3 μm) of the focused laser beam. Its height is limited by the confocal aperture (1.35 Airy units) to ~3 μm, giving the volume of 0.3 μm^3. There are ~400 fluorescent myosin molecules in this volume.

Labeling of myosin active site with Alexa-ATP. A muscle fiber was incubated with 0.1 μM Alexa-ATP in Ca-rigor for 10 min at room temperature. Excess dye was washed out with Ca-rigor solution. The degree of incorporation of Alexa-ATP into fiber was estimated by comparing the intensity of fluorescence of known concentration of the dye with the fluorescence of labeled fibers, like in the case of labeling with IATR-RLC. Typically 2-3 μM of myosin was labeled. There are ~500 myosin molecules labeled with Alexa-ADP in this volume.

Functionality of exchanged fibers. Tension development was studied by a MKB force transducer (Scientific Instruments, Heidelberg, Germany) coupled to an analog counter (Model 6024E, National Instruments, Austin, TX). Control (unlabeled) fibers developed 0.94±0.05 mN/fiber (mean±SEM, n=32) maximum isometric tension. Fibers exchanged with RLC fluorescently labeled at Cys 73 developed 0.96±0.03 mN/fiber tension. The lack of effect of exchange on tension is consistent with previous experiments with such fibers (*32*) and with experiments that used chicken gizzard RLC labeled at Cys108 (*21, 29, 31*). Likewise, labeling the myosin active site with ATP analogs had no effect on tension induced by normal ATP. Fibers labeled with 3 μM Alexa-ATP developed 0.92±0.02 mN/fiber (n=7) of tension. Fibers stimulated with 0.2 mM Alexa-ATP developed 0.68±0.14 (n=5) mN/fiber. The ATP turnover of myofibrils stimulated by control (regular) ATP was 1.8 sec^{-1}. The ATP turnover of myofibrils stimulated by Alexa-ATP was within 90% of control.

Experimental arrangement. The instrument to measure anisotropy of fluorescence was described elsewhere (*10, 22*). The current set-up differs from the earlier one in that the laser spot is not scanned and that the 633 nm excitation and Cy5 emission filters have been added to detect fluorescent ADP. Briefly, the experimental chamber was placed on stage of the confocal microscope (Zeiss, LSM 410, Thornwood, NY). A 633 nm visible light from a He/Ne laser was selected by the line selection filter to excite Alexa-ATP. A 568 nm light from Ar/Kr laser was selected by another line selection filter to excite IATR-RLC. The polarization of the laser beam could be rotated by a λ/2 plate and directed by the dichroic mirror onto an objective (Zeiss C-Apo, 40x, Numerical Aperture (NA)=1.2, water

immersion). The UV beam of an argon laser operating at 364 and 351 nm was used to photolyze the caged–nucleotide.

Photogeneration of ATP. The mounted muscle fiber was perfused with 2 mM of 5-dimethyoxy-2-nitrobenzyl-caged ATP (DMNPE-caged ATP). The UV beam was focused by the objective to a Gaussian spot with width and length equal to twice the lateral resolution of the UV beam (about 0.2 μm). The height equaled 3 μm. ~3 sec after beginning the scan, a shutter admitting the UV light was opened for exactly 10 msec. The energy flux through the illuminated area during the time ATP stayed in the experimental volume (~300 μsec) was 9 x 10^{-4} mJ/μm^2. The amount of released ATP was enough for a single turnover of ATP.

Anisotropy of solutions. Absorption spectra were measured in the Ca^{2+}-rigor buffer at room temperature in a Beckman DU650 absorption spectrophotometer. Fluorescence intensities were measured in an ISS K2 spectrofluorometer (Champaign, Illinois). Polarized fluorescence intensities were collected using Glan-Thompson polarizers in the excitation and emitted light paths. Excitation was vertically polarized. Experiments were done at 0°C in the Ca^{2+}-rigor buffer. Experiments on immobilized Alexa-ATP were performed at 0 °C in 90 % glycerol. All samples used in fluorescence measurements had absorption of <0.1.

Fluorescence intensity and anisotropy of fibers. Fluorescence was measured with a high aperture lens (C-Apo, 40x, NA=1.2) using confocal microscopy. Different sensitivities of detectors were compensated by adjusting photomultiplier voltages (in our microscope

detector #2 is 18% more sensitive than detector #1). Calculations showed that high NA of the objective causes minimal distortion to the polarized intensities (*33*).

The subscripts before and after the intensity indicate the direction of polarization of excited and emitted light relative to the axis of the muscle fiber. Perpendicular anisotropy was recorded with the λ/2 plate in place. The muscle axis was oriented horizontally on a stage of a microscope. Channels 1 & 2 recorded ${}_{\perp}I_{\perp}$ & ${}_{\perp}I_{\parallel}$, respectively. Parallel anisotropy was recorded with the λ/2 absent. Channels 1 & 2 recorded ${}_{\parallel}I_{\perp}$ & ${}_{\parallel}I_{\parallel}$, respectively. The absolute anisotropies are $r_{\perp}$ = (ch1-ch2) / (ch1+2*ch2) and $r_{\parallel}$ = (ch2-ch1) / (ch1+2*ch2).

RESULTS

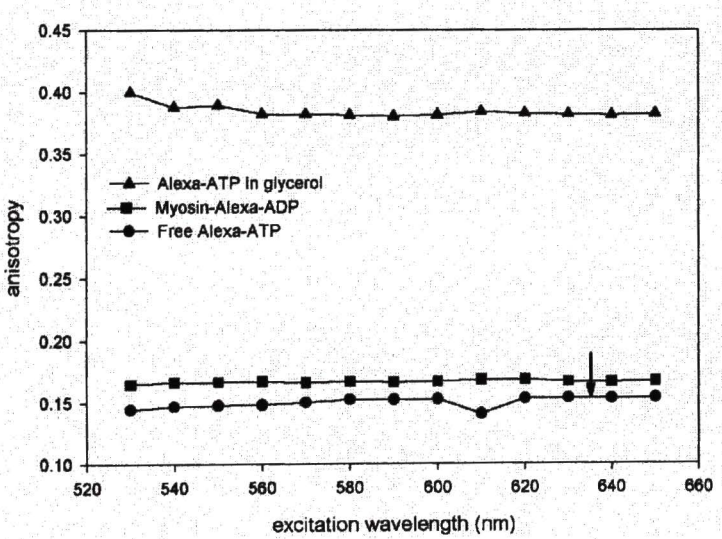

Figure 1. Excitation anisotropy of Alexa-ATP. Alexa-ATP immobilized in 90% glycerol at 0°C (▲), Alexa-ADP bound to myosin at low (100 mM) ionic strength (■) and free Alexa-ATP in Ca-rigor solution at 0°C (●). 1 μM Alexa-ATP, 2 μM myosin heads, λ_{em}=670 nm. Excitation slit=2 mm, emission. slit=1 mm. Arrow indicates the observed transition. All measurements at 0°C.

Enzymatic signal: This signal arises from the release of myosin bound Alexa-ADP to solution. Normally, free and bound dye should have different anisotropies (*23*). However, in

our case is not certain that this is so. Myosin-bound Alexa-ADP may be rotationally mobile, and it may have large residual anisotropy due to a short fluorescent lifetime[1]. The Perrin's equation is: $r = r_o/(1 + \tau/\theta)$. r = actual (or residual) anisotropy, r_o = anisotropy in the absence of rotational diffusion (or limiting anisotropy), τ = lifetime, θ = rotational correlation time. Ro was obtained from anisotropy in the presence of glycerol. The actual anisotropy is not close to zero, because the lifetime is short.

Figure 1 shows excitation anisotropies of solutions of substoichiometric Alexa-ATP added to myosin. The rotationally immobilized ATP (90% glycerol at 0°C) gave limiting anisotropies that were near their theoretical limit of 0.4 (▲) indicating that the absorption and emission dipoles of Alexa-ATP are parallel. Myosin does not rotate during the fluorescent lifetime of Alexa-ATP, yet the anisotropy of myosin-Alexa-ADP (■) (Alexa-ATP is hydrolyzed by myosin) was close to that of the free probe (●) suggesting that the bound probe has significant mobility. The free dye had somewhat lower anisotropy indicating a further increase in rotational mobility upon dissociation from the myosin active site. Thus in fiber experiments we can expect measurable change in steady-state anisotropy (arrow), especially since rigor anisotropy in fibers is likely to be greater than anisotropy of myosin in solution.

---

[1] The lifetime can be calculated as ~2 nsec from Perrin's equation using rotational correlation time (~2 nsec) and residual anisotropy (~0.15). Those results are similar to the data of Oiwa (*34*) for related fluorescent nucleotide analogs.

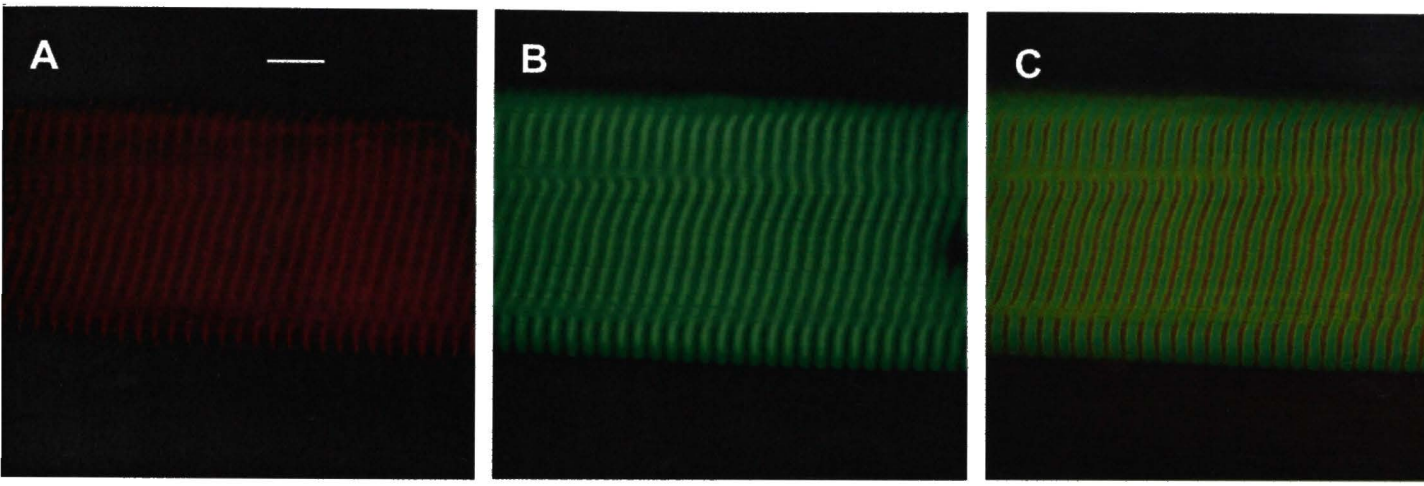

Figure 2. Myosin labeling with Alexa-ATP (red) and actin labeling with fluorescent phalloidin (green) in the same muscle fiber results in staining of A- and I-bands. **A)** Fiber labeled with 3 μM Alexa-ATP for 5' at RT followed by 15' wash with Ca^{2+}-rigor solution. **B)** The same fiber labeled with 0.3 μM FITC-phalloidin for ½ hr at RT followed by 15' wash with Ca^{+}-rigor solution. **C)** Superposition of A and B. Bar is 10 μm.

In muscle fibers, the changes were measured by polarized intensity or anisotropy of Alexa-ATP after displacement by ATP that was rapidly photogenerated from caged precursor. Even though the fibers were labeled with Alexa-ATP, most of the cross-bridges were in Actin-Myosin-ADP state because Alexa-ATP is rapidly hydrolyzed to Alexa-ADP.Pi. Pi was removed by thorough washing with rigor solution. **Figure 2** shows the appearance of muscle after incubation with Alexa-ATP. As a control, the I-bands of the same fiber were labeled with FITC-phalloidin. As expected, Alexa-ATP and FITC-phalloidin labeled the A- and I-bands, respectively. Alexa-ADP was displaced from the active site by 2 mM non-fluorescent ATP that was rapidly photogenerated from a caged precursor.

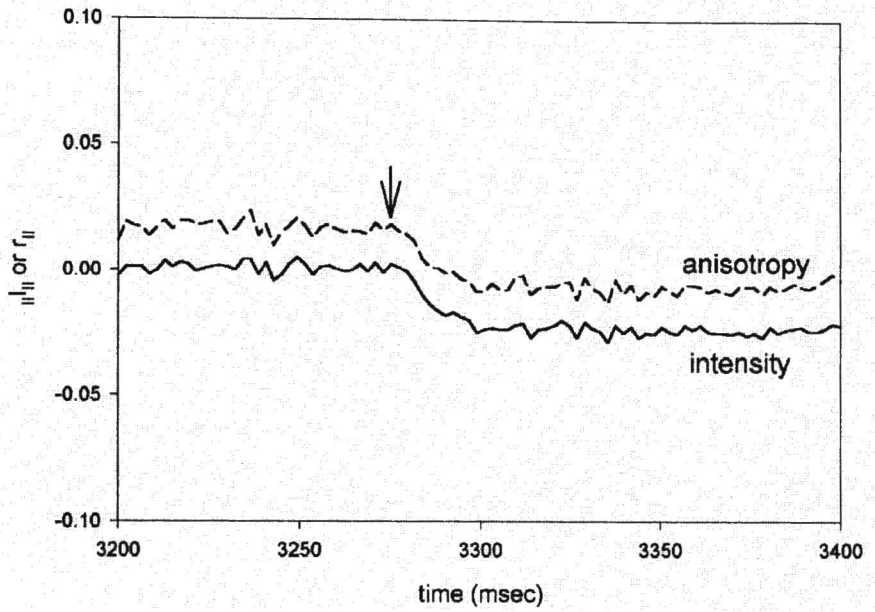

Figure 3. The parallel anisotropy (dashed line) and parallel polarized intensity (solid line) following ATP photogeneration (arrow) in the fiber labeled with Alexa-ATP. Signals have been corrected for photobleaching like in (*10*) i.e. they are set to baseline ~0 before the pulse.

Figure 3 shows the time courses of change of polarized intensity ($_{\parallel}I_{\parallel}$ = solid line) and anisotropy ($r_{\parallel}$= dashed line) upon generation (at the arrow) of 2 mM non-fluorescent ATP. The enzymatic signals consist of a rapid decrease corresponding to increased rate of rotation of Alexa-ADP. Since the diffusion coefficient of free ATP is large ($3.7x10^{-6}cm^2/sec$) (*35*), after a UV pulse there is practically no free ATP left in the experimental volume. Therefore anisotropy, or polarized intensity, reflects irreversible displacement of bound fluorescent-ADP by a single molecule of ATP. The average half-time of decay of anisotropy was 6.7 ± 1.0 msec (mean ± SEM of 5 experiments). The Alexa-ADP signal remains low after dissociation because release of Alexa-ADP is irreversible.

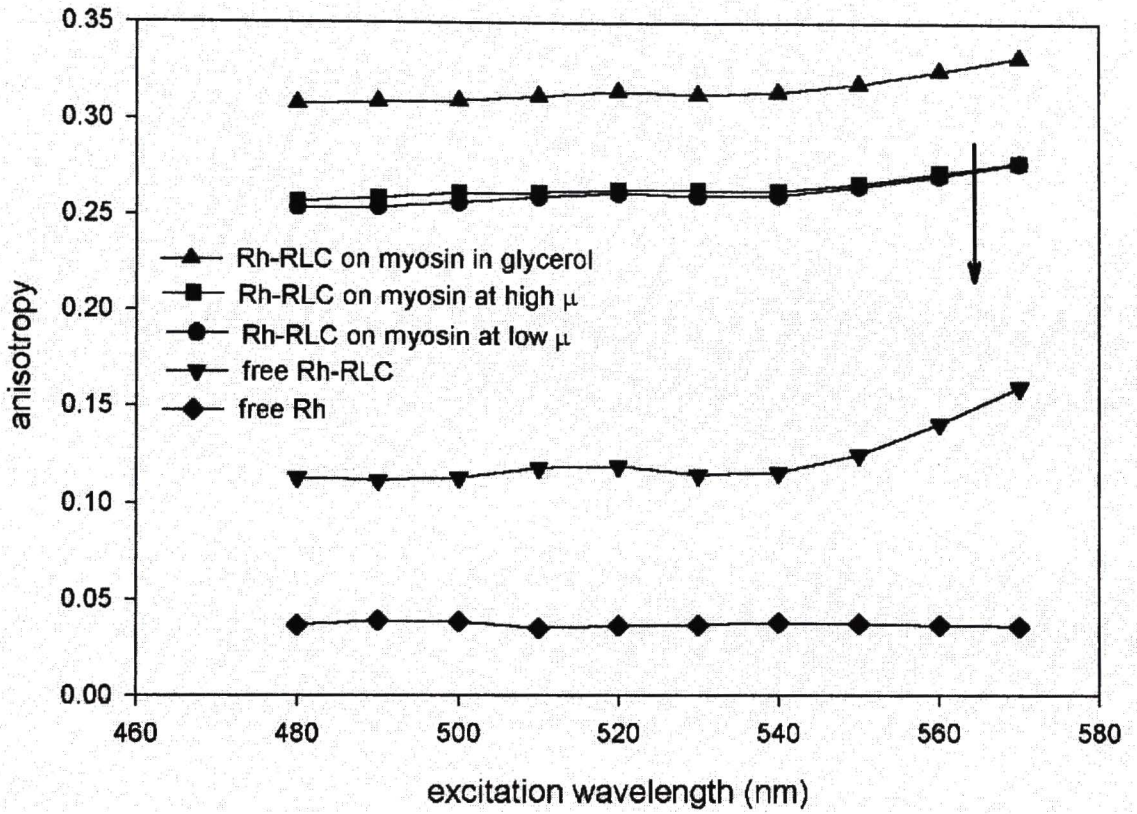

Figure 4. Excitation anisotropy of IATR-RLC. IATR-RLC exchanged to myosin immobilized in 90% glycerol at 0°C (▲), IATR-RLC bound to myosin at low (100 mM) (●) and high (0.6 M) ionic strength (■), free IATR-RLC (▼) and free rhodamine (♦). 0.5 μM IATR. λ_{em}=590 nm. Excitation slit=2 mm, emission slit=1 mm. Arrow indicates the observed transition. All measurements at 0°C.

Mechanical signal: The signal measured here is a change of steady-state anisotropy due to rotation of cross-bridge-bound IATR-RLC. However, it is not certain that such rotation must result in change of anisotropy. For example, RLC bound to myosin in rigor may be rotationally mobile. To assess mobility, we measured anisotropy of free, immobilized and myosin-bound IATR-RLC *in vitro*. **Figure 4** shows excitation anisotropies of solutions of IATR-RLC. The limiting anisotropy of myosin-IATR-RLC complex immobilized in 90%

glycerol at 0°C (▲) is 0.33 consistent with earlier results (*36*), and indicating that the angle between absorption and emission dipoles of the probe is 19.4°. The anisotropy of myosin-IATR-RLC is decreased, indicating motion of the probe and of myosin-bound RLC. Anisotropy is the same at low (●), high (■) ionic strength or in the presence of excess of F-actin (data not shown) indicating that the mobility of the RD is not affected by thick filament or actomyosin complex formation. This shows that anisotropy change *in vivo* is not due to cross-bridge dissociation from thin filaments, but reflects lever arm rotation, consistent with data from muscle fibers (*29*). The anisotropy of free IATR-RLC (▼) is larger than that of free rhodamine (♦) consistent with the larger molecular weight of the complex. The change in the steady-state anisotropy that is monitored in fiber experiments (arrow) is equal or greater than the change seen in solution because steady-state anisotropy of Alexa-ADP bound to myosin in fibers is greater.

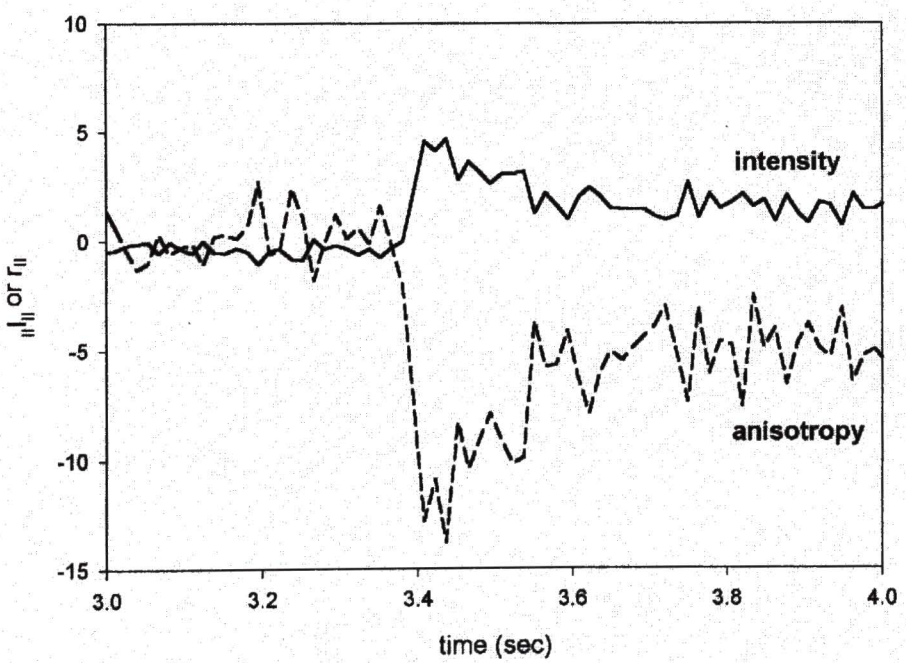

Figure 5. The parallel anisotropy (dashed line) and parallel polarized intensity (solid line) following ATP photogeneration (arrow) in the fiber labeled with IATR-RLC. Signals have been corrected for photobleaching.

We next measured the mechanical signal in muscle fibers by polarized intensity or anisotropy of IATR-RLC bound to RD of a cross-bridge after sudden release of ATP. The striation pattern of muscle exchanged with fluorescent RLC was very good (*10*). **Figure 5** shows the time course of parallel polarized fluorescence ($_{\parallel}I_{\parallel}$ = solid line) and of anisotropy ($r_{\parallel}$= dashed line). They reflect rotation of the RD during single turnover of ATP by cross-bridges. Consistent with earlier observations (*10, 22*), the mechanical signal consists of a rapid decline corresponding to cross-bridge dissociation. In contrast to the Alexa-ADP signal that remains low after dissociation, this phase is followed by a slow reversal corresponding to rebinding of cross-bridges to thin filaments. The average rate of anisotropy change was 3.6 ± 0.5 msec and of anisotropy rise 221 ± 40 msec (n=5). The difference between half times of relaxation of Alexa-ADP and RLC signals was not statistically significant (t=2.0, P=0.105).

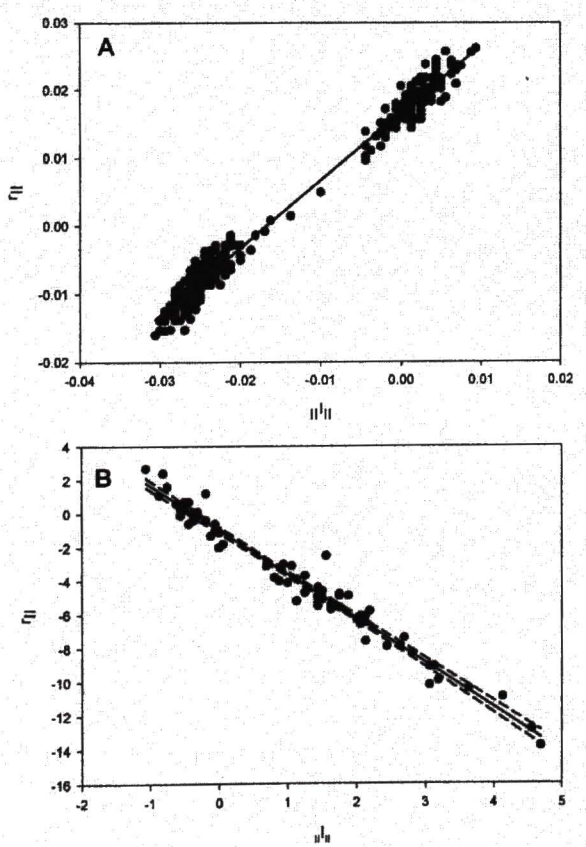

Figure 6. The correspondence between anisotropy and intensity signals. **A**) Data from Figure 4. **B**) Data from Figure 5. The solid lines are the linear regressions. Dashed lines in **B** indicate 95% confidence limits. In **A** they lie within the solid line.

Correspondence of changes of polarized intensity and anisotropy. Anisotropy measurements require 2 fluorescent channels – one for each polarized intensity. It would therefore require 4 channels to simultaneously measure rotations of RLC and Alexa-ATP, an impossible task using a regular confocal microscope that only has 3 fluorescence channels. To simultaneously measure time courses of RLC and Alexa-ATP rotations, it is therefore necessary to monitor polarized intensities. However, in contrast to anisotropy, which is a ratio of polarized intensities, intensity does not compensate for changes of observational volume caused by possible muscle movement. Fortunately, in the present experiments the anisotropy and polarized intensity were closely correlated as predicted by theory (*33*), i.e. the movement artifacts were negligible. In **Figure 6A** every value of intensity from **Figure 3** is plotted on the X-axis and the corresponding value of anisotropy from is plotted on the Y-axis. The solid line shows the linear regression, R^2=0.98. If the experimental volume changed during contraction, the correlation would not have been linear. The movement artifacts are absent because the amount of ATP generated by a short pulse of UV light in small volume is extremely small (0.6×10^{-18} moles). Good correlation is also obtained when comparing anisotropy and intensity of mechanical signal (**Figure 6B**).

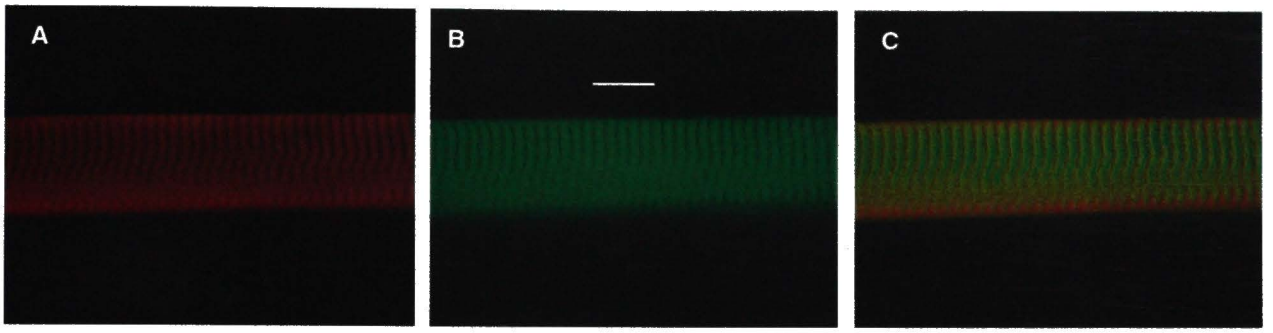

Figure 7. Images of a fiber labeled with IATR-RLC and viewed through LP 590 (rhodamine) filter (**A**) and Alexa-ATP viewed through LP 647 (Cy5) filter (**B**). The fiber labeled with Alexa is deep red, but was assigned to a green channel. **C**) Superposition of **A** and **B**. Scale shown in **B** is 10 μm.

Simultaneous measurements of enzymatic and mechanical signals. Because anisotropies and polarized intensities correspond to each other, it is possible to simultaneously measure time courses of enzymatic and mechanical events in a single contraction of small cross-bridge population of the same fiber. **Figure 7A** shows the confocal image of a fiber labeled with IATR-RLC. The average intensity of the bright (myosin) bands, measured by ImagePlus (Media Cybernetics, Silver Spring, MD) was ~70% larger than the intensity of dark (actin) bands. **Figure 7B** shows the confocal image of the same fiber labeled with Alexa-ATP. The average intensity of the bright (myosin) bands was ~75% larger than the intensity of dark (actin) bands. The two images are combined in **Figure 7C** to show that the both labels are co-localized in the A-band. The same result was obtained when myosin was exchanged with fluorescein-RLC.

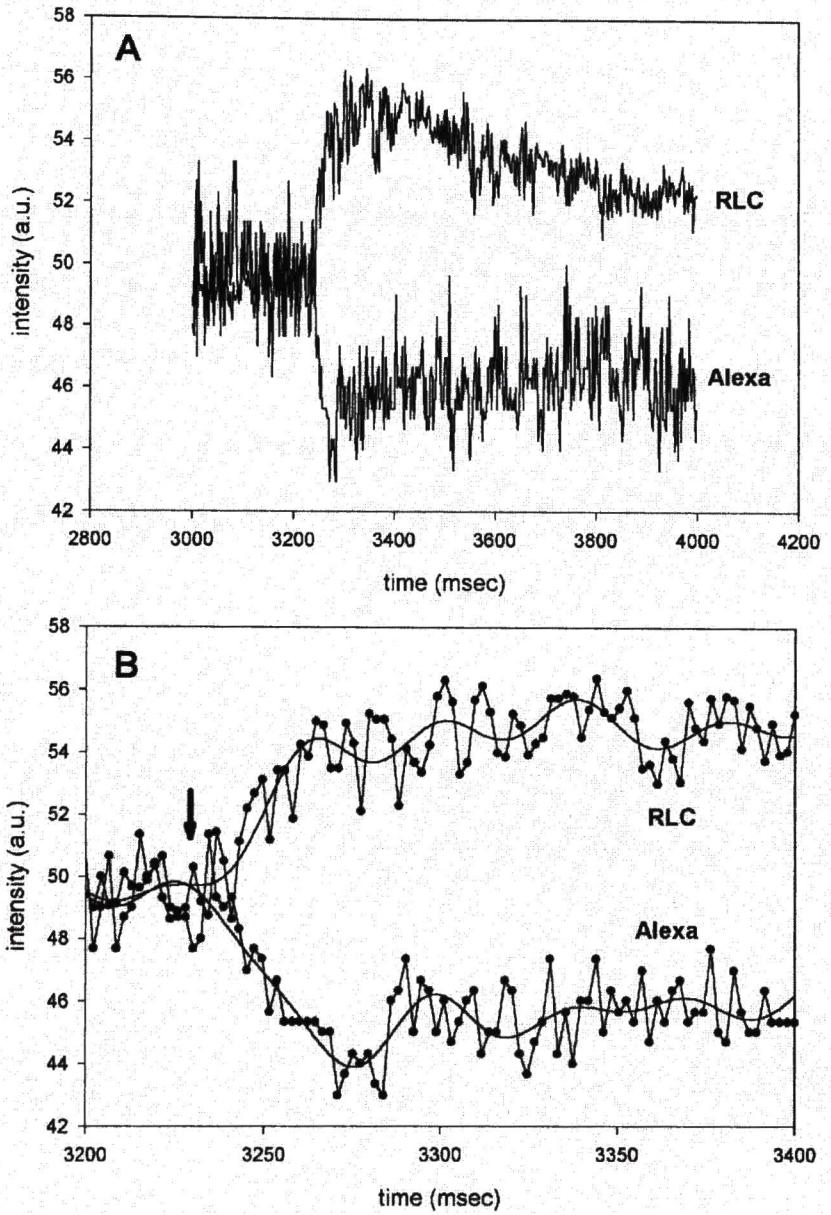

Figure 8. **A**) Correlation between rotations of perpendicular polarized intensity of RLC (top curve) and parallel polarized intensity of Alexa-ATP (bottom curve). **B**) The data drawn on expanded time scale. The true time resolution is 25 μsec, but to keep the data files to reasonable size, 87 points were pooled together and averaged to give a time resolution of 2.2 msec.

Figure 8A compares the time courses of change of mechanical and enzymatic signals. The enzymatic signal (red) has lower S/N ratio than the corresponding mechanical signal (green) because anisotropy of Alexa-ATP changes little upon dissociation (**Figure 1**) as a consequence of its short fluorescence lifetime. The RLC begins to rotate at the same time that ADP is released. There is no indication of mechanical change other than the slow rebinding. The expanded time scale (**Figure 8B**) shows that the two signals are coincident within at least 10 msec. The same result was obtained in 11 experiments using fluorescein labeled RLC and 5 experiments using IATR labeled RLC.

DISCUSSION

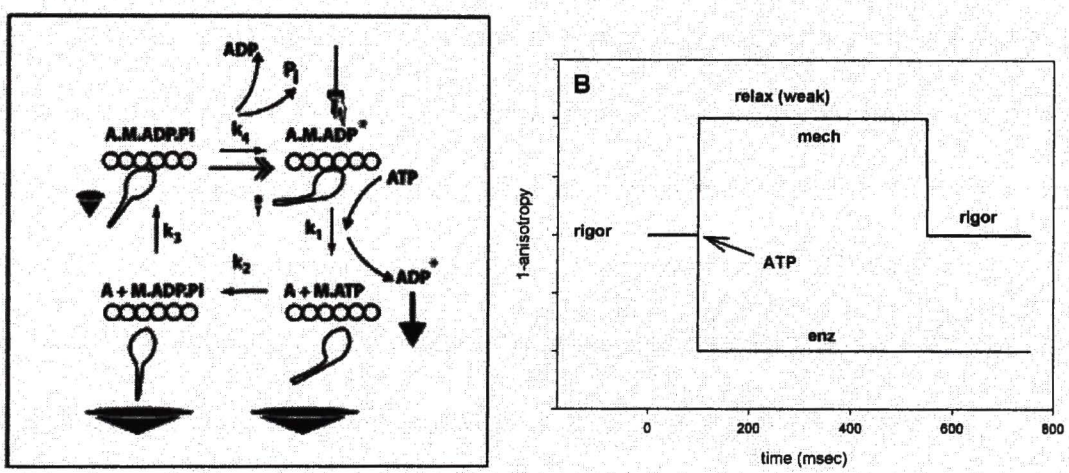

Figure 9. Conventional scheme of cross-bridge action. **A**) UV pulse (hand) causes release of fluorescent ADP (arrow), cross-bridge dissociation, ATP hydrolysis, cross-bridge rebinding to actin to form a weak binding state and force generation (double-headed arrow). Fluorescent ADP is indicated by an asterisk. Cones schematically represent extent of rotation of fluorescent dipoles on RLC. Hydrolysis of one molecule of ATP leads to a single dissociation-rebinding cycle of cross-bridges. **B)** The time course of anisotropy expected if a single cross-bridge was observed.

The present study shows that in contracting muscle the release of ADP is coincident with cross-bridge dissociation from thin filaments. This is consistent with the conventional view that hydrolysis of one ATP molecule is associated with a single mechanical cycle of cross-bridges, i.e. that mechanical and enzymatic events are tightly coupled (*37*). If they were not, cross-bridges would execute multiple reorientation cycles before dissociating from thin filaments. **Figure 9A** is a classical cross-bridge cycle. It begins with photocreation of ATP (black arrow) followed by dissociation, hydrolysis, rebinding in a weak state and the power stroke. **Figure 9B** illustrates the time course of anisotropy changes that are expected if we observed a single cross-bridge. Photocreation of ATP (black arrow) leads to an immediate release of fluorescent ADP from catalytic site and change of anisotropy (enz) (for clarity, the anisotropy change is shown as an increase). Simultaneously, a cross-bridge dissociates from a thin filament, which demonstrates itself as a rapid decrease of anisotropy due to the increased rate of rotation of the RD (relax). In this state a cross-bridge interacts weakly with actin. It remains in this state until ATP is hydrolyzed and Pi is released from active site. Pi dissociation marks the transition to a putative pre power stroke state, which may be short-lived (*5*). This transition is expected to be associated with anisotropy increase, because the cross-bridge rotation is inhibited by actin. Finally, cross-bridge executes a power stroke, which is expected to be accompanied by further anisotropy drop to the initial rigor value. The observed sequence of events (**Figure 8**) is consistent with the classical view, i.e. suggesting that the conventional scheme adequately represents events occurring in contracting muscle. The individual transitions were not resolved, perhaps because cross-bridges were not perfectly synchronized.

The confocal microscope defines a femtoliter volume that contains only ~400 fluorescent cross-bridges. It is crucial that the population under observation be small enough to have high degree of synchrony after the flash. The synchrony induced by uncaging ATP in such a small population is high, i.e. 400 cross-bridges rotate as one for at least 100 msec after the flash (*10*). The time course of rotation of a large population of cross-bridges, on the other hand, is the time average that may obscure small time differences. Another reason for requiring high degree of synchrony is that there are ~20,000 myosin molecules in our experimental volume. Out of this population, ~400 molecules are fluorescently labeled with IATR-RLC and ~500 with Alexa-ADP. It is statistically unlikely that the same myosin molecule carries both labels. Thus while our results do not reflect events occurring at the same molecule, they reflect the behavior of a small population of well synchronized cross-bridges.

Possible artifacts. It is unlikely that our results are due to damage of muscle by exposure to UV light. Control experiments in which there was no caged ATP present gave no change in intensity or anisotropy whatsoever (data not shown). It is also unlikely that the results are due to the fact that we compared polarized intensities rather than anisotropies. We have demonstrated that in our experiments anisotropy is equivalent to polarized intensities. This is because in our experiments the amount of photogenerated ATP is too small to cause shortening of muscle. It is enough only for a single cross-bridge turnover, which does not produce any mechanical artifacts. It is also improbable that any artifacts arise because of heating the muscle. We estimate that heating caused by the absorption of UV light by caged

ATP is ~2°C, too small to cause any damage. In addition to the above estimate, there are four experimental lines of evidence proving that anisotropy change is not due to a rise in temperature. First, caged EDTA (DMNP-EDTA), which has the same UV absorption as caged ATP, causes no change of anisotropy whatsoever (not shown). Second, there is no anisotropy change in fibers left for 24 hrs at room temperature (denatured) (data not shown). Third, fibers in EDTA-containing solution (50 mM KCl, 2 mM EDTA, 10 mM TRIS pH 7.6) do not show any polarized intensity change. Finally, fibers devoid of myosin did not give any anisotropy change upon stimulation by caged ATP (data not shown).

Kinetics of change. The beginning phases of cross-bridge rotation and of ADP dissociation are similar because they both reflect cross-bridge detachment. The overall time courses, however, are very different (**Figure 8A**). The dissociation of Alexa-ADP is irreversible event, i.e. once free Alexa-ADP never attaches to the active site again. Rotation of RLC, in contrast, is biphasic, i.e. after detachment from actin the RD continues to rotate reflecting cross-bridge attachment after photogenerated ATP diffuses away. The absolute values of rates of nucleotide dissociation and of orientation change measured here are smaller than reported elsewhere (*21, 26*). This is because ours are single-turnover experiments, in which the concentration of ATP is in large excess over bound ADP only for a few msec after the UV pulse. Diffusion of ATP away from experimental volume causes reattachment of cross-bridges following original detachment, creating a load which slows down the contraction. The dissociation is slowed down ~15 times and reattachment ~2.7 times (*10*), suggesting that

the half-times in isometrically contracting muscle are $1/k_1 \approx 0.3$ and $1/k_3 \approx 80$ msec, respectively.

The method to measure dissociation by changes of anisotropy of fluorescence was first used by Highsmith et al. (*24*). The displacement technique was first used by Bagshaw and collaborators (*26, 27*) to measure changes in intensity of fluorescence of excess Cy3-EDA-ATP bound to myofibrillar myosin. Those experiments differ from the present ones in that myofibrils were used with large excess of fluorescent ATP. Isolated myofibrils present an insignificant barrier to diffusion of ATP and so the nucleotide hydrolyzed at the active site was constantly replenished by fresh ATP. The predominant intermediate was therefore actin-myosin-ADP.Pi and the release of fluorescent nucleotide reflected the rate of ATP hydrolysis.

In conclusion: we incorporated Alexa-ATP and fluorescent RLC into catalytic site and lever arm of cross-bridges, respectively. We followed rotational motion of both dyes during a single-turnover of ATP. Both dyes rotated as predicted by the conventional model of muscle contraction, suggesting that enzymatic and mechanical events of a cross-bridge of contacting skeletal muscle are strongly coupled. The experiments were done on ~400 cross-bridges, which were synchronized by a sudden release of caged ATP. The final test of the model must wait until enzymatic and mechanical activities of a single cross-bridge of contracting muscle can be measured.

ACKNOWLEDGMENTS

Supported by NIH R21CA9732 and RO1AR048622 and by the grant 000130-0008-2001 from Texas Higher Education Coordinating Board. We thank Dr. Irina Akopova , Mr. John Talent & Ms. Mahalakshmi Ramani for expert technical assistance.

REFERENCES

1. Saito, K., Aoki, T., and Yanagida, T. (1994) Movement of single myosin filaments and myosin step size on an actin filament suspended in solution by a laser trap, *Biophys J 66*, 769-777.
2. Yanagida, T., Kitamura, K., Tanaka, H., Hikikoshi Iwane, A., and Esaki, S. (2000) Single molecule analysis of the actomyosin motor, *Curr Opin Cell Biol 12*, 20-25.
3. Ishijima, A., Kojima, H., Funatsu, T., Tokunaga, M., Higuchi, H., Tanaka, H., and Yanagida, T. (1998) Simultaneous observation of individual ATPase and mechanical events by a single myosin molecule during interaction with actin, *Cell 92*, 161-171.
4. Funatsu, T., Harada, Y., Tokunaga, M., Saito, K., and Yanagida, T. (1995) Imaging of single fluorescent molecules and individual ATP turnovers by single myosin molecules in aqueous solution., *Nature 374*, 555-559.
5. Warshaw, D. M., Hayes, E., Gaffney, D., Lauzon, A. M., Wu, J., Kennedy, G., Trybus, K., Lowey, S., and Berger, C. (1998) Myosin conformational states determined by single fluorophore polarization, *Proc Natl Acad Sci U S A 95*, 8034-8039.
6. Minton, A. P. (1998) Molecular crowding: analysis of effects of high concentrations of inert cosolutes on biochemical equilibria and rates in terms of volume exclusion, *Methods Enzymol 295*, 127-149.
7. Arakawa, T., and Timasheff, S. N. (1985) Theory of protein solubility, *Methods Enzymol 114*, 49-77.
8. Andreev, O. A., and Borejdo, J. (1991) Myosin head can bind two actin monomers., *Biochem. Biophys. Res. Comm. 177*, 350-356.
9. Andreev, O. A., Andreeva, A. L., Markin, V. S., and Borejdo, J. (1993) Two different rigor complexes of myosin subfragment-1 and actin., *Biochemistry 32*, 12046-12035.
10. Borejdo, J., and Akopova, I. (2003) Orientational Changes of Cross-Bridges During Single Turnover of ATP, *Biophys. J. 84*, 2450-2459.
11. Dos Remedios, C. G., Millikan, R.G., Morales, M.F. (1972) Polarization of tryptophan fluorescence from single striated muscle fibers. A molecular probe of contractile state., *J. Gen. Physiol. 59*, 103-120.
12. Cooke, R., Crowder, M. S., and Thomas, D. D. (1982) Orientation of spin labels attached to cross-bridges in contracting muscle fibres, *Nature 300*, 776-8.
13. Burghardt, T. P., Garamszegi, S.P., Park, S. & Ajtai, K. (1998) Tertiary structural changes in the cleft containing the ATP sensitive tryptophan and reactive thiol are consistent with pivoting of the myosin heavy chain at Gly699., *Biochemistry 37*, 8035-8047.
14. Highsmith, S., and Eden, D. (1993) Myosin-ATP chemomechanics., *Biochemistry 32*, 2455-2458.
15. Rayment, I., Rypniewski, W., Schmidt-Base, K., Smith, R., Tomchik, D. R., Benning, M. M., Winkelman, D. A., Wesenberg, G., and Holden, H. M. (1993) Three-

dimensional structure of myosin subfragment-1: a molecular motor., *Science 261*, 50-58.
16. Cooke, R. (1997) Actomyosin interaction in striated muscle, *Physiol Rev 77*, 671-697.
17. Goldman, Y. E. (1998) Wag the tail: structural dynamics of actomyosin, *Cell 93*, 1-4.
18. Dominguez, R., Freyzon, Y., Trybus, K. M., and Cohen, C. (1998) Crystal structure of a vertebrate smooth muscle myosin motor domain and its complex with the essential light chain: visualization of the pre-power stroke state, *Cell 94*, 559-571.
19. Houdusse, A., Kalabokis, V. N., Himmel, D., Szent-Gyorgyi, A. G., and Cohen, C. (1999) Atomic structure of scallop myosin subfragment S1 complexed with MgADP: a novel conformation of the myosin head, *Cell 97*, 459-470.
20. Warshaw, D. M., Guilford, W. H., Freyzon, Y., Krementsova, E., Palmiter, K. A., Tyska, M. J., Baker, J. E., and Trybus, K. M. (2000) The light chain binding domain of expressed smooth muscle heavy meromyosin acts as a mechanical lever, *J Biol Chem 275*, 37167-37172.
21. Allen, T. S.-C., Ling, N., Irving, M., and Goldman, Y. E. (1996) Orientation changes in myosin regulatory light chains following photorelease of ATP in skinned muscle fibers., *Biophys. J. 70*, 1847-1862.
22. Borejdo, J., Ushakov, D. S., and Akopova, I. (2002) The Regulatory and Essential Light Chains of Myosin Rotate Equally During Contraction of Skeletal Muscle, *Biophys. J. 82*, 3150-3159.
23. Pesce, A. J., Rosen, C-G., Pasby, T.L. (1971) In: "Fluorescence Spectroscopy", *Marcel Dekker New York.*
24. Highsmith, S., Mendelson, R. A., and Morales, M. F. (1976) Affinity of myosin S-1 for F-actin, measured by time-resolved fluorescence anisotropy, *Proc Natl Acad Sci U S A 73*, 133-137.
25. Weiss, S., Rossi, R., Pellegrino, M. A., Bottinelli, R., and Geeves, M. A. (2001) Differing ADP release rates from myosin heavy chain isoforms define the shortening velocity of skeletal muscle fibers, *J Biol Chem 276*, 45902-45908.
26. Chaen, S., Shirakawa, I., Bagshaw, C. R., and Sugi, H. (1997) Measurement of nucleotide release kinetics in single skeletal muscle myofibrils during isometric and isovelocity contractions using fluorescence microscopy, *Biophys J 73*, 2033-2042.
27. Shirakawa, I., Chaen, S., Bagshaw, C. R., and Sugi, H. (2000) Measurement of nucleotide exchange rate constants in single rabbit soleus myofibrils during shortening and lengthening using a fluorescent ATP analog, *Biophys J 78*, 918-926.
28. Tonomura, Y., Appel, P., and Morales, M. F. (1966) On the molecular weight of myosin. II., *Biochemistry 5*, 515-521.
29. Sabido-David, C., Hopkins, S. C., Saraswat, L. D., Lowey, S., Goldman, Y. E., and Irving, M. (1998) Orientation changes of fluorescent probes at five sites on the myosin regulatory light chain during contraction of single skeletal muscle fibres, *J Mol Biol 279*, 387-402.
30. Wolff-Long, V. L., Saraswat, L. D., and Lowey, S. (1993) Cysteine mutants of light chain-2 form disulfide bonds in skeletal muscle myosin, *J Biol Chem 268*, 23162-23167.

31. Ling, N., Shrimpton, C., Sleep, J., Kendrick-Jones, J. & Irving, M. (1996) Fluorescent probes of the orientation of myosin regulatory light chains in relaxed, rigor, and contracting muscle., *Biophys. J. 70* , 1836-1846.
32. Sabido-David, C., Brandmeier, B., Craik, J. S., Corrie, J. E., Trentham, D. R., and Irving, M. (1998) Steady-state fluorescence polarization studies of the orientation of myosin regulatory light chains in single skeletal muscle fibers using pure isomers of iodoacetamidotetramethylrhodamine, *Biophys J 74*, 3083-3092.
33. Burghardt, T. P., Cruz-Walker, A. R., Park, S., and Ajtai, K. (2001) Conformation of Myosin Interdomain Interactions During Contraction: Deductions from muscle fibers using polarized fluorescence., *Biochemistry 40*, 4821-4833.
34. Oiwa, K., Jameson, D. M., Croney, J. C., Davis, C. T., Eccleston, J. F., and Anson, M. (2003) The 2'-O- and 3'-O-Cy3-EDA-ATP(ADP) Complexes with Myosin Subfragment-1 are Spectroscopically Distinct, *Biophys J 84*, 634-642.
35. Hubley, M. J., Locke, B. R., and Moerland, T. S. (1996) The effects of temperature, pH, and magnesium on the diffusion coefficient of ATP in solutions of physiological ionic strength, *Biochim Biophys Acta 1291*, 115-121.
36. Ajtai, K., Ilich, P. J., Ringler, A., Sedarous, S. S., Toft, D. J., and Burghardt, T. P. (1992) Stereospecific reaction of muscle fiber proteins with the 5' or 6' isomer of (iodoacetamido)tetramethylrhodamine, *Biochemistry 31*, 12431-12440.
37. Lymn, R. W., and Taylor, E. W. (1971) Mechanism of adenosine triphosphate hydrolysis by actomyosin., *Biochemistry 10*, 4617-4624.

CHAPTER 4

CHANGES IN ORIENTATION OF ACTIN DURING CONTRACTION OF MUSCLE

Rationale:

The previous two chapters reported results regarding the rotation of myosin. My next challenge was to examine rotation of actin in skeletal muscle. The convention regarding F-actin in skeletal muscle holds that it is a rigid structural support molecule acting as a rail for myosin to slide against. However, actin is an abundant and highly conserved protein functioning in cell motility and transport in other cells. It has been shown that actin monomers change conformation when they polymerize into F actin through ATP hydrolysis. Given that both monomeric and filamentous actin display many internal degrees of freedom, and emerging reports have shown *in vitro* a change in probes attached to F-actin during in the presence or absence of S1, the possibility exists that actin might rotate during skeletal muscle contraction. The hypothesis to be tested was whether actin rotates during the cross bridge cycle. To accomplish this, actin was labeled actin in a single fiber in rigor with phalloidin-fluoroscein containing caged ATP. A brief pulse of UV light released ATP from its caged precursor and synchronized a small population of cross-bridges to undergo one cross-bridge cycle during which the polarization of actin was monitored over time.

ABBREVIATIONS

IATR-phalloidin: phalloidin coupled to 5'-iodoacetamido-tetramethyl-rhodamine.

FITC-phalloidin: phalloidin coupled to fluorescein-5(6)-isothiocyanate

Caged ATP: 5-dimethyoxy-2-nitrobenzyl-caged ATP (DMNPE-caged ATP)

Caged EDTA: 1-(4,5-dimethoxy-2-nitrophenyl)-1,2- diaminoethane-N,N, N',N'-tetra acetic acid (DMNP-EDTA)

5'-IATR: 5'-iodoacetamido-tetramethyl-rhodamine

ABSTRACT. It is well documented that muscle contraction results from cyclic rotations of actin-bound myosin cross-bridges. The role of actin is hypothesized to be limited to accelerating phosphate release from myosin and to serving as a rigid substrate for cross-bridge rotations. In order to test this hypothesis, actin rotations were measured during contraction of a skeletal muscle. Actin filaments of rabbit psoas fiber were labeled with rhodamine-phalloidin. Muscle contraction was induced by a pulse of ATP photogenerated from caged precursor. ATP induced a single turnover of cross-bridges, the appropriate amount of which had been previously determined by our lab. The rotations were measured by anisotropy of fluorescence originating from a small volume defined by a narrow aperture of a confocal microscope. The anisotropy of phalloidin-actin changed rapidly at first and was followed by a slow relaxation to a steady-state value. Extracting myosin abolished anisotropy changes. To test whether actin rotated during muscle contraction *in vivo*, actin with fluorescent phalloidin was labeled. The time course of anisotropy change of fluorescent nucleotide was recorded. These results suggest that actin reorientation occurs by dissociation and rebinding of myosin cross-bridges.

INTRODUCTION

Actin serves as a basis of motility in the cell. Actin reorganization during the formation of lamellipodia in concert with microtubule-dependent tail retraction is critical for cell migration (*1*). Rotational motions associated with muscle contraction may occur in myosin, actin or in both (*2*). Rotations of myosin cross-bridges are well documented (*3-11*), but changes in actin have not been thoroughly investigated. *In vitro* studies of isolated S1 have shown that S1 preferentially binds F-actin over the conformer of G-actin (*12*). The 3D structure of G-actin is similar to ATP-dependent chaperone HSP70 (heat shock protein 70) and a high sequence homology at the putative ATPase domain exists between actin, hsp70, hexokinase, glucokinase and glycerol kinase (*13*). F-actin (*14, 15*) and G-actin (*16, 17*) are dynamic structures displaying many internal degrees of freedom, so it is likely that the interactions with myosin have an affect on conformation. Indeed, dissociation of myosin heads from actin results in a change of fluorescence polarization (*18-20*) and in change of microsecond rotational motion detected by saturation transfer electron paramagnetic resonance (ST-EPR) spectra of spin labels on Cys-374 of actin (*21*). Probe fluorescence on cys10 on subdomain 1 of actin has been modified following activation of S1 ATPase, inferring actin-myosin interactions as inducing dynamic, allosteric changes in actin structure (*22*). However, active interaction of heads with actin were found not to induce microsecond rotational motions of Cys-374 (*23*). It is possible that not all amino acids rotate on actin, which explains conflicting reports. More

recently, probes bound to the myosin binding site of actin showed greater polarization changes (*24*).

In this chapter, the kinetics of orientation changes of actin during the power-stroke of skeletal muscle were studied. A narrow aperture of a confocal microscope defined a small volume within a thin filament. Rotational motion of a small number of actin monomers within this volume was synchronized by rapidly stimulating muscle by a short pulse of ATP. The amount of photogenerated ATP was enough for a single turnover of nucleotide by the cross-bridges. The anisotropy of phalloidin bound to actin changed rapidly at first and was followed by a slow relaxation back to a steady-state value, which was different from the original anisotropy.

The observed rotations of actin could be induced passively i.e. be imposed by myosin heads, or actively i.e. reflect hydrolytic activity of actin itself. Active involvement of actin was postulated earlier (*25-27*) and is consistent with the fact that actin polymerization-depolymerization may play a role in contraction of smooth muscle (*28*). The interest in the active involvement of actin has recently been reactivated by the demonstration that *in vitro* interactions of the myosin motor domain with actin change the actomyosin interface to produce "hot-spots" of activity (*29, 30*). These spots propagate along actin filaments to enable myosin V or VI to produce large processive steps during translocation along actin. The active or passive role of actin requires that it display anisotropy over time i.e. that during contraction, fluorescently labeled actin displays a distinct dipole moment which is altered in orientation during one contractile cycle. To test whether such rotation of actin occurs during contraction, we have incorporated

fluorescent phalloidin into actin and followed its rotation after photogenerating ATP in the solvent. If the fluorescently labeled actin were stationary during contraction, the anisotropy of fluorescent moiety would not change. Instead, anisotropy changes of fluorescent nucleotide were identified and recorded during one cross bridge cycle. This suggests that contraction of muscle involves rotation of actin during muscle contraction. Whether this rotation is active or passive is the hypothesis of the following chapter.

MATERIALS AND METHODS

Chemicals and solutions. Standard chemicals, nucleotides and FITC-phalloidin were from Sigma (St Louis, MO). 5'-iodoacetamido-tetramethyl-rhodamine-phalloidin (IATR-phalloidin) and 5-dimethyoxy-2-nitrobenzyl-caged ATP (DMNPE-caged ATP), were from Molecular Probes (Eugene, OR). Fibers isolated from young adult New Zealand White psoas muscle were stored in glycerinating solution contained 80 mM K-Acetate, 0.2 mg/mL PMSF, 2 mM mercaptoethanol and 50% glycerol.

Labeling actin in muscle fibers with phalloidin: Muscle fibers were glycerinated and isolated as described earlier (*10*). Fibers were mounted on a microscope slide containing aluminum clips glued ~5 mm apart. Tautly stretched fibers were attached to clips. Mounted fibers were thoroughly washed with 200 μL rigor solution (50mM KCl, 2mM $MgCl_2$, 10mM Tris-Cl pH 7.5). 0.3 μM 5'-IATR-phalloidin was added onto the fiber and the fiber incubated at 30°C for 30 minutes. The fiber was rinsed with 300uL calcium-

rigor solution (50mM KCl, 2mM $MgCl_2$, 10mM Tris-Cl pH 7.5, and 0.1mM $CaCl_2$). 50uL 2mM caged ATP + 10mM reduced glutathione was added to the fiber prior to confocal analysis. A glass cover slip was placed over the fiber and rested on ~2 mm layer of Vaseline lined along the edge of the microscopic slide to prevent evaporation and drying out of the fiber.

Tension development was studied by MKB force transducer (Scientific Instruments, Heidelberg, Germany). Control (unlabeled) fibers developed 0.96±0.05 mN/fiber of maximum isometric tension (n=32, mean±SEM). Fibers labeled with 0.3 μM IATR-phalloidin developed tension within 10% of control. The lack of effect on tension is in agreement with earlier results (*31*). The degree of labeling was estimated by comparing fluorescent intensity of fiber with the intensity of known concentrations of IATR-phalloidin. After 15' of incubation with 0.3 μM phalloidin, the concentration of fluorescent phalloidin in muscle was ~4-5 μM. The number of actin molecules observed by the confocal microscope is equal to this concentration multiplied by the experimental volume. The confocal volume was ~0.3 μm^3. There were ~1,000 labeled actin monomers in this volume.

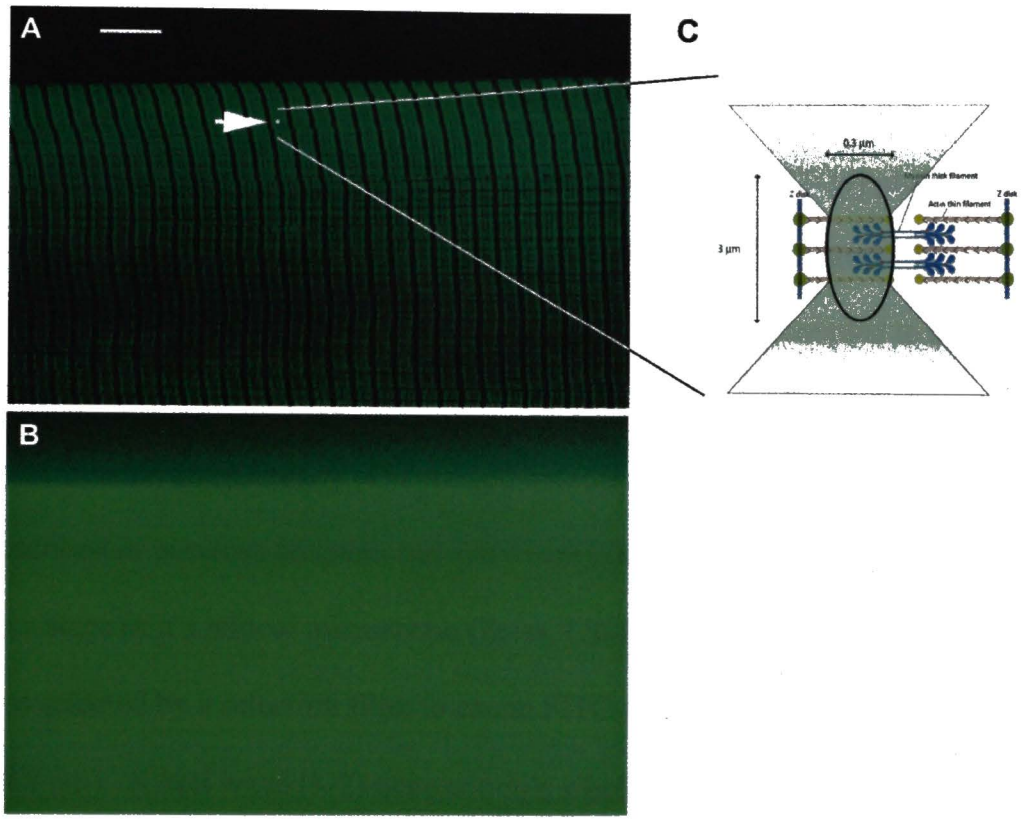

Figure 1. Labeling of thin filaments in a fiber. **A)** Fiber labeled with FITC-phalloidin viewed through confocal aperture. Fluorescein filter (band pass 515<λ<565 nm). The arrowhead points to a spot that indicates the position of the laser beam. Bar=10 μm, sarcomere length =2.8 μm. **B)** the same fiber viewed without confocal aperture. **C)** Schematic illustration of the experimental volume. Laser beam is focused to a diffraction limit. The light is collected from a volume defined by ellipsoid of revolution with diameters 0.3 and 3 μm. There are ~ 1000 fluorescent actin monomers in this volume.

Specificity of labeling. The specificity of labeling was assessed by inspecting the striation pattern. To maximize the resolution and reduce thickness of the section, the diameter of the confocal pinhole was minimized to 26.3 μm. **Figure 1A** shows the confocal image of FITC-phalloidin labeled fiber. The striation pattern is impossible to visualize without a confocal aperture (**Figure 1B**). The white spot (indicated by an arrowhead) shows the relative size of the probing laser beam. The observed volume is shown schematically in **Figure 1C**. The volume width and depth are approximately

equal to the diffraction limit (~0.3 μm) of the illuminating laser spot. Its height is limited by the confocal aperture (1.35 Airy units) to ~3 μm, giving the volume of 0.3 μm^3. In agreement with earlier observations on isolated myofibrils (*32-34*) phalloidin was not distributed uniformly along the length of a thin filament. This non-uniformity was independent of labeling times, the stretch or the type of dye coupled to phalloidin.

Experimental arrangement. The instrument to measure anisotropy of fluorescence was described in previous chapters and elsewhere (*10, 11*). Briefly, a muscle fiber was placed on a stage of a confocal microscope (Zeiss, LSM 410, Thornwood, NY). An Ar/Kr laser was selected by a selection filter to excite FITC-phalloidin (488 nm) or IATR-phalloidin (568 nm). A half wave (λ/2) plate controls whether the excitation light is horizontally or vertically polarized. The laser light is directed by the dichroic mirror onto an objective (Zeiss C-Apo, 40x, NA 1.2, water immersion). The UV beam of an argon laser operating at 364 and 351 nm is used to photolyze caged nucleotide. The UV light is admitted by the shutter. Dichroic combiners merge the UV and visible beams. The objective focuses the exciting light on muscle, collects it and projects fluorescent light onto the photomultipliers through orthogonally polarized analyzers.

Photogeneration of ATP. In order to photolyze ATP from the caged precursor, the fibers were perfused with 2 mM 5-dimethyoxy-2-nitrobenzyl-caged ATP (DMNPE-caged ATP) prior to confocal analysis. The UV beam was focused by the objective to a Gaussian spot with width and length equal to twice the lateral resolution of the UV beam (about 0.2

μm). The height equals to the depth of focus of the objective (about 3 μm, as confocal aperture does not decrease the depth-of-focus of excitation). A few seconds after the beginning of the experiment, the shutter admitting the UV light was opened for exactly 10 msec. The laser power incident on the illuminated area (0.04 μm^2) was 0.12 mJ/sec. The energy flux through the illuminated area was 0.12 mJ/(sec x 0.04 μm^2)=3.0 mJ/(sec x μm^2). ATP stayed in the experimental volume on the average for 300 μsec. The energy through the illuminated area during this time is 9×10^{-4} mJ/μm^2. This is larger than the energy flux obtainable with the frequency-doubled ruby laser (about 3×10^{-5}mJ/μm^2) (*35*). The amount of released ATP was enough for a single turnover of ATP by cross-bridges (*10, 11*).

Measuring anisotropy. The polarization direction of exciting light was kept constant to minimize distortion of polarized light by microscope optics. To measure orthogonal polarizations, fiber axis was rotated by 90°. Otherwise, the measurements were made as described before (*10*). Anisotropy was measured with a high aperture lens (C-Apo, 40x, NA=1.2) using confocal microscopy. To estimate sensitivities, the analyzers in front of both photomultipliers were placed in the same orientation. In this case, both channels must produce identical images. Let the subscripts before and after the intensity indicate the direction of polarization of exiting and emitted light relative to the axis of the muscle fiber. Perpendicular anisotropy is recorded with the λ/2 plate in place. With muscle axis oriented horizontally on a stage of a microscope, channels 1 & 2 record $_{\perp}I_{\perp}$ & $_{\perp}I_{\parallel}$, respectively. Parallel anisotropy is recorded with the λ/2 absent. With muscle axis

horizontal, channels 1 & 2 record $_{\parallel}I_{\perp}$ & $_{\parallel}I_{\parallel}$, respectively. The "on-screen-anisotropy" $R_{\perp}$ is defined as (ch1-ch2) / (ch1+2*ch2) * 256+128 and $R_{\parallel}$ as (ch2-ch1) / (ch1+2*ch2) * 256+128. Factors 256 and 128 make R visible on an 8-bit display. The absolute anisotropies were $r_{\perp}$ = (ch1-ch2) / (ch1+2*ch2) and $r_{\parallel}$ = (ch2-ch1) / (ch1+2*ch2) (*36*).

RESULTS

Controls:

EDTA-Rigor. To confirm that contraction requires calcium and magnesium, the fiber was perfused with EDTA-Rigor, which is a chelator of calcium and magnesium in place of the calcium rigor solution. The EDTA Rigor consisted of: 50mM KCl, 2mM EDTA, 10mM Tris-Cl pH 7.5. 100uL of 1uM Fluorescein-phalloidin conjugated to actin was used to label a fiber. If no calcium and magnesium is present in the muscle, contraction cannot occur and anisotropy should not change during one cross bridge cycle. This was indeed the case (data not shown). This confirmed that 1) the anisotropy change due to rotation of the fluorophore is not an artifact of the confocal instrument, shutter release, etc., because if it were, anisotropy change would be seen whether or not calcium/magnesium was present in the fiber. 2) The amount of calcium and magnesium was sufficient to allow contraction. The concentration of calcium and magnesium is 0.1mM in the form of $CaCl_2$ and 2mM in the form of $MgCl_2$. Such concentrations are based on the procedure of Ling (*37*). If the concentrations were too low, no contraction would occur. Also, the dye does not disrupt contraction, because if it did, no contraction

would be seen with or without the calcium and magnesium. In my case, anisotropy was observed with calcium rigor solution in an actin-labeled fiber. However, the calcium and magnesium is sufficient in concentration and amount to allow contraction in the presence of fluorescently labeled actin.

Rotation is not affected by type of fluorophore used. The present experiments were performed with both fluorescein-phalloidin and rhodamine phalloidin. The same results were achieved wither fluorescein or rhodamine was used. This confirms that results are not dependent or altered by the type of dye used.

Triple vs. single labeled fibers produce the same results. A fiber was triple labeled with RLC-Rh, fluorescein-phalloidin, and Alexa ADP, then analyzed for anisotropy of RLC alone, as well as anisotropy of rhodamine-phalloidin-actin alone. The results were similar to a singly labeled fiber of RLC-Rh alone and singly labeled rhodamine-phalloidin-actin alone. Experimentally, this confirms the theoretical basis that 1) fluorescence intensity of a fluorescently labeled protein from a triple-labeled fiber is the same as anisotropy of the same fluorescently labeled protein from a singly-labeled fiber. 2) bleedthrough of emissions wavelengths through another filter is prevented.

Bleedthrough. A second way bleedthrough was confirmed as negligible, was performed by preparing a 10uM capillary containing free rhodamine dye. If this dye is excited using a 488nm wavelength (568 is required for rhodamine) and viewed through emission filters specific to fluorescein, no image of the capillary is visualized. This confirms that the fluorophores, laser beam and filters are operating correctly. If bleedthrough were

present, the capillary containing rhodamine would have been able to be visualized using settings for fluorescein. This was not the case.

Changes of anisotropy of actin labeled with IATR-phalloidin. The rationale was to observe a small population of actin monomers, to synchronize motion by rapid application of ATP and to follow the orientation changes associated with binding and hydrolysis by myosin of a single molecule of ATP. Muscle actin was labeled with IATR-phalloidin, the fiber was placed horizontally on a stage of a confocal microscope and observed through long pass filter (λ>590 nm). The objective focused visible laser light onto the I-band (white spot in **Figure 1A**). The laser beam was focused slightly off-center of the fluorescent band to avoid taking measurements from the Z-line and from the tips of the actin filaments. The laser beam was not scanned, i.e. the same actin molecules were observed throughout the experiment. This has an important advantage over earlier experiments (*10*) in that the same cross-bridges are observed throughout the entire experiment and that only a short pulse of UV radiation is necessary to produce ATP. Unfortunately, it causes considerable photobleaching because the same fluorophores are under constant illumination. To decrease photobleaching the laser beam was attenuated 300-1000x. 262,144 (512x512) measurements are taken every 25 μsec for a total of 6.55 sec. 570 or 130 data points are averaged to display anisotropy every 14.25 or 3.25 msec. The video card (Matrox Imaging Series) calculates in real time the perpendicular or parallel on-screen-anisotropy.

The rotations were synchronized by the sudden photogeneration of ATP from caged precursor. ~3 sec after the beginning of the experiment, the shutter admitting the UV light is opened for exactly 10 msec. It produces 2 mM ATP in the illuminated volume. The diffusion coefficient of ATP is $3.7 \times 10^{-6} cm^2/sec$ (*38*), so ATP diffuses away from the experimental volume in ~300 μsec. While the actual diffusion coefficient in filament lattice of muscle fiber may be smaller, this order-of-magnitude calculation shows that soon after the application of a pulse there is practically no free nucleotide in the experimental volume. The sole nucleotide remaining in the volume is the one bound to the cross-bridge. The anisotropy change following the pulse reflects actin rotation induced by a turnover of this molecule of ATP.

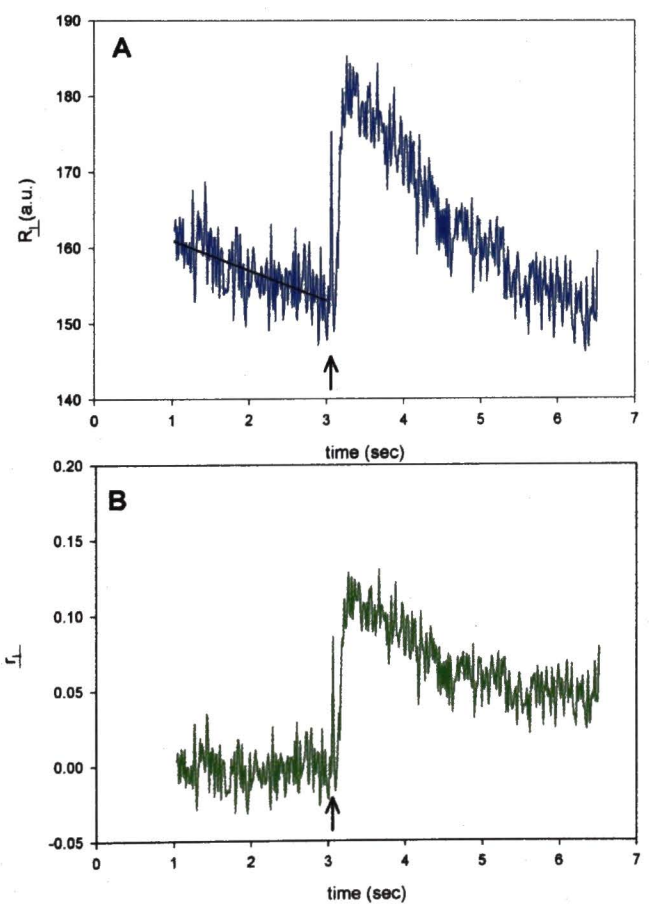

Figure 2. Perpendicular anisotropy of IATR-phalloidin bound to thin filaments of muscle fiber. **A)** The on screen anisotropy is calculated as: $R_\perp(t)=[({}_\perp I_\perp(ch1)-{}_\perp I_\parallel(ch2))/({}_\perp I_\perp(ch1)+2{}_\perp I_\parallel(ch2))]*256+128$. The solid line is a fit used to detrend the data to account for photobleaching. **B)** Data after correcting for photobleaching. The anisotropy $r_\perp(t)=[({}_\perp I_\perp(ch1)-{}_\perp I_\parallel(ch2))/({}_\perp I_\perp(ch1)+2{}_\perp I_\parallel(ch2))]$ has been adjusted to 0 before photogeneration of ATP. The fiber is initially in Ca^{2+}-rigor solution. A pulse of ATP is generated at the arrows. A separate spike is sometimes observed at this pulse, a deflection from the pulse of ATP itself.

Figure 2A is a plot of the perpendicular anisotropy of fluorescence of actin labeled with IATR-phalloidin and initially in Ca^{2+}-rigor solution. The on-screen-anisotropy $R_{\perp}(t)=[({}_{\perp}I_{\perp}(t)-{}_{\perp}I_{\parallel}(t))/({}_{\perp}I_{\perp}(t)+2{}_{\perp}I_{\parallel}(t))]*256+128)$ was calculated in real-time. 3.25 sec after the beginning of experiment, a 10 msec pulse of UV light was applied to muscle (arrow). Photobleaching was subtracted from the raw data, which after conversion to $r_{\perp}$ gave the data of **Figure 2B.** The anisotropy changes consisted of a rapid increase followed by a slow relaxation to a new steady-state level. The average half-time of this process was 478 ± 36 msec (n=16). About 1.5 sec after the pulse, the anisotropy assumed new steady-state value. This was always different from the initial rigor value. It is speculated that this reflects different states of actin before and after creation of ATP.

Anisotropy of "ghost" fibers. In order to see whether myosin was necessary for the reorientation of actin, experiments were done on "ghost" fibers devoid of thick filaments. A fiber was first tested for rotation of actin. Myosin was then extracted from the same fiber by the application of Hasselbach-Schneider solution (0.47 M KCl, 5 mM $MgCl_2$, 10 mM PP_i 0.1 M PO_4 buffer pH 6.4) for 10 min at room temperature followed by extensive washing with Ca^{2+}-rigor solution. After myosin extraction, there was no change of anisotropy following photogeneration of ATP (not shown). The same results were obtained in 3 experiments on 3 different batches of fibers.

DISCUSSION

Actin is one of the most highly conserved eukaryotic proteins (*39*). Modeling has suggested images of actin containing many internal degrees of freedom within the actin filament which allows it to interact with diverse proteins (*17*). Structural homologs of actin such as hexokinase (*40*) and Hsc 70 undergo various tilts, twists, and "propeller-like" rotations, suggesting that actin could too. It is possible that the actin binding proteins, which are far less conserved, might render specificity of the actin filament as to its function. Actin coupled to myosin VI and may facilitate membrane invagination or vesicle movement during endocytosis however its interface structure is unknown (*41*).

So far, crystallization of F-actin his not been possible, however monomeric ATP-bound actin has been crystallized and used to construct a helical model of F-actin (*42*). Modeling has also shown that F-actin bound to various molecules exhibit different conformations (*43*).

The anisotropy change of phalloidin-fluorescein bound to actin reflects the rotation of actin during one cross-bridge cycle. How the conformation of actin is changed to allow this is unknown. In smooth muscle, caldesmon (793 amino acids), which is similar to troponin in skeletal muscle, binds to actin to modulate the structural transition of actin monomers between an "off" and "on" conformation conducive to myosin binding (*44*). Similarly, perhaps when calcium binds troponin C, the troponin complex would, in concert with tropomyosin, induce a conformational change in actin itself to further expose the myosin S1 binding site.

Ruling out the artifacts. The artifacts may arise because of: 1) Heating of the muscle, 2) Damage to muscle fiber induced by the UV light, 3) Gross motion of fiber occurring. An argument is presented that none of the above is responsible for the present observations. This is applicable to the experiments in all chapters.

1. Heating: The heating is caused by the absorption of UV light by caged ATP. The extinction coefficient of caged-ATP at 364 nm is 4,400 $M^{-1}cm^{-1}$, i.e. a 3 μm thick section of muscle perfused with 2 mM precursor absorbs 0.264% of the incident UV light. Because the beam diameter used here is small, heat associated with this absorption dissipates in less than ~70 nsec (*45*). The UV laser delivered 0.9×10^{-11} J in 70 nsec, i.e. the temperature rise during the experiment is less than 2°C. The experimental support of this argument is the observation that the UV pulse did not cause a change in the control anisotropy (data not shown). Three additional lines of evidence exist suggesting that anisotropy is not influenced by a temperature rise in the experimental volume. Caged EDTA (DMNP-EDTA), which has the same UV absorption as caged ATP, caused no change of anisotropy whatsoever (data not shown). There is no anisotropy change in denatured fibers (left for 24 hrs at room temperature, data not shown). Fibers devoid of myosin did not give any anisotropy change upon stimulation by caged ATP (ghost fibers).

2. Damage: Muscle damage caused by the exposure to the UV light can be eliminated as a possible source for artifact generation because there was no anisotropy change whatever

in fibers which did not contain caged ATP but were exposed to the UV pulse (data not shown).

3. Gross motions of the fiber: The mean concentration of ATP in the experimental chamber photogenerated in each experiment is ~6 x 10^{-8} mM. This is too small to induce a global contraction. When the image of a fiber taken before stimulation of a contractile cycle is subtracted from the image taken after the contraction, the result is 0 (black) everywhere except in the area where photobleaching occurred (data not shown). If gross motions had occurred, remnants would have likely been seen marked by a difference in image intensity.

The results presented here suggest that the whole thin filament is rotating as originally proposed by Oosawa (*46*). The kinetics of change revealed that actin rotated in two phases. The experiments using ghost fibers show that myosin is necessary for all phases to occur. The first phase was a fast reorientation. The half-time of this process was ~80 msec, not significantly different than the rate of cross-bridge dissociation (*11*). Coincidence of changes in actin and dissociation are consistent with earlier observation that ST-EPR spectra of spin labels on Cys-374 of actin changed upon dissociation of S1 (*21*) and with observation that binding of S1 to actin labeled with spin labeled analogues of ATP resulted in some change in actin conformation (*47*). However, we cannot rule out the possibility that the changes in actin occur before changes in myosin. Rapid changes in actin could be due to the activation process. This may be related to earlier findings

(*48, 49*) that there was a small decrease in the spacing of the axial repeat of actin during contraction against the negligible load. Since contraction against zero load is comparable to the early stages of contraction, this data led to the suggestion that actin filaments twist and shorten before any tension is developed (*49*).

The second phase of the anisotropy change was slow relaxation to a steady-state value. The half-time of this process was ~480 msec, again not significantly different from cross-bridge binding to thin filaments in single-turnover experiments (*11*) and this process reflects binding of cross-bridges.

The second phase of anisotropy change ended with a resumption of a new steady-state value, typically 1.5-2 sec after the pulse. This value was always different from the initial rigor value. A possible explanation of the present results is that thin filaments are in different state before and after the exposure to a pulse of ATP. Before the exposure the thin filaments are under stress because muscle develops full rigor tension when it is transferred from relaxing (glycerinating) solution to rigor solution. Following the exposure, however, the filaments are unstressed because muscle develops very little rigor tension. This state then stays constant until ATP is available in the medium again.

The results of these experiments suggest that actin rotates during the contractile cycle and is not simply a "static rail" along which myosin filaments slide.

ACKNOWLEDGMENTS

Supported by NIH R21CA9732 and by the Texas Higher Education Coordinating Board grant 000130-0008-2001.

REFERENCES

1. Ballestrem, C., Wehrle-Haller, B., Hinz, B., and Imhof, B. A., Actin-dependent lamellipodia formation and microtubule-dependent tail retraction control-directed cell migration, *Mol Biol Cell, 11*, 2999 (2000).
2. Huxley, A. F., and Simmons, R. M., Proposed mechanism of force generation in striated muscle, *Nature, 233*, 533 (1971).
3. Dos Remedios, C. G., Millikan, R. G., and Morales, M. F., Polarization of tryptophan fluorescence from single striated muscle fibers. A molecular probe of contractile state, *J Gen Physiol, 59*, 103 (1972).
4. Nihei, T., Mendelson, R. A., and Botts, J., Use of fluorescence polarization to observe changes in attitude of S-1 moieties in muscle fibers, *Biophys J, 14*, 236 (1974).
5. Thomas, D. D., and Cooke, R., Orientation of spin-labeled myosin heads in glycerinated muscle fibers, *Biophys J, 32*, 891 (1980).
6. Borejdo, J., Assulin, O., Ando, T., and Putnam, S., Cross-bridge orientation in skeletal muscle measured by linear dichroism of an extrinsic chromophore, *J Mol Biol, 158*, 391 (1982).
7. Sabido-David, C., Brandmeier, B., Craik, J. S., Corrie, J. E., Trentham, D. R., and Irving, M., Steady-state fluorescence polarization studies of the orientation of myosin regulatory light chains in single skeletal muscle fibers using pure isomers of iodoacetamidotetramethylrhodamine, *Biophys J, 74*, 3083 (1998).
8. Allen, T. S., Ling, N., Irving, M., and Goldman, Y. E., Orientation changes in myosin regulatory light chains following photorelease of ATP in skinned muscle fibers, *Biophys J, 70*, 1847 (1996).
9. Hopkins, S. C., Sabido-David, C., Corrie, J. E., Irving, M., and Goldman, Y. E., Fluorescence polarization transients from rhodamine isomers on the myosin regulatory light chain in skeletal muscle fibers, *Biophys J, 74*, 3093 (1998).
10. Borejdo, J., Ushakov, D. S., and Akopova, I., Regulatory and essential light chains of myosin rotate equally during contraction of skeletal muscle, *Biophys J, 82*, 3150 (2002).
11. Borejdo, J., and Akopova, I., Orientational changes of crossbridges during single turnover of ATP, *Biophys J, 84*, 2450 (2003).
12. Ballweber, E., Kiessling, P., Manstein, D., and Mannherz, H. G., Interaction of myosin subfragment 1 with forms of monomeric actin, *Biochemistry, 42*, 3060 (2003).
13. Flaherty, K. M., McKay, D. B., Kabsch, W., and Holmes, K. C., Similarity of the three-dimensional structures of actin and the ATPase fragment of a 70-kDa heat shock cognate protein, *Proc Natl Acad Sci U S A, 88*, 5041 (1991).
14. Oosawa, F., Actin-actin bond strength and the conformational change of F-actin, *Biorheology, 14*, 11 (1977).
15. Oosawa, F., Maeda, Y., Fujime, S., Ishiwata, S., Yanagida, T., and Taniguchi, M.,

Dynamic characteristics of F-actin and thin filaments in vivo and in vitro, *J Mechanochem Cell Motil, 4*, 63 (1977).
16. Page, R., Lindberg, U., and Schutt, C. E., Domain motions in actin, *J Mol Biol, 280*, 463 (1998).
17. Galkin, V. E., VanLoock, M. S., Orlova, A., and Egelman, E. H., A new internal mode in F-actin helps explain the remarkable evolutionary conservation of actin's sequence and structure, *Curr Biol, 12*, 570 (2002).
18. Borovikov, Y. S., and Chernogriadskaia, N. A., Studies on conformational changes in F-actin of glycerinated muscle fibers during relaxation by means of polarized ultraviolet fluorescence microscopy, *Microsc Acta, 81*, 383 (1979).
19. Borovikov, Y. S., Levitskii, D. I., Kirillina, V. P., and Poglazov, B. F., Effect of Ca2+ binding to 5,5'-dithiobis(2-nitrobenzoic acid) light chains on conformational changes of F-actin caused by myosin subfragment-1, *Eur J Biochem, 125*, 343 (1982).
20. Prochniewicz-Nakayama, E., Yanagida, T., and Oosawa, F., Studies on conformation of F-actin in muscle fibers in the relaxed state, rigor, and during contraction using fluorescent phalloidin, *J Cell Biol, 97*, 1663 (1983).
21. Thomas, D. D., Seidel, J. C., and Gergely, J., Rotational dynamics of spin-labeled F-actin in the sub-millisecond time range, *J Mol Biol, 132*, 257 (1979).
22. Eli-Berchoer, L., Reisler, E., and Muhlrad, A., Structural implications of the chemical modification of Cys(10) on actin, *Biophys J, 78*, 1482 (2000).
23. Ostap, E. M., and Thomas, D. D., Rotational dynamics of spin-labeled F-actin during activation of myosin S1 ATPase using caged ATP, *Biophys J, 59*, 1235 (1991).
24. Borovikov, Y. S., Dedova, I. V., dos Remedios, C. G., Vikhoreva, N. N., Vikhorev, P. G., Avrova, S. V., Hazlett, T. L., and Van Der Meer, B. W., Fluorescence depolarization of actin filaments in reconstructed myofibers: the effect of S1 or pPDM-S1 on movements of distinct areas of actin, *Biophys J, 86*, 3020 (2004).
25. Schutt, C., and Lindberg, U., Actin as the generator of tension during muscle contraction, *Proc Natl Acad Sci U S A, 89*, 319 (1992).
26. Schutt, C. E., and Lindberg, U., A new perspective on muscle contraction, *FEBS Lett, 325*, 59 (1993).
27. Schutt, C. E., and Lindberg, U., Muscle contraction as a Markov process. I: Energetics of the process, *Acta Physiol Scand, 163*, 307 (1998).
28. Barany, M., Barron, J. T., Gu, L., and Barany, K., Exchange of the actin-bound nucleotide in intact arterial smooth muscle, *J Biol Chem, 276*, 48398 (2001).
29. Tanaka, H., Homma, K., Iwane, A. H., Katayama, E., Ikebe, R., Saito, J., Yanagida, T., and Ikebe, M., The motor domain determines the large step of myosin-V, *Nature, 415*, 192 (2002).
30. Nishikawa, S., Homma, K., Komori, Y., Iwaki, M., Wazawa, T., Hikikoshi Iwane, A., Saito, J., Ikebe, R., Katayama, E., Yanagida, T., and Ikebe, M., Class VI myosin moves processively along actin filaments backward with large steps, *Biochem Biophys Res Commun, 290*, 311 (2002).

31. Bukatina, A. E., Fuchs, F., and Watkins, S. C., A study on the mechanism of phalloidin-induced tension changes in skinned rabbit psoas muscle fibres, *J Muscle Res Cell Motil, 17*, 365 (1996).
32. Szczesna, D., and Lehrer, S. S., The binding of fluorescent phallotoxins to actin in myofibrils, *J Muscle Res Cell Motil, 14*, 594 (1993).
33. Ao, X., and Lehrer, S. S., Phalloidin unzips nebulin from thin filaments in skeletal myofibrils, *J Cell Sci, 108 (Pt 11)*, 3397 (1995).
34. Zhukarev, V., Sanger, J. M., Sanger, J. W., Goldman, Y. E., and Shuman, H., Distribution and orientation of rhodamine-phalloidin bound to thin filaments in skeletal and cardiac myofibrils, *Cell Motil Cytoskeleton, 37*, 363 (1997).
35. Goldman, Y. E., Hibberd, M. G., and Trentham, D. R., Initiation of active contraction by photogeneration of adenosine-5'-triphosphate in rabbit psoas muscle fibres, *J Physiol, 269*, 55 (1984).
36. Lackowicz, J., *Principles of Fluorescence Spectroscopy*, Kluwer Academic/Plenum Publishers, New York, NY (1999).
37. Ling, N., Shrimpton, C., Sleep, J., Kendrick-Jones, J., and Irving, M., Fluorescent probes of the orientation of myosin regulatory light chains in relaxed, rigor, and contracting muscle, *Biophys J, 70*, 1836 (1996).
38. Hubley, M. J., Locke, B. R., and Moerland, T. S., The effects of temperature, pH, and magnesium on the diffusion coefficient of ATP in solutions of physiological ionic strength, *Biochim Biophys Acta, 1291*, 115 (1996).
39. Sheterline, P., Clayton, J., and Sparrow, J., Actin, *Protein Profile, 2*, 1 (1995).
40. Bennett, W. S., Jr., and Steitz, T. A., Glucose-induced conformational change in yeast hexokinase, *Proc Natl Acad Sci U S A, 75*, 4848 (1978).
41. Schafer, D. A., Coupling actin dynamics and membrane dynamics during endocytosis, *Curr Opin Cell Biol, 14*, 76 (2002).
42. Holmes, K. C., Popp, D., Gebhard, W., and Kabsch, W., Atomic model of the actin filament, *Nature, 347*, 44 (1990).
43. Sablin, E. P., Dawson, J. F., VanLoock, M. S., Spudich, J. A., Egelman, E. H., and Fletterick, R. J., How does ATP hydrolysis control actin's associations?, *Proc Natl Acad Sci U S A, 99*, 10945 (2002).
44. Borovikov, Y. S., Avrova, S. V., Vikhoreva, N. N., Vikhorev, P. G., Ermakov, V. S., Copeland, O., and Marston, S. B., C-terminal actin-binding sites of smooth muscle caldesmon switch actin between conformational states, *Int J Biochem Cell Biol, 33*, 1151 (2001).
45. Denk, W., Piston, D. W., and Webb, W. W., *Two-photon Molecular Excitation in Laser-Scanning Microscopy*, Plenum Press, New York and London (1995).
46. Ishiwata, S., and Oosawa, F., A regulatory mechanism of muscle contraction based on the flexibility change of the thin filaments, *J Mechanochem Cell Motil, 3*, 9 (1974).
47. Naber, N., and Cooke, R., Mobility and orientation of spin probes attached to nucleotides incorporated into actin, *Biochemistry, 33*, 3855 (1994).
48. Huxley, H. E., Stewart, A., Sosa, H., and Irving, T., X-ray diffraction measurements of the extensibility of actin and myosin filaments in contracting

muscle, *Biophys J, 67*, 2411 (1994).
49. Bordas, J., Svensson, A., Rothery, M., Lowy, J., Diakun, G. P., and Boesecke, P., Extensibility and symmetry of actin filaments in contracting muscles, *Biophys J, 77*, 3197 (1999).

CHAPTER 5

CHANGES IN ACTIN ORIENTATION DURING MUSCLE CONTRACTION ARE PASSIVE

A. A. Shepard, D. Dumka, I. Akopova, J. Talent & J. Borejdo

Dept of Molecular Biology and Immunology

University of North Texas

3500 Camp Bowie Blvd, Fort Worth, TX 76107

In Press. *Journal of Muscle Research and Cell Motility*. Accepted 9/2004.

Rationale:

In the previous experiments, actin appeared to rotate, but whether this rotation initiates cross-bridge dissociation, or if actin rotation occurred simply as a consequence of cross-bridge dissociation is not known.

A working hypothesis was formed to test whether actin rotation is passive or active. To accomplish this, the polarized emission intensities of RLC, actin, and nucleotide during one cross-bridge cycle within one isolated fiber beginning in a state of rigor were simultaneously measured as a reflection of anisotropy. The changes in orientation of regulatory light chains were measured by following anisotropy of recombinant fluorescent regulatory exchanged into muscle fibers. The changes in orientation of actin monomers were measured by following anisotropy of phalloidin added to endogenous actin in muscle fibers. The enzymatic activity of myosin was measured by following dissociation of fluorescent ADP from its active site on myosin.

One possibility is actin rotates before the movement of myosin, inferring actin is actively participating in myosin dissociating from actin. A second possibility is that actin rotation occurs after dissociation of nucleotide or movement of the myosin head, implying actin is passive and rotates as a consequence of cross-bridge dissociation. A third possibility is that all three molecules rotate at the same time.

Abbreviations

caged ATP: 5-dimethyoxy-2-nitrobenzyl-caged adenosine 5'-triphosphate

5'-IATR or Rh: 5'-iodoacetamido-tetramethyl-rhodamine

FITC-Ph: 5'-iodoacetamido-fluorescein phalloidin

Alexa-ATP: Alexa Fluor® 647 2'-(or-3')-O-(N-(2-aminoethyl)urethane)

RD or lever-arm: regulatory domain of myosin

ABSTRACT. Muscle contraction results from the interaction between myosin cross-bridges and actin. It is believed that this interaction involves rotation of the lever-arm of cross-bridges, and that actin's role is limited to accelerating Pi release and guiding motion of myosin. However, earlier work showed that both cross-bridges and actin monomers rotated during muscle contraction. To find out whether rotation of actin is active or whether it is caused by interaction with cross-bridges, we measured rotations of actin and myosin simultaneously. The changes in orientation of cross-bridges were measured by following anisotropy of recombinant fluorescent regulatory light chains exchanged with native regulatory light chains in muscle fiber. The changes in orientation of actin monomers were measured by following anisotropy of phalloidin added to endogenous actin in muscle fibers. As a reference, we measured enzymatic activity of myosin by following dissociation of fluorescent ADP from the active site. The fluorescence originated from a femtoliter volume defined by a narrow aperture of a confocal microscope. Molecules in such a small volume behave as one when muscle contraction is initiated by a sudden release of caged ATP. The onset of all three events occurred at the same time suggesting that rotation of actin filaments is entirely passive.

INTRODUCTION

It is believed that muscle contraction results from rotation of the lever-arm of myosin cross-bridges. The role of actin is believed to be passive -- limited to accelerating phosphate release from myosin and serving as a rigid substrate for cross-bridge rotations (1). However, earlier work revealed that both cross-bridges and actin monomers changed orientation during muscle contraction (2). To find out whether reorientation of actin monomers was caused by the interaction with myosin cross-bridges or whether it was active, rotation of a single cross-bridge between actin and myosin should be studied at the same time. If actin were to rotate before cross-bridge detachment (and force generation), it would suggest that actin twists or shortens before any tension is developed (3, 4), perhaps reflecting Ca binding to the regulatory proteins. If actin were to reorient itself during force generation (after cross-bridge reattachment) it would suggest that actin is an active structure capable of generating force on its own.

In muscle fiber it is still impossible to study a single cross-bridge, but it is possible to synchronize a small number of cross-bridges and actin monomers. Such a synchronized population is expected to be equivalent to a single molecule (5). The introduction of extremely small observational volumes defined by diffraction-limited laser beams and confocal detection (6) made it possible to observe an *in vivo* population as small as 400 molecules. In this paper, we report the simultaneous measurement of orientation changes of myosin lever-arm and actin actin monomers. Release of ADP after hydrolysis by the

same myosin heads was measured as a reference. The changes in orientation of cross-bridges were followed by measuring anisotropy of fluorescent myosin regulatory light chains (RLC) exchanged with native light chains of muscle fiber. The changes in orientation of RLC reflect changes of orientation of the lever-arm of cross-bridges (7). Changes of orientation of actin monomers were followed by measuring anisotropy of fluorescent phalloidin added to muscle fibers. Enzymatic event was followed by measuring dissociation of fluorescent ADP from myosin active site. The onset of all three events occurred at the same time suggesting that actin filaments are passive structures whose motion is caused by binding/dissociation of myosin cross-bridges.

Experimental Procedures

Chemicals and solutions. 5-dimethyoxy-2-nitrobenzyl-caged ATP (caged ATP), Alexa Fluor® 647 2'-(or-3')-O-(N-(2- aminoethyl)urethane) (Alexa-ATP) and 5'-iodoacetamido-tetramethyl-rhodamine (5'-IATR or Rh) were from Molecular Probes (Eugene, OR). Fluorescein-5-isothiocyanate phalloidin (FITC-Ph) was from Sigma (St. Louis, MO). Rigor solution contained 50 mM KCl, 2 mM $MgCl_2$, 0.1 mM $CaCl_2$, 10 mM TRIS buffer pH 7.5, 10 mM reduced glutathione. Relaxing solution had the same composition, but 5 mM EGTA was substituted for $CaCl_2$ and 5 mM ATP was added. The glycerinating solution was the same as relaxing except that 80 mM K-Acetate was substituted for KCl and it contained in addition 0.2 mg/mL PMSF, 2 mM mercaptoethanol and 50% glycerol.

Muscle fibers. Single fibers were dissected from rabbit psoas muscle bundles kept in glycerinating solution. Fibers were transferred to a microscope slide to which aluminum clips were glued ~5 mm apart. Fibers were tautly stretched, attached to clips and covered with a cover glass separated from a microscope slide by ~0.2 mm thick layer of vaseline. Mounted fibers were thoroughly washed with rigor solution. Muscle bundles were stored in glycerol for no more than 3 months. Opened bottles containing glycerinated bundles were discarded after a week.

Expressing and labeling regulatory light chain. The regulatory light chain (RLC) containing a single cysteine at position 73 (8) was prepared by expression of RLC in a pT7-7 plasmid in BL21(DE3) cells. The construct was a gift from Dr S. Lowey (University of Vermont). A one liter culture was prepared and RLC isolated as described in (9). Newly purified RLC in 10 mM KP_i buffer pH 7.5 & 2 mM DTT was dialyzed overnight at 4°C against 50 mM KCL, 10 mM TRIS-Cl pH 7.5 and incubated with a 10 fold excess of 5'-IATR for 7 hrs on ice in the dark. Excess IATR was removed by overnight dialysis at 4°C against 50 mM KCl, 20 mM EDTA, 0.01 M KP_i buffer pH 7.0 and 0.5 mM DTT. The degree of labeling was 14%.

Exchanging IATR-RLC with native RLC of fibers. Labeled RLC was exchanged into fibers as described earlier (7). After the exchange fibers were rinsed 3 times with 100 μL rigor solution. and 50 μL of 2 mM caged ATP in rigor solution was added. The

concentration of fluorophore incorporated into muscle was estimated as ~ 2 μM by comparing intensity of fluorescence of muscle with intensity of capillaries containing known concentration of fluorophore. The number of fluorescent myosin molecules observed by the confocal microscope was estimated as ~400.

Labeling of actin in muscle fibers with phalloidin. The fibers in the relaxing solution were labeled with 0.3 μM of FITC-phallodin for 15' at room temperature. After labeling, the fibers were thoroughly washed with the relaxing and rigor solutions. The degree of labeling was ~4-5 μM. The number of actin molecules observed by the confocal microscope was ~1,000.

Labeling fibers with Alexa-ATP. A muscle fiber was incubated with 0.1 μM Alexa-ATP in rigor solution for 10 min at room temperature (RT). Excess dye was washed out with rigor solution. The degree of incorporation of Alexa-ATP into fiber was estimated by comparing the intensity of fluorescence of known concentration of the dye with the fluorescence of labeled fibers. Typically 2-3 μM of myosin was labeled. There are ~500 myosin molecules labeled with Alexa-ADP in this volume.

Functionality of exchanged fibers. Tension development was studied by a MKB force transducer (Scientific Instruments, Heidelberg, Germany) coupled to an analog counter (Model 6024E, National Instruments, Austin, TX). Control (unlabeled) fibers developed normal amount of maximum isometric tension (0.94±0.05 mN/fiber, mean±SEM, n=32).

Fibers exchanged with fluorescently labeled RLC developed 0.96±0.03 mN/fiber tension. The lack of effect of exchange on tension is consistent with previous experiments with such fibers (10). Fibers labeled with 0.3 μM Rh-phalloidin developed tension within 10% of control. The lack of effect on tension is in agreement with earlier results (11). Labeling myosin active site with Alexa-ATP also had no effect on tension induced by normal ATP - fibers labeled with 3 μM Alexa-ATP developed 0.92±0.02 mN/fiber (n=7) of tension.

Experimental arrangement. The instrument to measure anisotropy of fluorescence was described elsewhere (5, 12). The current set-up differs from the earlier one in that the 633 nm excitation and Cy5 emission filters have been added to detect fluorescent ADP. ATP was photogenerated from caged precursor by perfusing fibers with 2 mM of 5-dimethyoxy-2-nitrobenzyl-caged ATP (DMNPE-caged ATP) in rigor solution. The UV beam was focused by the objective to a Gaussian spot with width, length and depth of ~0.2x0.2x3 μm. Approximately 3 sec after beginning the scan, a shutter releasing the UV light was opened for exactly 10 msec. The energy flux through the illuminated area was 9×10^{-4} mJ/μm^2. ATP stayed in the experimental volume (~300 μsec). The amount of released ATP was enough for a single turnover of ATP.

In vitro anisotropy of solutions. Isolated myosin, prepared according to (13) was exchanged with IATR-RLC as in (7). Isolated actin, prepared according to (14), was 50% labeled with FITC-Ph and 50% with unlabeled phalloidin. Isolated myosin was

labeled with equimolar concentration of Alexa-ATP. Fluorescence anisotropy was measured in an ISS K2 spectrofluorometer (Champaign, Illinois). Experiments were done at 0°C in the rigor solution. Experiments on immobilized proteins were performed at 0 °C in 90 % glycerol. All samples used in fluorescence measurements had absorption <0.1.

Fluorescence intensity and anisotropy of fibers. Fluorescence was measured with a high aperture lens (C-Apo, 40x, NA=1.2) using confocal microscopy. High NA of the objective causes minimal distortion to the polarized intensities (15). The subscripts after the intensity indicate the direction of polarization of emitted light, relative to the axis of the muscle fiber. The excitation light was always parallel to the axis of fiber. Muscle fibers were aligned horizontally on a stage of a microscope. Channels 1 & 2 recorded $I_{\perp}$ & $I_{\parallel}$, respectively. The absolute anisotropy is $r_{\parallel}$ = (ch2-ch1) / (ch1+2*ch2).

RESULTS:

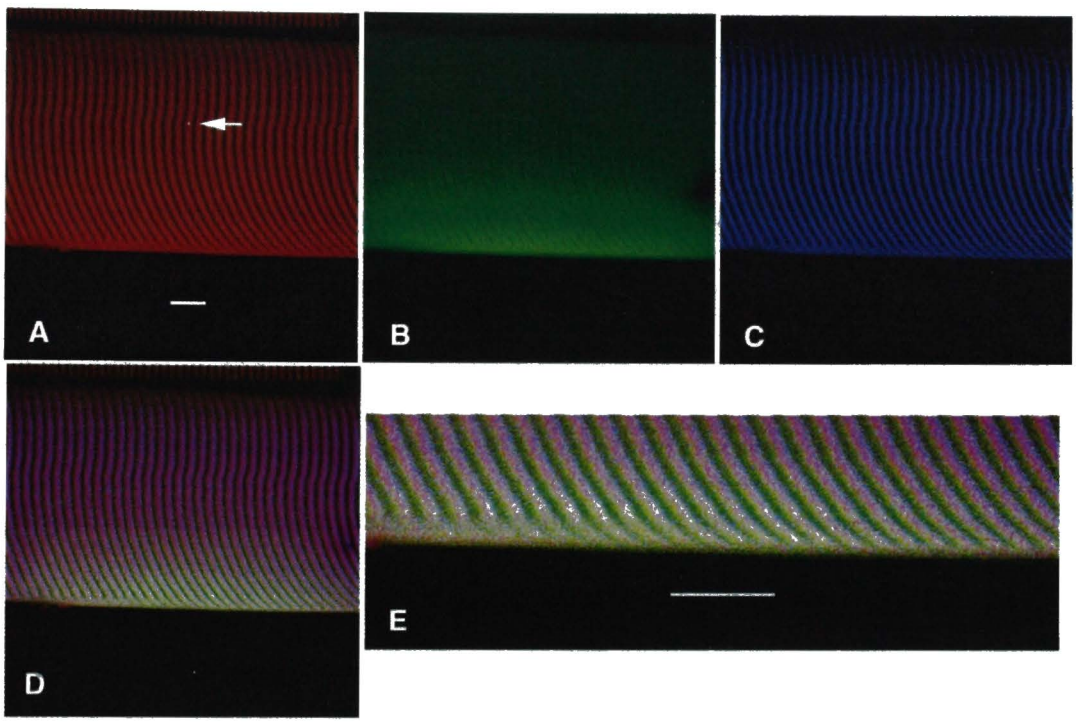

Fig. 1. Triple labeling of muscle. **A**) Myosin exchanged with IATR-RLC (red) and viewed through rhodamine filter (long pass λ>590 nm), **B)** Actin labeled with FITC-phalloidin (green) and viewed through fluorescein filter (band pass 515<λ<565 nm), **C)** myosin active site labeled with Alexa-ATP (blue) and viewed through Cy5 filter (long pass 670<λ nm). **D**) Composite of A, B and C. **E**) Magnified view of selected area of D. White spot in **A**, pointed to by the arrow, gives an approximate dimension of the illuminated area. Bar = 10 μm, sarcomere length = 2.62 μm.

Figure 1 is an image of a triple-labeled fiber in which native RLC was exchanged with Rhodamine-RLC (A, red), actin was labeled with FITC-phalloidin (B, green) and the active site of myosin was labeled with Alexa-ATP (C, blue). The fibers do not stain well with phalloidin, regardless of whether it is added before or after the other dyes. In contrast, when phalloidin is the only dye used, thin filaments label nicely (2, 16, 17). The 3 images are superimposed in (D). The A-bands are violet, because both IATR-RLC

(red) and Alexa-ATP (blue) colocalize there (violet=red+blue). The area of the image that contains all three labels (**Figure 1E**) shows that RLC and Alexa-ATP label the A-bands and that phalloidin labels the I-bands.

A triple-labeled muscle fiber was placed on the stage of a confocal microscope and illuminated with 488, 568 and 633 nm laser light. To avoid bleedthrough, narrow band-pass filters were used in the red (Band Pass 575-640 nm) and the green (BP 510-525 nm) channels. Cy5 long-pass filter (λ_{em}>670 nm) was used in the blue channel. In order to record signals simultaneously, polarized intensities -- not the anisotropies -- had to be measured. Conventional confocal microscope has only 3 fluorescence channels. To record anisotropy, two channels are needed (one each for orthogonally polarized intensities) so six channels would be required for 3 probes. Fortunately, polarized intensity is a good indicator of rotational motion (15), providing that the observational volume does not change during the experiment.

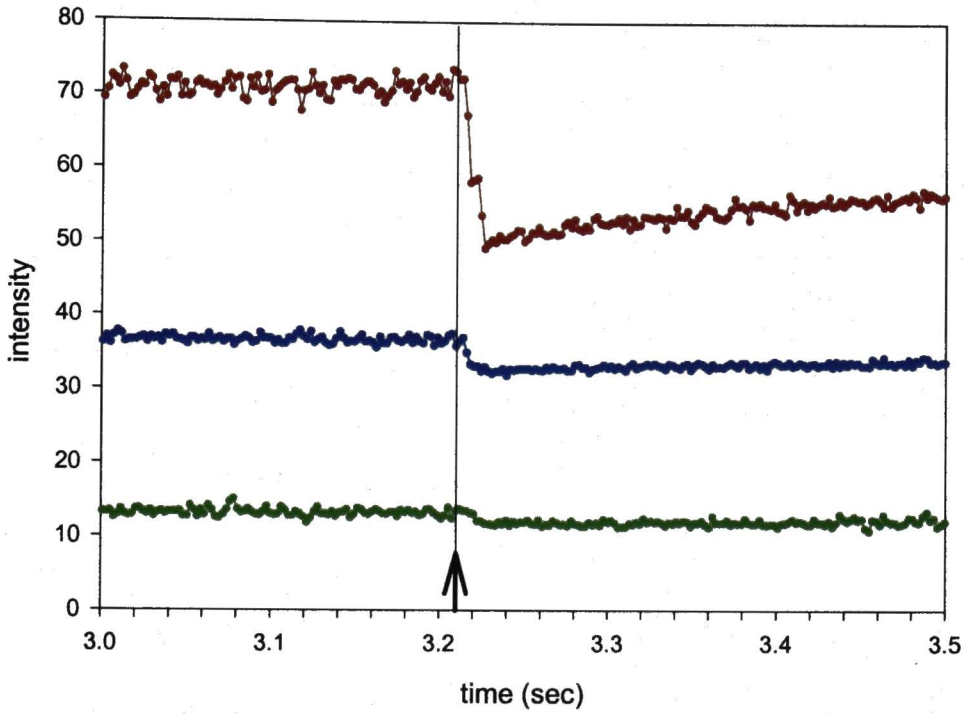

Fig. 2. Simultaneous measurement of polarized intensities: IATR-RLC incorporated into cross-bridges (red), FITC-phalloidin incorporated into actin (green) and Alexa-ADP incorporated into active site of myosin (blue). The muscle was illuminated with 488, 568 and 633 nm laser light. Emission filters: red channel BP 575-640 nm, green channel: BP 510-525 nm, blue channel: λ_{em}>670 nm.

Figure 2 is a typical experiment of simultaneous recording of perpendicularly polarized intensities of IATR-RLC on the RD of myosin (red), FITC-phalloidin on actin (green) and of Alexa-ADP on active site of myosin (blue). Polarized intensity of IATR-RLC and of FITC-phalloidin reported rotations of the lever-arm of S1 and of actin monomers, respectively. Photogeneration of ATP (at arrow) caused sudden drop of polarized intensity of lever-arm (red) indicating dissociation of cross-bridges from thin filaments. This change was followed by a slow recovery, indicating rebinding of cross-bridges to

thin filaments (5). The rapid change of orientation of the lever-arm was paralleled by a change of polarized intensity of actin (green) indicating reorientation of actin monomers. Polarized intensity of Alexa-ADP (blue) reported dissociation of ADP from the active site. ATP photogenerated by the UV pulse displaced fluorescent ADP bound to the active site (18). Displaced Alexa-ADP rotated faster than the immobilized dye (18), which was demonstrated here as a drop of polarized intensity. The three events occurred at the same time, with no exception, in all 49 experiments. The significance of this finding is explored in the Discussion.

Having established that the events occur simultaneously, the anisotropies of the three events were measured separately and superimposed on each other. This was done because there is 3 advantages of measuring anisotropy, rather than polarized intensity. First, all bleedthrough is eliminated. Second, anisotropy corrects for changes in observational volume. In our experiments these changes are negligible, because no global muscle shortening occurs (5), but measuring anisotropy corrects for any local changes in volume as well. Third, the measurements are done in fibers that are labeled separately by rhodamine, fluoresceine and Alexa-ATP, i.e. the fact that triple-labeled fibers do not label well with phalloidin is sidestepped.

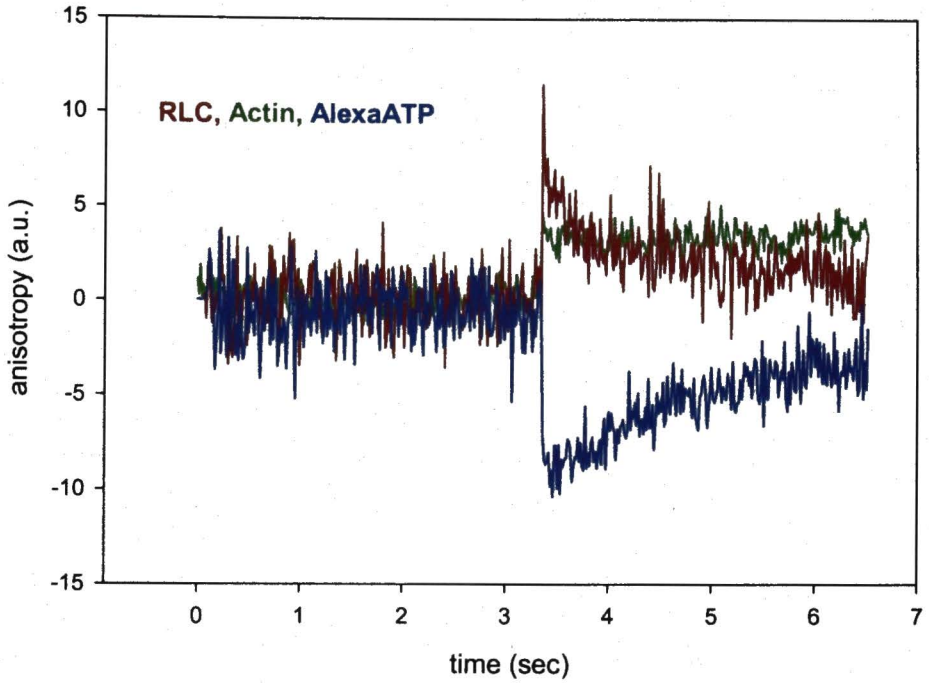

Fig. 3. Anisotropies of myosin and actin. Anisotropies of RLC (red), actin (green) and Alexa-ADP (blue) were fit to 80.5+1.40t, 34.2+0.58t and 122+13.7(1-$e^{-0.60t}$), respectively. Data was subtracted from fitted lines. Data was collected separately from different fibers and adjusted to begin at the same time.

Figure 3 is the superposition of all 3 anisotropies measured separately. Photogeneration of ATP (at arrow) causes dissociation of cross-bridges from thin filaments. Myosin anisotropy (red) behaves like reported before (5). Dissociation is followed by a slow recovery indicating rebinding of cross-bridges to thin filaments. Anisotropy of phalloidin (green) shows that the initial rotation of actin is followed by a new steady-state, indicating that actin assumes a different rigor conformation before and after the brief appearance of ATP (see Discussion for explanation of this effect). Finally, anisotropy of Alexa-ADP (blue) changes after the flash (18) indicating dissociation of ADP from

myosin active site. Ideally, after the rapid drop, this signal should not change with time. The fact that it does suggests that there is some non-specific binding of Alexa-ATP, or that some fluorescent nucleotide cannot be displaced by photogenerated ATP.

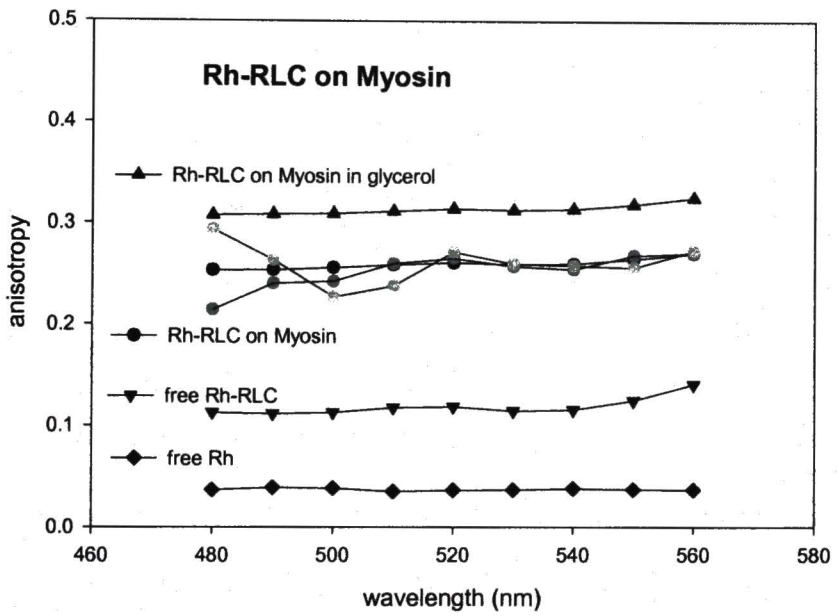

Fig. 4. Excitation anisotropy spectra of free RLC labeled with rhodamine and IATR-RLC incorporated into myosin. Measurements were taken when the dye was immobilized in 90% glycerol at 0°C (▲), when myosin was at low (100 mM) ionic strength (●) and when it was bound to F-actin (shaded circles. Dark gray actin:myosin ratio=1, light gray actin:myosin ratio=5). Controls -- free IATR-RLC (▼) and free rhodamine (♦). The final concentration of rhodamine was 0.1 μM, myosin and F-actin-phalloidin 0.7 μM. Black circles: myosin alone, red circles: myosin bound to equimolar actin, green circles: myosin bound to 5 molar excess of F-actin. λ_{em}=590 nm. Exc. slit=2 mm, em. slit=1 mm. All measurements at 0°C.

It is conceivable that the steady-state anisotropy of muscle fibers changed because dissociation of cross-bridges caused increase of rotational freedom of light chains or of dye itself, i.e. that the observed anisotropy changes do not reflect rotation of the lever-

arm at all. To check for this possibility, we measured excitation anisotropies of solutions of IATR-RLC incorporated into myosin (**Fig. 4**). The limiting anisotropy of immobilized myosin-IATR-RLC complex (▲) at 560 nm is 0.325, giving the angle between absorption and emission dipoles of the probe of 20.7°. The anisotropy of myosin-IATR-RLC at 560 nm is decreased to 0.270 (●). Since myosin at low ionic strength is filamentous and does not execute any nanosecond-time-scale motions, this decrease indicates collective motion of the probe and of myosin-bound RLC. The anisotropy of free IATR-RLC (▼) at 560 nm is 0.141 suggesting that rotation of RLC on myosin is restricted by the interactions with the heavy chain. The residual anisotropy of free rhodamine (♦) is 0.037. Anisotropy is the same in the presence of increasing excess of F-actin over myosin (shaded circles). This is important observation, suggesting that the nanosecond-time-scale mobility of the RD is not affected by the formation of actomyosin complex. It is possible, in principle, that anisotropy remains the same because an increase in rotational correlation time of a fluorophore is exactly compensated by equal increase in its fluorescent lifetime. However, this was not the case: fluorescence lifetimes in the absence and presence of actin were the same. Polarized intensities were well fitted by double exponential decay. In the absence of actin, the lifetimes were 1.53 and 4.44 nsec, with respective intensities at 1:1.18 ratio. In the presence of actin, the lifetimes were 1.75 and 4.50 nsec, with respective intensities at 1:1.28 ratio. The differences in lifetimes were not statistically significant. This proves that anisotropy of the RD is unaffected by the formation of actomyosin complex and that anisotropy change observed in fibers reflects lever-arm rotation.

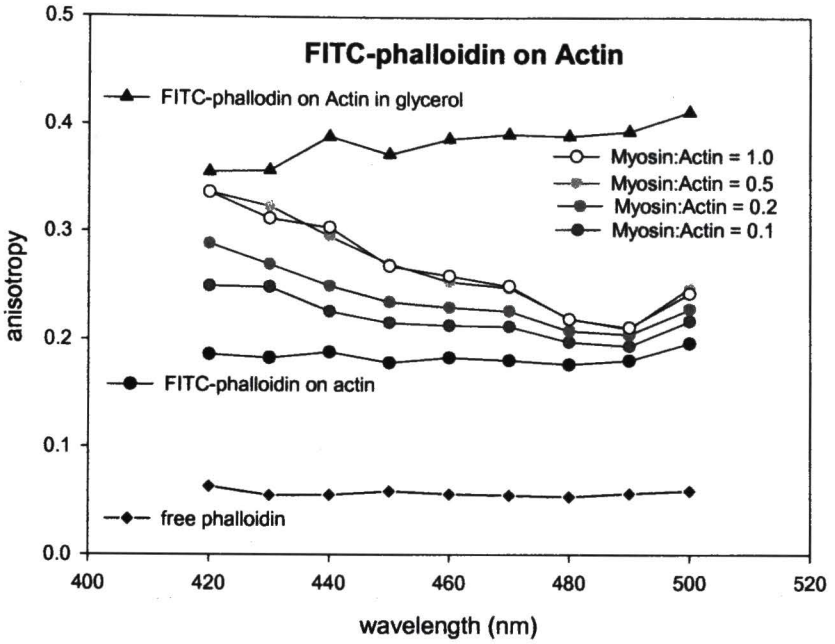

Fig. 5. Excitation anisotropy spectra of FITC-phalloidin incorporated into F-actin. Measurements taken when the dye was immobilized in 90% glycerol at 0oC (▲), when actin filaments were devoid of myosin (●) and when increasing concentrations of myosin at low ionic strength were added (color circles). (♦) – 0.5 μM free FITC-phalloidin. Final concentration of actin was 1 μM, FITC-phalloidin was 0.5 μM, unlabeled phalloidin 0.5 μM. Molar ratios of myosin to actin are indicated on the graph. λ_{em}=516 nm. Exc. slit=1 mm, em. slit=1 mm. All measurements at 0°C.

It is also conceivable that dissociation of cross-bridges from thin filaments results in change of intrinsic anisotropy of FITC phalloidin on actin, and does not reflect rotation of actin. The excitation anisotropies of solutions of FITC-phallodin on actin are shown in **Figure 5**. The limiting anisotropy of immobilized phalloidin on immobilized F-actin (▲) at 490 nm is 0.394, suggesting that the absorption and emission dipoles of the FITC probe are nearly parallel. The anisotropy of phalloidin on F-actin is significantly decreased (●, 0.181 at 490 nm). Since F- and G-actin are not expected to execute any nanosecond-time-scale motions, this decrease indicates rotation of the dye itself. The residual anisotropy of free FITC-phalloidin (♦) is 0.056 at 490 nm. Adding increasing

amounts of myosin (circles) increases anisotropy slightly. Bulk of this increase is due to the increase in the light scattering by acto-myosin, as evidenced by the increase in the polarized intensity with lowering the wavelength. We conclude that anisotropy changes observed during muscle contraction result from rotation of actin, and not from the increase in the intrinsic anisotropy.

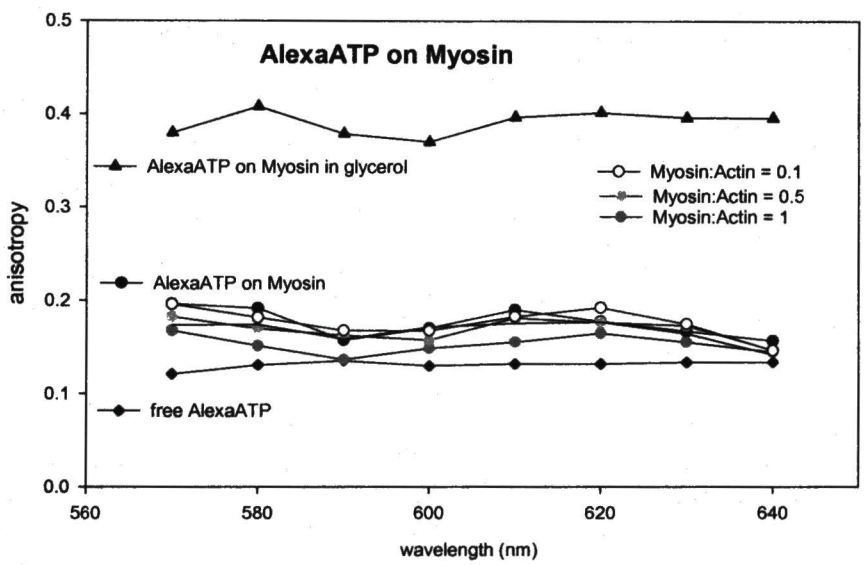

Fig. 6. Excitation anisotropy spectra of Alexa-ATP incorporated into active site of myosin. Myosin immobilized in 90% glycerol at 0°C (▲), myosin at low (100 mM) ionic strength (●), and myosin in the presence of increasing concentrations of F-actin (circles). Free Alexa-ATP has significant residual anisotropy because of short fluorescence lifetime (♦). Final concentration of Alexa-ATP was 0.2 μM, myosin 0.4 μM, F-actin-phalloidin 0.4 μM. Molar ratios of myosin to actin are indicated on the graph. λ_{em}=667 nm. Exc. slit=1 mm, em. slit=1 mm. All measurements were performed at 0°C.

Finally, it is conceivable that dissociation of cross-bridges from thin filaments results in change of intrinsic anisotropy of Alexa-ATP, and does not reflect on dissociation of the dye from myosin. **Figure 6** shows the excitation anisotropies of solutions of Alexa-ATP.

The limiting anisotropy of immobilized myosin containing Alexa-ATP (▲) at 620 nm is 0.396, suggesting that the absorption and emission dipoles of the probe are parallel. The anisotropy of Alexa-ATP on myosin without glycerol (●) is significantly decreased suggesting that the dye retains significant mobility when bound to the active site (since myosin at low ionic strength is filamentous and does not execute any nanosecond-time-scale motions). The residual anisotropy of free Alexa-ATP (♦, 0.134 at 620 nm) results from its short fluorescent lifetime (~2 nsec). Addition of increasing concentrations of actin (circles) makes little difference to the intrinsic anisotropy, suggesting that dissociation of cross-bridges from thin filaments is not responsible for observed changes.

DISCUSSION

The time relationship can be reliably studied in the present experiments because motion is synchronized by rapid release of caged ATP in a small experimental volume. This volume (0.3 μm^3) contains ~400 myosin cross-bridges labeled at the regulatory domain (RD), ~1000 actin monomers labeled with phalloidin, and ~500 cross-bridges labeled at myosin active site with Alexa-ADP. In such small population, the synchrony persists for at least 100 msec after the release of ATP (5). While it is statistically unlikely that the same myosin molecule is labeled at both the RD and the active site and that at the same time actin monomer to which it binds is observed, the anisotropy originates from the same small population of well synchronized cross-bridges.

The comparison of the time courses of cross-bridge rotation and of actin reorientation revealed that the two events begun at the same time (red and green in **Figure 2**). This is consistent with earlier observation that ST-EPR spectra of spin labels on Cys-374 of actin changed upon dissociation of S1 (19) and with observation that binding of S1 to actin labeled with spin labeled analogues of ATP resulted in some change in actin conformation (20). The results are consistent with a suggestion that actin reorientation is not an active event, i.e. that it occurs in response to cross-bridge dissociation from thin filaments. The results suggest that actin does not twist or shorten before any tension is developed (3, 4). The fact that orientation of actin is different before and after the release of caged ATP can be explained by realizing that the stress sustained by thin filaments is different before and after the photogeneration of ATP. Before the appearance of ATP the filaments are under rigor stress, but during a single cross-bridge cycle little tension is generated and filaments are under little or no stress.

The comparison of the time courses of cross-bridge rotation and ADP dissociation revealed that the two occurred at the same time (red and blue in **Figure 2**). If cross-bridge rotation occurred after ADP dissociation (i.e. after ATP binding to myosin), it would have opened a possibility that myosin stays attached to actin even after hydrolysis of ATP (21). If cross-bridge rotation occurred before ATP binding to myosin, it would have suggested an entirely different ATPase mechanism of actomyosin. The simultaneous cross-bridge rotation and ADP dissociation is consistent with the results reported earlier (18).

ACKNOWLEDGEMENTS

We thank Dr. Irina Akopova and Mr. John Talent for their assistance in the steady state experiments.

REFERENCES

1. Holmes, K. C., and Geeves, M. A., The structural basis of muscle contraction, *Philos Trans R Soc Lond B Biol Sci, 355*, 419 (2000).
2. Borejdo, J., Shepard, A., Dumka, D., Akopova, I., Talent, J., Malka, A., and Burghardt, T. P., Changes in orientation of actin during contraction of muscle, *Biophys. J.*, in press (2004).
3. Bordas, J., Svensson, A., Rothery, M., Lowy, J., Diakun, G. P., and Boesecke, P., Extensibility and symmetry of actin filaments in contracting muscles, *Biophys J, 77*, 3197 (1999).
4. Huxley, H. E., Stewart, A., Sosa, H., and Irving, T., X-ray diffraction measurements of the extensibility of actin and myosin filaments in contracting muscle, *Biophys J, 67*, 2411 (1994).
5. Borejdo, J., and Akopova, I., Orientational Changes of Cross-Bridges During Single Turnover of ATP, *Biophys. J., 84*, 2450 (2003).
6. Eigen, M., and Rigler, R., Sorting single molecules: application to diagnostics and evolutionary biotechnology, *Proc Natl Acad Sci U S A, 91*, 5740 (1994).
7. Ling, N., Shrimpton, C., Sleep, J., Kendrick-Jones, J., and Irving, M., Fluorescent probes of the orientation of myosin regulatory light chains in relaxed, rigor, and contracting muscle., *Biophys. J., 70*, 1836 (1996).
8. Sabido-David, C., Hopkins, S. C., Saraswat, L. D., Lowey, S., Goldman, Y. E., and Irving, M., Orientation changes of fluorescent probes at five sites on the myosin regulatory light chain during contraction of single skeletal muscle fibres, *J Mol Biol, 279*, 387 (1998).
9. Wolff-Long, V. L., Saraswat, L. D., and Lowey, S., Cysteine mutants of light chain-2 form disulfide bonds in skeletal muscle myosin, *J Biol Chem, 268*, 23162 (1993).
10. Sabido-David, C., Brandmeier, B., Craik, J. S., Corrie, J. E., Trentham, D. R., and Irving, M., Steady-state fluorescence polarization studies of the orientation of myosin regulatory light chains in single skeletal muscle fibers using pure isomers of iodoacetamidotetramethylrhodamine, *Biophys J, 74*, 3083 (1998).
11. Bukatina, A. E., Fuchs, F., and Watkins, S. C., A study on the mechanism of phalloidin-induced tension changes in skinned rabbit psoas muscle fibres, *J Muscle Res Cell Motil, 17*, 365 (1996).
12. Borejdo, J., Ushakov, D. S., and Akopova, I., The Regulatory and Essential Light Chains of Myosin Rotate Equally During Contraction of Skeletal Muscle, *Biophys. J., 82*, 3150 (2002).
13. Tonomura, Y., Appel, P., and Morales, M. F., On the molecular weight of myosin. II., *Biochemistry, 5*, 515 (1966).
14. Spudich, J., and Watt, S., Regulation of rabbit muscle contraction., *J. Biol.Chem., 246*, 4866 (1971).

15. Burghardt, T. P., Cruz-Walker, A. R., Park, S., and Ajtai, K., Conformation of Myosin Interdomain Interactions During Contraction: Deductions from muscle fibers using polarized fluorescence., *Biochemistry, 40*, 4821 (2001).
16. Szczesna, D., and Lehrer, S. S., The binding of fluorescent phallotoxins to actin in myofibrils, *J Muscle Res Cell Motil, 14*, 594 (1993).
17. Ao, X., and Lehrer, S. S., Phalloidin unzips nebulin from thin filaments in skeletal myofibrils, *J Cell Sci, 108*, 3397 (1995).
18. Shepard, A., and Borejdo, J., Correlation between mechanical and enzymatic events in contracting skeletal muscle fiber, *Biochemistry, 43*, 2804 (2004).
19. Thomas, D. D., Seidel, J. C., and Gergely, J., Rotational dynamics of spin-labeled F-actin in the sub-millisecond time range, *J Mol Biol, 132*, 257 (1979).
20. Naber, N., and Cooke, R., Mobility and orientation of spin probes attached to nucleotides incorporated into actin, *Biochemistry, 33*, 3855 (1994).
21. Yanagida, T., Loose coupling between chemical and mechanical reactions in actomyosin energy transduction, *Adv Biophys, 26*, 75 (1990).

CHAPTER 6

CONCLUSION

In summary, the key findings of this thesis are:

1) ELC and RLC rotate during contraction and the movement of the lever arm power stroke appears to occur approximately 200 milliseconds after release of ATP into a fiber in the rigor state.

2) The release of nucleotide is coupled to one mechanical movement of the lever arm.

3) Actin rotates during contraction and is not simply a passive rail for myosin filaments to slide against.

4) The rotation of actin appears to be passive, i.e. it does not in itself rotate prior to release of nucleotide or prior to rotation of the lever arm within a fiber beginning in the rigor state.

The present experiments monitored orientation changes of actin, myosin, and nucleotide, in non-diseased contracting muscle fibers, in a small illumination volume, during a single cross-bridge cycle. Defects in sarcomeric proteins have been shown to underlie blindness, deafness, and various cardiomyopathies. Hopefully, by understanding the mechanism of muscle contraction in the healthy scenario, better treatments or preventative measures stemming from defects in sarcomeric proteins will become available in the future.